Towards a Better Physical Understanding of Human Hair: Development of Fiber-Tribology-Methods at the Micro- and Nanoscale

Dissertation

zur Erlangung des akademischen Grades eines
Doktors der Naturwissenschaften
–Dr. rer. nat.–
der Fakultät Biologie, Chemie und Geowissenschaften
der Universität Bayreuth

vorgelegt von
Eva C. Max
geboren in Hof/Saale

Bayreuth, im Mai 2010

Die vorliegende Arbeit wurde in der Zeit von September 2006 bis Januar 2010 am Lehrstuhl Physikalische Chemie II der Universität Bayreuth in der Arbeitsgruppe von Herrn Prof. Dr. Andreas Fery angefertigt.

Vollständiger Abdruck der von der Fakultät für Biologie, Chemie und Geowissenschaften der Universität Bayreuth zur Erlangung des akademischen Grades eines Doktors der Naturwissenschaften genehmigten Dissertation.

Dissertation eingereicht am:	25.05.2010
Wissenschaftliches Kolloquium:	29.07.2010
Amtierender Dekan:	Prof. Dr. Stephan Clemens

Prüfungsausschuss:

Prof. Dr. Andreas Fery	(Erstgutachter)
Prof. Dr. Thomas Scheibel	(Zweitgutachter)
Prof. Dr. Josef Breu	(Vorsitz)
Prof. Dr. Volker Altstädt	

Meinen Eltern

List of Publications

List of Publications Resulting from this Thesis:

Max, E.; Häfner, W.; Bartels, F.; Wood, C.; Sugiharto, A.; Fery, A. A Novel AFM Based Method for Force Measurements between Individual Hair Strands, *Ultramicroscopy*, **2010**, *110*, 320-324

Wood, C.; Max, E.; Fery, A.; Sugiharto, A. AFM Based Single Hair Interaction Measurements, *SOFW Journal*, **2009**

Max, E.; Bartels, F.; Wood, C.; Sugiharto, A.; Fery, A. AFM Single-Hair-Force Spectroscopy: "In-situ" Measurements, *EDC Preprints*, **2009**

Wood, C; Max, E.; Bartels, F.; Fery, A. From Conditioning Shampoo to Nano Mechanics and Haptics on Human Hair, *IFSCC Preprints*, **2008**, *25*

Max, E.; Bartels, F.; Fery, A. Meso- and Nanoscale Analysis of the Conditioning Effect on Human Hair, *Liquid Matter Preprints*, **2008**

Max, E.; Bartels, F.; Fery, A. Haptics on Human Hair: From Automated Touches to Single Hair Interaction Measurements, *ECIS Preprints*, **2007**

List of Publications Resulting from Collaborative Research Projects:

Le-Troedec, M.; Peyratout, C.; Max, E.; Kaftan, O.; Smith, A.; Fery, A. Influence of Chemical Treatments on Adhesion Properties of Hemp Fibers, *Submitted*

Kunz, D. A.; Max, E.; Weinkamer, R.; Lunkenbein, T.; Fery, A.; Breu, J. Deformation Measurements on Thin Clay Tactoids, *Small*, **2009**, *5(16)*, 1816-1820

Max, E.; Hund, M.; Tsarkova, L. Depth Profiling of Lamella-Forming Block Copolymer Films Using Quasi In-situ SFM Design, *Abstr. Pap. Am. Chem. Soc.*, **2008**, *99*, 689-690

Max, E.; Zettl, H.; Freitag, P.; Oellerich, S.; Krausch, G.; Köhler, J. Diffusion of Individual Polymer Chains, *International Summer School @ University Bremen*, **2006**

List of Prizes and Press Coverage:

Max, E.; Bartels, F.; Wood, C.; Sugiharto, A.; Fery, A. Haptics on Human Hair: from Automated Touches to Single Hair Interaction Measurements, *HairS'09*, **2009** (Best Lecture Award)

Max, E.; Bartels, F.; Wood, C.; Fery, A. Meso- and Nanoscale Analysis of the Conditioning Effect on Human Hair, *Abstr. Pap. Am. Chem. Soc.*, **2008**, *19*, (Public to Science Talk, Autumn Meeting of the American Chemical Society 2008)

Sampson, M. Heads-up Study of Hair Dynamics May Lead to Better Hair-care Products, ASC Homepage, **2008**

DPA, Forscher liefern Schlüssel für neue Haarpflege, *Deutsche Presse Agentur*, **2008**

UPI, Hair Study May Lead to Better Shampoos, *United Press International*, **2008**

Halford, Untangling Hair Dynamics, *Chemical & Engineering*, **2008**, *86* 34

Henderson, M. Microscopic Solution to Giving Bad Hair Days a Wave Goodbye, *The Times*, **2008**

Yuxia J. Bye-bye to Bad Hair Days as Experts Entangle Hair, *China Daily*, **2008**

Bayrischer Rundfunk, Hilfe bei sprödem Haar, 5 min. Contribution in TV, **2008**

Max, E. Hair, Interview by *Radio New Zealand International*, **2008**

ANI 31, Bad Hair Days May Soon be History, *The Times of India*, **2009**

Contents

1 Introduction

For centuries, natural fats, oils and products derived from animals were used by human beings all over the world to improve their well-being and to take care of their scalp, hair and skin. In *Victorian* and *Edwardian* times, it was common place for men to use *macassar oil* as a hair conditioner, yet this has the side-effect of feeling heavy or greasy. However, hair conditioners were not widely used until the mid-20th century, and it is still common to incorporate a variety of natural fats and oils in cosmetic products like shampoos and conditioners; for example coconut fat, avocado oil, jojoba oil, ylang-ylang oil or horse milk.

The main goal of hair conditioning is to improve combability and the haptic perception of hair, hair shininess, avoidance of flyaway hair due to static electricity, and protection against harmful influences like wear and tear or UV-light.

Modern science can advance the hair conditioner industry by inclusion of silicone oils, fatty alcohols, and quaternary ammonium compounds etc., these chemical compounds (used at the right concentration) condition hair without feeling greasy, fatty or heavy.

Combing of hair is influenced by the lubrication (by active agents) of the hair fiber surface. This activity is due to the binding or sorption of lubricants onto the hair surface, and it is therefore essential to study these interactions where they are occurring (for example near or on the fiber surface).

Figure 1.1 illustrates how conditioners, especially their active agents (cationic polymers) can influence the surface of hair. Research on the structure of hair itself, more specifically, the chemistry and physics of the surface of hair, is necessary to reveal the interactions between hair and these active agents. The structure and the composition of a hair fiber is already very well investigated[1–4]. Studies of mechanical behavior have until now been carried out mostly in the micro force regime, and investigation of the nano force regime

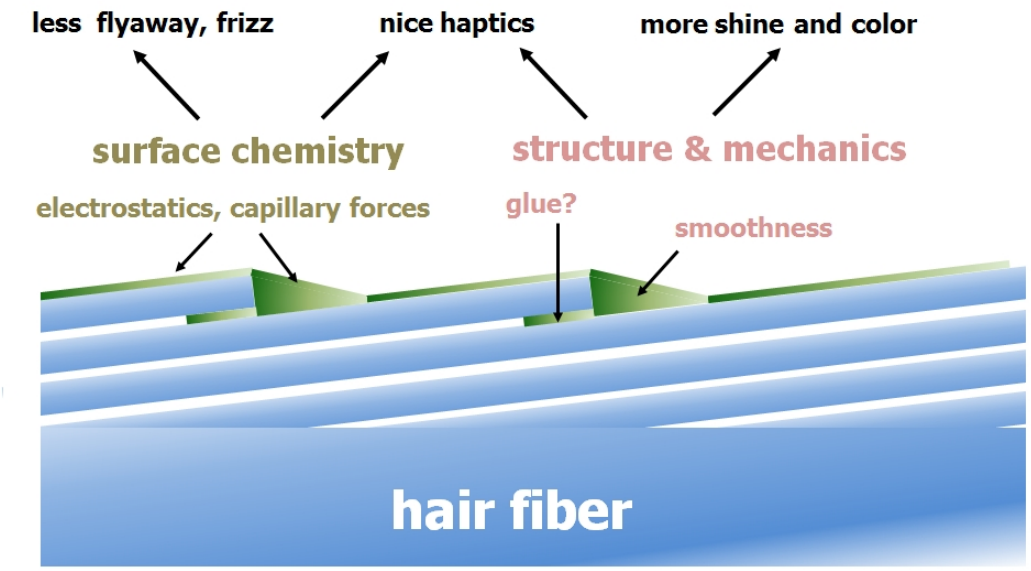

Figure 1.1: Possible effects of conditioning the surface of hair.

is still in its infancy in comparison to all other research about conditioners[5–7]. Initial investigations of their behavior on the surface of hair have been reported by several groups[8–12].

In this thesis, modified physical measurement methods concerning the interactions between conditioners and the surface of hair fibers are investigated. In doing so, the aspect of haptic perception plays an important role. Therefore, in the first part of the thesis the frictional behavior on the surface of hair is studied with a so called Universal Surface Tester. It is possible with this instrument to measure the behavior of friction in the micro force regime. The set up of the instrument was modified and several different conditioner formulations are compared to each other. These results are correlated to the measurements using the Comb Force Method, which is widely spread for studying the effects of different shampoo formulations.

The main part of this thesis deals with the nano force regime. An investigation of single hair measurements was achieved using an Atomic Force Microscope, and the modifications to the set up are also discussed. Furthermore it was possible to determine the effect of adhesion forces. In addition we studied the frictional behavior between two

single hairs. An investigation of *in situ* measurements of them with different active agents from conditioning formulas gave us initial information about the friction reduction that occurs when polymer adsorption takes place on an untreated hair surface.
Over-all we saw, that results from Haptic Panel Tests could be related to both experimental data, from the measurements using the Universal Surface Tester and the measurements using the Atomic Force Microscope.

2 Status of the Field

The motivation for this work was to find a way to understand the interactions between conditioner polymers with the surface of hair in more detail. To approach the system, this Chapter introduces the following points:

- Morphological Structure and Physical Behavior of Hair
- Effect of Conditioning Polymers on the Surface of Hair
- State of the Art Concerning Existing Physical Methods
- Theoretical Background of Methods

Section 2.1 focuses on the morphological structure of hair and its anatomy from the inner layers to the outer ones, which is essential for the physical behavior of the fibers. Systematic studies that facilitate improvements to the quality of hair care products are of great interest. Interactions between cationic polymers (active agents in shampoos and conditioners) and the hair surface are presented in Section 2.2, also how the interactions change if a polymer/surfactant complex is adsorbing at the surface of hair. Section 2.3 *State of the Art* gives an introduction to research from the last decades and informs the reader about the current science, most pertinent to this thesis.
There is also a focus on the mechanical properties like the tensile strength, torsion, bending and the friction of hair, the description of these behaviors in a mathematical way and how to handle these experimental data.

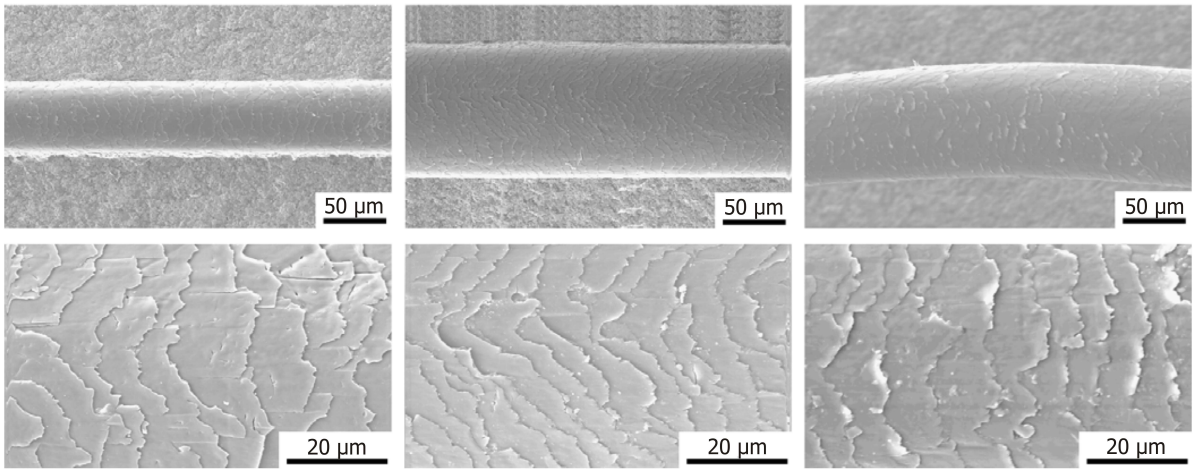

Figure 2.1: SEM pictures of different hair. Caucasian on the left, Asian in the middle and African on the right. The diameter of the hair is different. Asian is the thickest (middle) and Caucasian the thinnest (left)[13].

2.1 Science of Hair

2.1.1 Morphological Structure of Hair

Hair provides protective, sensory, and sexual attractiveness functions. The main focus of this work is on the physical behavior of the human scalp hair as opposed to hair of other parts of the body (therefore when hair is mentioned it refers to human scalp hair). On the scalp there are approx. 200 hairs/cm^2, yielding a total of up to circa 150.000 hairs[14]. Human hair is a complex system which consists of several morphological components. Each has different chemical compositions and can therefore be regarded as a separate unit with respect to its chemical and physical behavior. Human hair consists of approximately (approx.) 65 to 95% proteins (polymers composed of amino acids). The rest of the contents are water, lipids, pigments and micronutrients. Chemically, the hair of all ethnic groups all around the world is found to have similar protein structure and composition[15,16]. In Figure 2.1 Scanning Electron Microscopy (SEM) pictures of hairs from people of different ethnic backgrounds (from left to right: Caucasian, Asian and

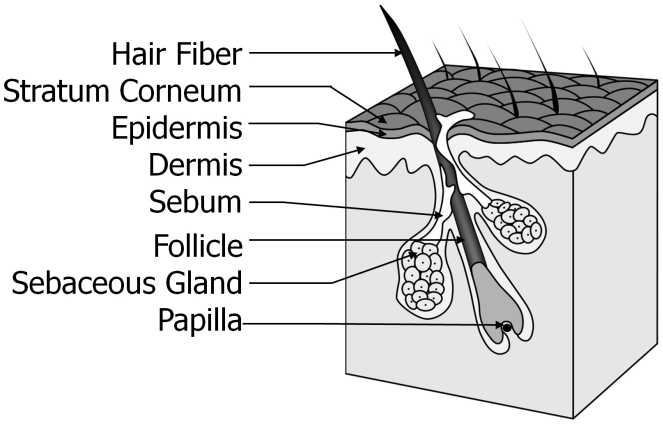

Figure 2.2: Diagram of the structural organization of a hair follicle as a fiber emerges from the scalp.

African) and their contrasts in thickness are shown, the Asian hair is clearly the thickest, and the Caucasian the thinnest. A follicle with an active human hair bulb and its structural organization is illustrated in Figure 2.2. A hair fiber arises from the subcutaneous tissue of skin, the base of the hair follicle is a large structure that is called the dermal papilla, which is the control center of the three distinct stages of human hair growth. The stages are called *anagen* (growing stage), *catagen* (transition stage) and *telogen* (resting stage), respectively. In the hair bulb the growing stage is characterized by intense metabolic activities which can take from two to six years, and on average a hair grows 16 cm each year[17]. The *catagen* stage occurs within a few weeks, during which the bulb drifts upwards in the skin towards the epidermal surface, while the metabolic activity is slowing down. At the *telogen* stage (also a few weeks) growth stops completely and the bulb reaches the stage of atrophy while a new fiber starts to grow and pushes out the old one.

A scheme of the build-up of a hair fiber in which all important dimensions and ratios are indicated is shown in Figure 2.3. Hair fibers have an elliptic shape. The cortex is surrounded by the cuticle (see Figure 2.3 (A)) and consists of spindle-shaped cells aligned along the fiber axis (not shown here). The medulla is the inner most layer of the hair shaft, which is a more loosely packed porous region of aligned cells than the cortex.

The cuticle consists of flat cells which overlap each other (overlay$\sim$5μm). Their orientation is from the proximal end (root) to the distal end (tip) of the hair fiber. This orientation affects the frictional behavior of hair enormously[18]. The hair fiber diameter is typically between 40-120 μm[19]. The cuticle is normally 5 to 10 μm thick, and they are unbroken just next to the scalp and near the root, yet the farther away from the scalp the more mechanical deterioration is detectable[20]. In detail (Figure 2.3 (C)) the cuticle consists of a thin outer membrane (approx. 50-100 Å), which is covered by a monolayer of 18-methyleicosanoic acid (18-MEA), called the F-layer[21]. The A-layer beneath the cell membrane complex has a high content of cystine (>30%), the exocuticle (also called the B-layer) which has $\sim$15% content of cystine, and the endocuticle which is low in cystine content ($\sim$3%)[22]. The complex surface of the fiber is one of the factors which govern the diffusion of ingredients into the hair.

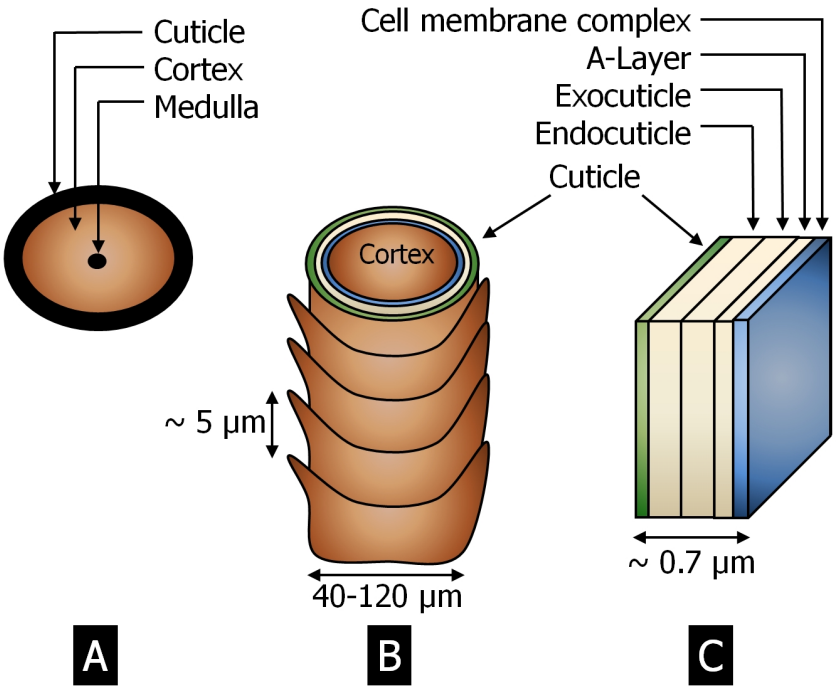

Figure 2.3: Illustration of a cross section of a human hair fiber (A). (B) is the fiber structure and (C) presents the substructures of the cuticles. The cortex is composed of micro fibrils (not shown).

2.1.2 Physical Properties of Hair

As mentioned before, in the last decades the physical properties of hair were studied mostly in the regime of the microscale. This means that most of the physical properties like modulus of elasticity or the shear modulus were established by collecting e.g. forces in micro Newton via bending or tensile tests. For the nano regime, the friction behavior was also investigated in the nano newton regime. Table 2.1 presents the most important physical properties of virgin and untreated hair[14,23,24]. Hereby E_S is the elastic modulus, which is in the same range as the elastic modulus for bending E_B. E_T is the torsional modulus and R is the electrical resistance. How these values can be determined experimentally is described in more detail in Section 2.3.

Table 2.1: Important physical properties of virgin untreated human hair[14,23,24]. All values were investigated at a relative humidity between 60-80% RH (relative humidity).

E_S [MPa]	E_T [MPa]	E_B [MPa]	R [Ω]
3890	890	3790	1.0-1.7 $\times 10^{12}$

2.2 Conditioning of Hair

Over the past decades polymers have become increasingly important as active agents of different cosmetics, like conditioners[17]. They are responsible for many effects not only for conditioning hair. They have been used to improve combing, manageability, curl retention, the substantivity of other ingredients to hair, emulsion stability and to thicken formulations. The main aim for researchers and industry is to develop polymers in cosmetics that are more compatible with water and more environmentally friendly. The important areas of application of polymers in hair products are the following:

- Interactions of Polymers Binding to the Hair Surface

- The Chemical Behavior of Polymers
- Formation of Films and Adhesional Behavior of Polymers
- Cationic Polymer/Surfactant Complexes

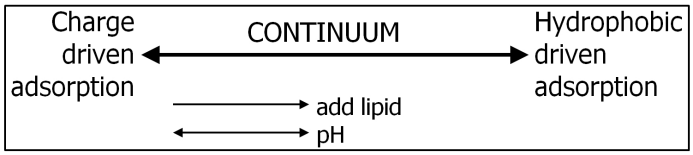

Figure 2.4: Schematic of mechanism for adsorption of polymers to keratins, suggested by Robbins et al.[25].

2.2.1 Adsorption of Polymers

From an aqueous solution the amount of sorption of chemicals by hair is driven by its binding interactions to the keratin, its hydrophilicity and the diffusibility into the hair. Research has been done in the field of adsorption of conditioning polymers to human hair, so far[5,26,27]. Robbins et al. suggested that the adsorption to keratin surfaces is a continuum between a charge-driven and a hydrophobically driven process[25]. Figure 2.4 illustrates this suggestion.

The main factors this depends upon are the chemical structure of the adsorbing species and the pH of the system.

There are three main types of bonding possibility between a polymer and a predominantly hair:

1. Ionic and Covalent Bonds
2. Primary Polar Interactions
3. *Van der Waals* Forces

It is not possible to separate these different types from each other because intermediate binding forms occur[28]. But it is possible to describe the trend of the different types.

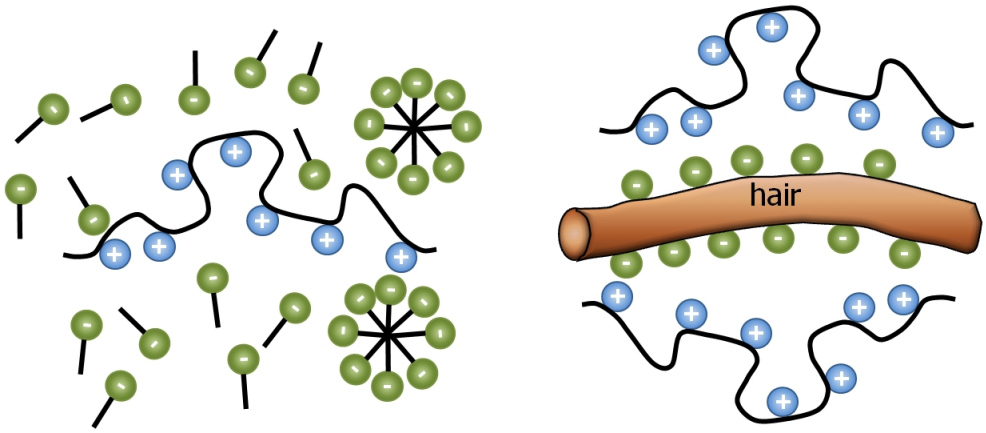

Figure 2.5: Effect of cationic polymers in a conditioning formulation. The surfactant forms micelles. After a rinse-off the positively charged molecules are attracted to the negative charged net on the hair surface if the pH is above the isoelectric point (pH 3.67).

The strongest binding forms are the primary valence bonds including ionic and covalent bonds, for which 50-200 $\frac{\text{kcal}}{\text{mol}}$ are the normal energies. Hydrogen bonds are the most important polar interactions and the second strongest binding forces, having values of 4-10 $\frac{\text{kcal}}{\text{mol}}$[29]. With approx. 1 $\frac{\text{kcal}}{\text{mol}}$ *Van der Waals* attractions are relatively weak[29].

If the molecule is very large, the entropy is equally or more important than the attractive forces between polymer and hair. The entropy is inversely related to the amount of structural organization of the total system. Thus these forces drive large hydrophobic polymers out of the solvent phase onto the hair surface. It was described, that the forces involved in such multiple bindings in polymers resulting in molar cohesion[30]. The molecular size to the substance activity of polymers to hair is very important. Pauling et al. showed that the stronger bond types are much more important to the substantivity than the molecular size[28].

Figure 2.5 depicts a water-soluble cationic surfactant in an aqueous solution adsorbing onto a hair above its isoelectric point. Main active agents of polymers used in hair products are cationic. They have a very high affinity to hair because of the low isoelectric point (approx. pH 3.67) in cosmetically untreated hair which is even lower in

bleached hair[31]. As shown in Figure 2.5 positively charged polymers are attracted to the negatively charged net of the hair surface if the pH is above the isoelectric point. Most cosmetic hair treatments are above this pH, so polycationics getting more attractive to hair. Because cationic polymers are difficult to remove by rinsing they are said to be substantive to hair. The desorption is much slower than expected from a simple law of diffusion calculated by the square root of time law[31].
The flattening effects which occur by the interaction forces mentioned above improve shine, color and results finally in detangling of hair and more smooth combability[32].

2.2.2 Adsorption of Polymer/Surfactant Complexes

For cleaning effects in a conditioning formula there are additional active surfactants. They form associations with the cationic polymers in solution[33].
Generally this can be explained like this: the entropic driving force of mixing two polymers (e.g. a polymer with a surfactant) in a common solvent is weak and they typically segregate into a two-phase solution. One of them is rich in one polymer, and one rich in the other. If the molecular weight is increasing, the tendency of the phase separation increases, too.
Surfactants (also called amphiphiles) typically have a hydrophilic head group and a hydrophobic tail. They normally start to form micelles at a critical micelle concentration (CMC). Since a micelle is characterized by a high molecular weight, the expectation of segregative phase separation could be a common phenomenon.
There are attractive interactions between an ionic surfactant with an oppositely charged polymer. In this case an associative phase separation occurs. One phase contains high concentrations of both polymers (polymer and surfactant) and one phase is a dilute solution. The degree of phase separation will in both cases increase with the molecular weight of the polymer and the surfactant[34]. A characteristic ternary phase diagram for a mixture of an ionic surfactant and an oppositely charged polymer in water is presented in Figure 2.6. The tie-lines in the two-phase region are given to show the compositions

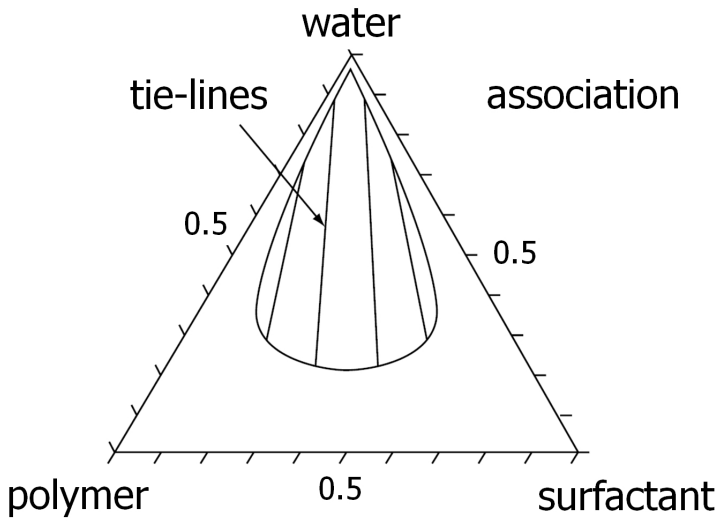

Figure 2.6: Ternary phase diagram for a mixture of ionic surfactant and a oppositely charged polymer gives an associative phase separation. The tie-lines are given to show the compositions of co-existing solution phases in the two-phase region[34].

of co-existing solution phases. By increasing the length of the alkyl chains of the surfactant and the polymer molecular weight, the extent of phase separation in the system also increases. Of course it is important, if the polymer is water-soluble or not. The solubilization of water-insoluble polymers is included in the phase behavior effects. The addition of an ionic surfactant can achieve the depression of clouding (increase the cloud point) of a polymer solution.

Solvency effects always play a crucial role in material adsorption. Therefore a surfactant strongly affects the adsorption of an oppositely charged polymer[34]. Qualitatively, the kinetics of the adsorption process from polymer/surfactant complexes to *hair-like surfaces* (modified silica surfaces) show two different stages: a rapid increase in adsorption within the first minutes, followed by a slow adsorption that reaches a plateau.

Terada et al. compared the adsorption behavior of polymer/surfactant complexes to hydrophobized silica within different conditions[35]. They used this surface as a hair model surface. They tested the adsorption by first, preadsorbing a polymer layer to the surface

and adding stepwise the surfactant sodium dodecyl sulfate (SDS) and second, adsorbing a premixed surfactant/polymer solution to the surface. From a premixed surfactant/-polymer, SDS completely inhibits the adsorption of polymer molecules on the surface at high SDS concentrations above the critical micelle concentration (CMC). In addition to that they studied the desorption behavior in the post-precipitation regime, by diluting the system with water. The adsorption (or desorption) behavior during the rinsing process strongly depends on the hydrophobicity of the polymer and the state of the surface. Goddard et al. studied interactions between the surfactant SDS and a polymer called JR, which is often used in conditioning formulae[36]. They found out, that the interactions between the mentioned molecules take place in two stages, as noted above. First there is a primary layer adsorption of surfactant to the polymer, which results in neutralization of the cationic polymer. The solubility decreases and the surface interaction of this new complex is very high.

If the ratio of anionic surfactant to cationic polymer increases, a second layer adsorbs by reversing the net charge and the complex becomes more water soluble. It was also found out, that at the theoretical charge neutralization ratio the complex is precipitated[37]. It takes place if the concentration is above 0.010 wt% polymer and anionic surfactant. At lower concentrations of polymer, a fixed concentration of SDS is needed for precipitation. It is inversely related to the charge density of the polymer and decreases if the density increases. The importance of the space length of the quaternary derivatives of polymer is less than the charge density. Another notable factor is the relaxation rate of polymer/surfactant mixed micelle complexes, which depends on the structure of the polymer. The substantivity of these anionic cationic complexes to the hair surface is very high. Water can just remove 30% of such complexes from the hair surface. There is not a closed film of complex over the entire hair surface[13]. The majority of complexes that remain on the hair after application, deposit near the scale edge base, and layers with thicknesses of up to 100 nm were found[38].

2.3 State of the Art of Physical Characterization Methods

Many methods have been developed for characterizing the physical behavior of hair and the influence of different treatments to it. All physical properties of hair are influenced by shampoos and conditioners, so it is worth having a closer look at these conditioning effects. This Section deals with the following physical properties and how they can be investigated:

- Mechanical Properties of Hair
- Frictional Properties of Hair
- Static Charge of Hair
- Haptic of Hair and the Influence of Conditioners
- Physical Properties of Hair in the Nanoscale and the Influence of Conditioners

2.3.1 Mechanical Properties

The elastic and tensile deformations of hair were investigated by a lot of different methods. A common procedure to evaluate tensile properties is via load-elongation experiments, however, the stretching properties are based on the behavior of the whole fiber. The surface of hair acts in a different way, and Robbins and Crawford demonstrated with an Instron Tensile Tester that damage processes to the cuticles have no influence on the tensile properties[24].

Whereas Wolfram et al. pointed out the enormous influence of relative humidity (RH) and room temperature (RT) to the elastic modulus E_S within a ratio of 2.62 determined for $\frac{65\%\ \mathrm{RH}}{100\%\ \mathrm{RH}}$ [39]. Comparing this elastic modulus (also called the Young's Modulus) of 3890 MPa (RT, 60% RH) measured by Robbins et al. to a value of 3000 MPa (RT,

50% RH) reported by Orfanos, this ratio is confirmed[14,24]. A single hair fiber has also a tensile strength of 2 Newtons[14]. The effect of increasing the temperature is similar to the effect of relative humidity i.e. upon increasing temperature, there is also a direct proportionality of the fiber diameter to the tensile properties[40,41]. Chemical damage like bleaching, permanent waving and light radiations also known to affect the mechanical properties[42–44]. Mechanical damage occurring from large physical forces or temperatures which degrade and wear the outer cuticle layers, commonly caused by combing, scratching, cutting or blow-drying, and not only the tensile properties are affected by all these factors.

The torsion and the hair fiber rigidity can be determined via several methods. Most popular for studying this is the Torsion Pendulum Procedure (TPP), in which a small pendulum from a fiber has to be set into a free rotational oscillation[45]. To determine the torsional modulus E_T it is necessary to have the period of oscillation P, the moment of inertia of the pendulum I, the fiber diameter D and the length of the fiber:

$$E_T = \frac{128\pi IL}{(PD^2)^2} \tag{2.1}$$

The rigidity P can be calculated within the same dimensions:

$$P = \frac{8\pi IL}{P^2} \tag{2.2}$$

With a value of 890 MPa (RT, 65% RH) E_T is smaller than the stretching modulus E_S[19]. One reason for this is, that in contrast to tensile stress the cuticles play an important role for the torsion.

The stiffness coefficient is directly proportional to fiber linear density, meaning that the stiffness increases with fiber diameter[46]. This was determined via the so called Balanced Fiber Method (BFM), in which small equal weights are mounted on the ends of a fiber, and each one was threaded through a short piece of plastic tubing, and a cone-shaped metal pen is inserted in the other end of the tubing. It is possible to hang the hair over a

fine wire hook and to measure the distance d as it is shown in 2.7, allowing the stiffness coefficient to be calculated from this distance:

$$G = \frac{Td^2}{8} \tag{2.3}$$

In which T is the force applied to each fiber end. The elastic modulus of bending E_B can be described with d, where A is the cross sectional area of the fiber:

$$E_B = \frac{\pi T d^2}{2A^2} \tag{2.4}$$

Compared to the Young's modulus for stretching E_S, E_B has a value of 3790 MPa in the same region. It should not be disregarded, that with the elliptical diameter of the hair fiber the orientation for the bending is always over the minor axis in a Hanging Bending Test.

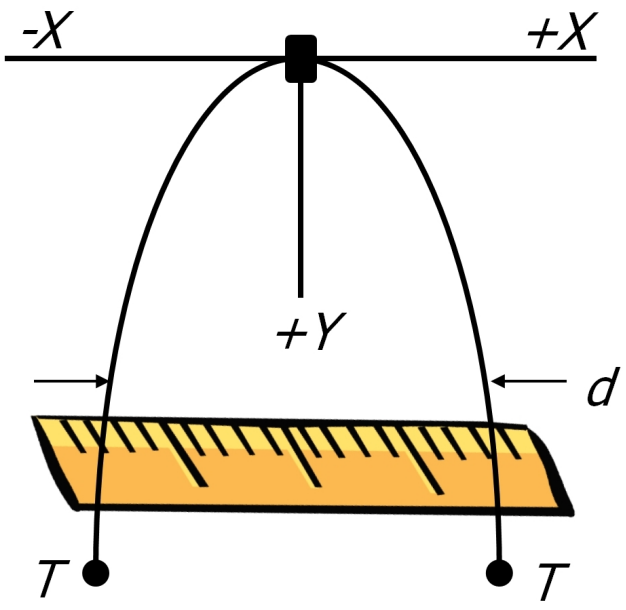

Figure 2.7: Schematic set up of a Hanging Bending Test (HBT) with human hair. The distance d is measured by varying the weights T on each end of the hair fiber.

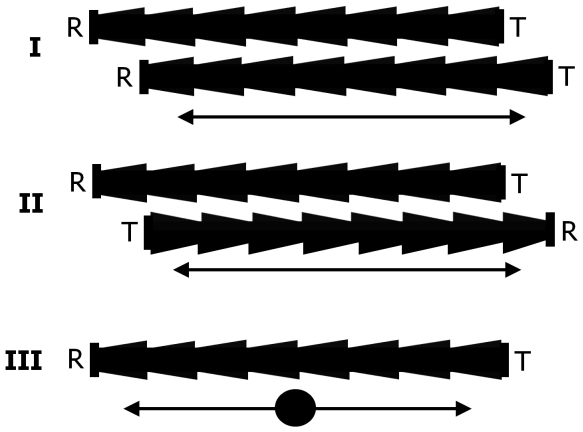

Figure 2.8: Directional effects in hair friction. In all three possibilities the top hair is stationary and the bottom hair is moving. R = root and T = tip.

2.3.2 Frictional Properties

At the contact area of two hair fibers dissipative forces (known as friction forces) exist. The *Coulomb* friction of one body with another is:

$$F = \mu F_N \tag{2.5}$$

F_N is the normal load, μ is the coefficient of friction, whereas μ_S is the coefficient of the static friction and the coefficient of the kinetic friction is μ_K. These two forces are necessary to initiate the movement, in general $\mu_S \geq \mu_K$, and μ_K can be calculated directly. The laws of friction apply to dry, unlubricated surfaces, except the lubricants represented as thin solids or non fluid films.

The relative humidity is relevant to friction as well. Experiments between individual hairs are more difficult to describe than experiments between hair and another material. The coefficient of kinetic friction can be calculated by tension measurements, in which a hair fiber is moved over an axis and weighted at the tip end[47].

$$\mu_K = \frac{1}{\phi} ln \frac{T_2}{T_1} \tag{2.6}$$

ϕ is the angle of wrap in radians, T_1 and T_2 the tension before and after passing the axis. The directional effect was introduced by Schwartz et al., Figure 2.8 shows the three important principles[48]. In diagram **I**, the scale edges of only one of the fibers is rasping, no matter what the direction of relative motion. In **II** the friction is either lower than in **I**, if the bottom hair is moving from tip (T) to root (R) or higher, if the bottom hair is ranging from root to tip. If the hairs are perpendicular to one another there is only movement with or against the scales. All cases of hair-hair friction can be explained with Figure 2.8. In this thesis stage **III** was used for single hair measurements with a AFM described in more detail in Section 4.2.

The production of natural fats decreases the roughness, as well as the talc which is filling up the cuticles[49]. In general the friction increases in proportion to the diameter of the hair fiber.

A widely used approach for hairs is measuring friction effects via the so called Combing Force Method (CFM). In combing force measurements, various interactions are involved: adhesion between comb and hair, friction of hair fibers with each other and maybe even entanglement of hair fibers. Wood et al. performed the wet combing force reduction for different conditioning systems with standard shampoo formulations (like it is shown in Table 4.1)[50]. The combing force reduction is defined as:

$$F_R = 100 - \frac{x_{treated} \times 100}{x_{untreated}} \tag{2.7}$$

Hereby $x_{treated}$ refers to the combing force of conditioner-treated hair, and $x_{untreated}$ to the combing force of untreated hair. Figure 2.9 illustrates the force reduction F_R of three different polymers. The structure and properties of these polymers are illustrated in more detail in Section 3.1. As part of this work the combing force reduction was correlated with the Universal Surface Tester (UST) technique in Section 4.1.

Figure 2.9 indicates a higher combing force reduction when the applied amount of the cationic polymer is also increased. The addition of silicone oil has a very strong effect

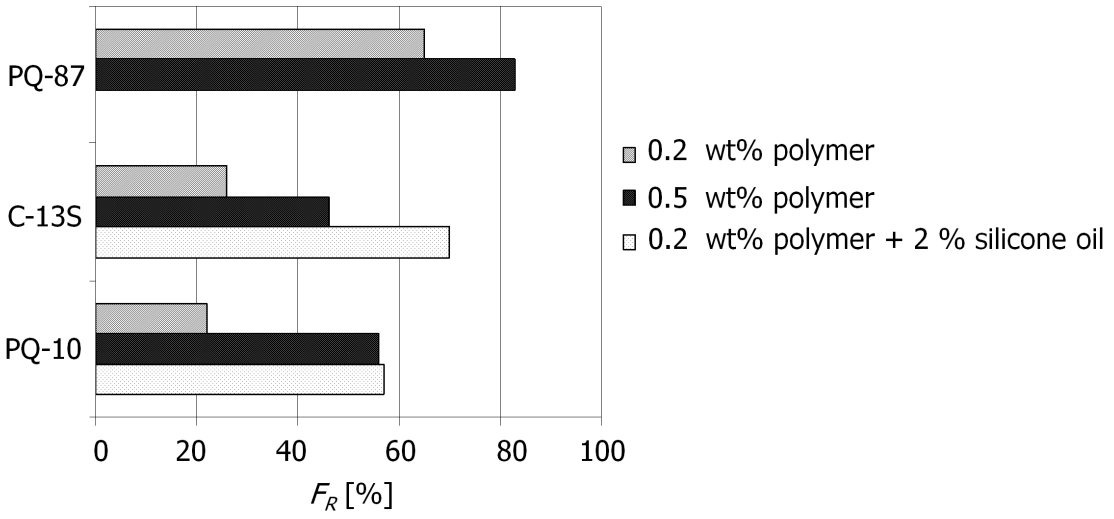

Figure 2.9: Wet combing force reduction by applying different conditioning systems in SLES/CAPB shampoo to bleached hair. It is shown that the highest reduction F_R is achieved with the polymer PQ-87 within a concentration of 0.5 wt%. The reduction is also very high, when silicone oil is added to the system with the polymer Jaguar C-13S.

on combing when combined with the cationic polymer Jaguar C-13S.

Nevertheless, Polyquaternium-87 shows the highest values for combing force reduction of over 80% at 0.5 wt% use level, which cannot be improved by the addition of silicone oil.

2.3.3 Static Charges of Hair

Static charges of hair (better known as flyaway hair) are influenced by different factors. Mechanical pressure, like compressing hair fibers, generates separation of the charge, which leads to triboelectricity and piezoelectricity. The electrical resistance is appropriate to the speed of relieving these charges. Thus it appears that flyaway hair is caused by a high electrical resistance. The type of hair is very important, if hair is curled for example, the grade of integration hinders single hair to stick out[17].

The direction dependency of friction causes an interesting effect. If one hair is pulled

out of a bunch of equally orientated hairs, charges occur on the surface of this hair. The polarization depends on the direction of this procedure, it is positive if the fiber is excerpted on the tip end and negative by excerpted on the root end. If the single fiber is directed oppositely to the others there is no charge. Increasing the relative humidity leads to a decrease of the electrical resistance (the resistance of hair is 1.0-1.7$\times 10^{12}$ Ω), and the tendency of charge formation is therefore lower if hair is wet[23]. The electrical resistance can also be influenced by the concentration of electrolytes because the keratin of hair is highly hygroscopic.

Shampoos and conditioners decreasing the electrical resistance and friction, followed by less comb assignment and so less charge formation. If the electrical resistance is below $R = 10^8 \ \frac{\Omega g}{cm^2}$, the charge can spread over the entire hair.

2.3.4 Haptics of Hair and the Influence of Conditioners

Haptic attributes are usually addressed by sensory assessment during product development and in panel tests. External objects or forces are perceived via contact with the body, especially the hands. The complexity of Haptic Panel Tests (HPT) is even greater due to the mechanisms of human haptic perception. There are cutaneous sense organs with tactile receptors in skin. The highest density of them are on the tip of tongue and on the finger pad, and it is possible to sense differences in fine structures. Tactile contact quality is realized by sensoric panel tests on human hair, see Figure 2.10. The sensoric or subjective estimation of hair after different applications was done in the BASF SE practice lab by the following grades: 1 $\widehat{=}$ very good to 3 $\widehat{=}$ weak (not good). The detangling of hair was evaluated after conditioning, and a description of the touch was also given from trained testers as well as from untrained test persons[51]. The sensory assessment of the wet-use attributes and the dry hair attributes after shampoo application shows differences in the hair feel depending on the type of conditioning system. In shampoo application, the panel perceived a slipperiness during rinse with the PQ-87 shampoo as well as with the C-13S/silicone oil combination, and wet hair feels with these two

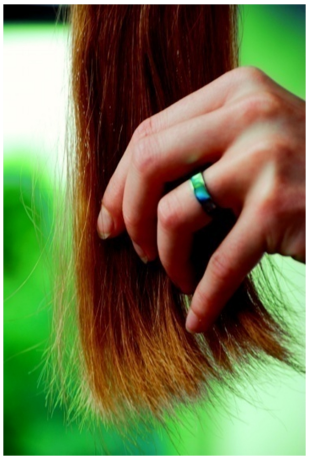

Figure 2.10: Tactile contact quality is realized by sensoric panel tests on human hair.

systems slick and well conditioned.
The hair is easy to comb with a very low friction. After shampoo application and drying, the panel noticed sensoric differences between the PQ-87 shampoo and the silicone oil combinations: while the PQ-87 provides the soft hair feel, the silicone oil gives smoothness to hair feel. These panel tests are further evaluated in Section 4.3.

2.3.5 Physical Properties of Hair at the Nanoscale and the Influence of Conditioners

Until 2000 most physical tests were done in the microscale range. A major focus of research in the last decades has been the analysis of the chemical composition of the fiber, its microscale structure, and hair growth. Most information about the detailed structure of human hair was obtained via different techniques like Scanning Electron Microscopy (SEM) and Transmission Electron Microscopy (TEM)[17,52,53]. Other publications on hair on the macroscale dealt with bending tests, torsional and tension measurements[54–56]. It should also be mentioned that in all cases the complete fiber was used as a sample.
Resent research has focused on the use of micro- and nanoscale experimental methods such as Atomic Force/Friction Force Microscopies (AFM/FFM) to answer the complex

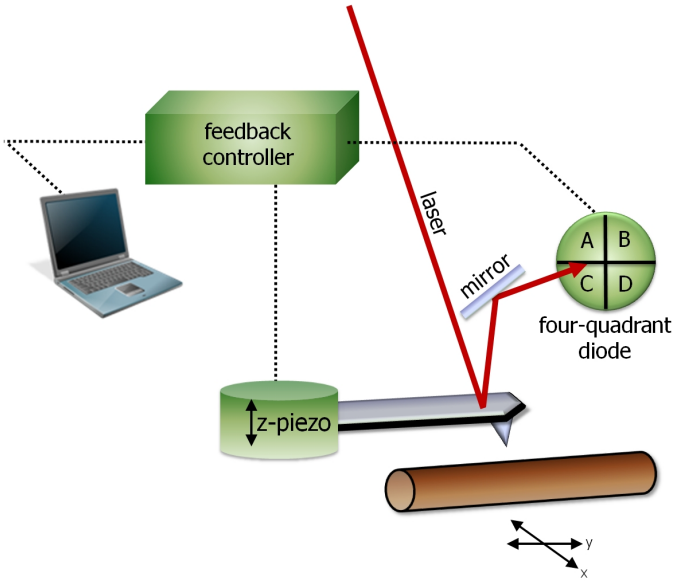

Figure 2.11: Schematic diagram of an Atomic Force Microscope (AFM) with a human hair as sample. A more detailed description of this method is in Section 2.4.

questions surrounding the structure and properties of the hair surface[11,13,57–59]. A lot of interesting research into the nanotribology of hair was carried out by Bhushan et al.[13,32,57,58,60].

O'Connor et al. used an AFM set up as shown in Figure 2.11, to provide quantitative real-time analysis of human hair morphologic changes under ambient conditions, in Section 2.4 the method is described in more detail[61]. *The Mechanics of Fracture of Human Hair* was published by Swift in 2001, who reported that bending and associated longitudinal shear processes played an important role in the strength of hair and not the tensile mechanical properties of the hair fiber itself as previous thought[62].

Lateral force measurements in combination with AFM can provide fundamental information about the physical and chemical properties of a surface. McMullen et al. therefore investigated the morphologic and surface changes associated with various surface modifications to human hair (these included extraction with a series of solvents, bleaching, and treatment with a cationic polymer[63]).

Friction Force Microscopy (FFM) that visualizes the frictional distribution of the sample surface by detecting the torsion of the cantilever is particularly useful for examining the frictional properties of heterogeneous surfaces[8,9]. It is useful to study the surface of human hair with this technique.

Wei and Bushan did systematic nanoscratching tests in single and multiple cuticles, finding the coefficient of friction of conditioner treated hair is lower than virgin hair for Caucasian and Asian hair in both cases of single cuticle scratches. This thin conditioner layer acts as a layer of lubricant and thereby reduces the coefficient of friction during scratching[11,13].

The investigation of scale effects (macro/micro/nano) and directionality dependence of hair on friction and adhesion of human hair using AFM and macroscale friction test apparatus was done by LaTorre and Bhushan. They used the schematic set up depicted in Figure 2.11 to image the hair surface and they measured the friction dependency of the direction of the cuticles. They modified a cantilever with a SiO_2 sphere and a diameter of 4 μm and compared than this data received from a micro-sphere with a normal cantilever, where the tip is just a few nanometer[64].

Saidae et al. employed a cantilever modified with a self-assembled monolayer (SAM) consisted of octadecanethiols as a *hair model probe* for FFM to measure friction acting between hair and hair like surfaces. They have detected anisotropic frictional properties on the cuticle surfaces which are ascribed to the striations observed on cuticle cells parallel to the long axis of the hair fiber[65]. Also effects on the 18-MEA surface layer investigated by AFM were done by Breakspears et al.[66].

The researches discussed above give an insight to physical and morphological behavior of human hair at the macro/micro and nano scale. Unfortunately, even with the investigation of Saidae et al. real single hair interactions could not be measured.

The main focus of this thesis was to find a way to study single hair interactions and how they are influenced by conditioners. For this we modified a AFM set up in a special way, which is presented in more detail in Section 4.2.

2.4 Status Methods

This Section gives an introduction to the theory of the instruments, which were used in this thesis.

To analyze interaction forces of hair in the micro Newton regime a so called Universal Surface Tester (UST) was used and is described in Section 2.4.1. This method is often applied in industry panel tests to study surfaces, like ceramics or plastics in their physical behavior.

According to the research with a Scanning Electron Microscope (SEM) the main principle of this method is also presented in Section 2.4.2.

A description of Atomic Force Microscopy (AFM) is illustrated in Section 2.4.3, a common application of the instrument is the so called imaging AFM, based on the optical lever technique (OLT)[67]. In this thesis the main method was force-distance methodology and friction force measurements, both of which are also related to the OLT and are discussed here.

2.4.1 Basics of Universal Surface Tester (UST)

The Universal Surface Tester is a well known DIN-standard instrument which is commonly used for testing industrial products, like plastics, coatings and fabrics, polymers, metals, ceramics etc.. In engineering science it gives information of micro-mechanical, micro-tribological and functional properties of different materials in the sub-micrometer range.

The testing method is based on mechanical scanning of a surface along a straight line in three steps. Figure 2.12 gives a schematic view of this so called MISTAN® process[68]. First, the surface profile is determined. Afterwards the total deformation is defined with an applied load and in the last step the recovery of the elastic portion is scanned. Within step **I** almost a load free scanner is moving on a defined path on a surface. Thereby the vertical displacement (height profile) is detected continuously. Afterwards at step **II** the

same path is scanned with the scanner and an additional load. The surface is deformed. The height profile generated by the software is the deformation over all. In the last step **III**, the scanner is moving on the path without any load again. The elastic part of the deformation is deferred and the height profile is calculated from the deformation. With this process it is also possible to measure the occurring micro-friction on hair surfaces. A more detailed description of the measuring conditions, which were used for this thesis is given in Section 4.1.1.

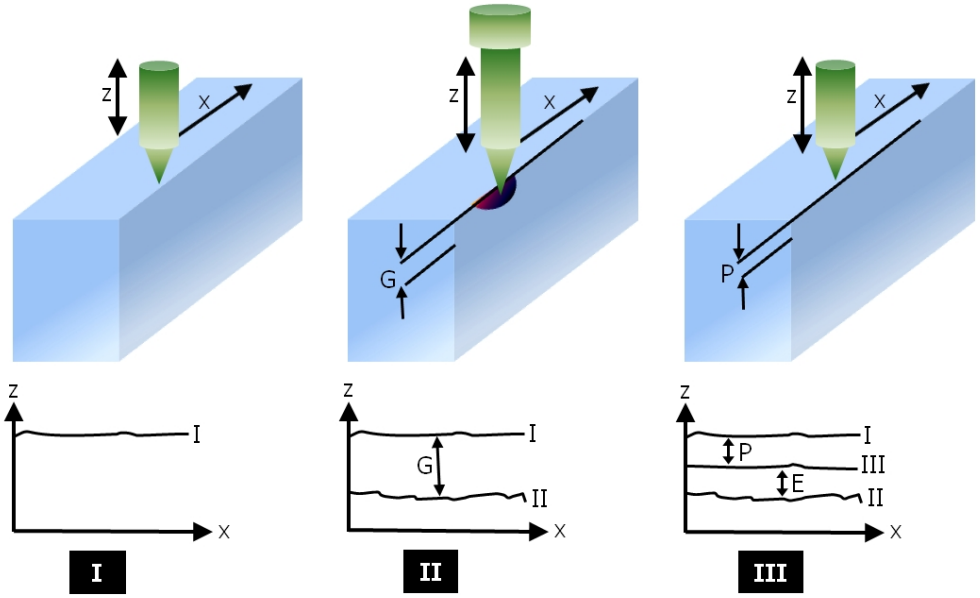

Figure 2.12: So called Mistan® Process, where a surface is scanned mechanically along a straight line in three steps. The basic principle is the following: there is a load free deformation over all in step **I**. Afterwards, in **II**, there is an elastic deformation with an additional load. Step **III** gives finally the permanent deformation.

2.4.2 Basics of Scanning Electron Microscopy (SEM)

With the Scanning Electron Microscope (SEM) it is possible to image a surface of a sample. The principle based on scanning the sample with a high-energy beam of electrons. The first SEM picture was reported by Knoll et al. in 1935[69].

In the opposite of magnification of a optical microscope (max. thousandfold magnification) it is possible to reach hundred thousandfold magnification. The resolution limit is within a few nano meters. The scanning electron microscopes have opened new areas for studies in different fields of science, like medicine, biology or physics.

Before the measurements can be carried out, a high vacuum with a pressure between 10^{-7} and 10^{-12} hPa is generated. Because of this all samples should be free of water, solvent, or other material that could vaporize. A regular SEM requires a conductive sample, non-metallic samples need to be coated (for example with gold) before they are placed into the SEM.

Figure 2.13 illustrates the most important components of an SEM. The electron beam, which typically has an energy ranging from 0.5 keV to 40 keV, is induced by a electron gun. Attractive forces for electrons are formed by the positive charged anode. In the cylindrical magnetic lens the electrons spiraling down perpendicular to the axis of the magnetic lens. The scan coils induce a magnetic field which deflects the beam back and forth in a controlled pattern.

By varying the voltage by a scan generator the scan coils are energized. This varying voltage is also applied to the Cathode-Ray Tube (CRT). This causes also a pattern of light deflected back and forth on the surface of the CRT. The pattern of deflection of the spot of light on the CRT is the same as the pattern of deflection of the electron beam. Finally the electron beam hits the sample, photons and electrons are emitted.

The signals that are present in the SEM are *Auger* electrons, X-rays, Cathodoluminescence, primary backscattered electrons (BSE) and secondary electrons (SE). The signals most commonly detected via SEM are the BSE and SE. BSE are elastic scattered ones. There is just a small (< 1 eV) or no change in energy of the electrons. Elastic scattering occurs between the negative electron and the positive nuclei of the sample. SE are specimen electrons that obtain energy by inelastic collisions with beam electrons. They are defined as electrons emitted from the specimen with low energy (< 50 eV). The *Everhart-Thornley* detector provides topographical information. Whereas the contrast

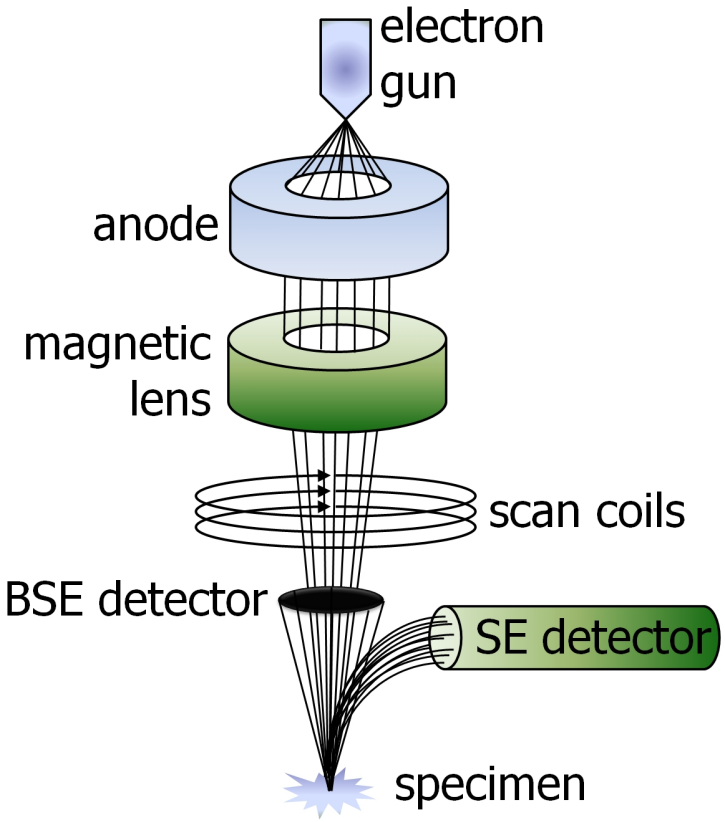

Figure 2.13: Basic principle of the SEM technique for imaging conductive surfaces in the regime of just a few nanometers. An electron beam is induced via an electron gun and hits after more cylindrical parts the specimen. The secondary electron (SE) detector and the backscattered electron (BSE) detector convert the radiation to an electrical signal. The whole apparatus is under high vacuum.

is generated by the different number of emitted electrons, which depend upon the atomic number.

The SE detector and also the BSE detector convert the radiation of interest into an electrical signal.

Hair morphology was measured using a P Cambride Stereoscan 200 SEM from Zeiss GmbH, Germany. Before doing SEM, the hair samples were coated with a thin layer of platinum (about 20nm thick) by sputtering using a sputter coater (Balzers Union SCD 040, Balzers-Pfeifer GmbH, Germany).

2.4.3 Basics of Atomic Force Microscopy (AFM)

In the end of the 1980s the Atomic Force Microscopy (AFM) was revolutionary, because it opened new ways to observe surfaces on the nano scale. Optical effects could be eliminated and the physical behavior of the surface itself was not altered completely, like with Transmission Electron Microscopy (TEM) or Scanning Electron Microscopy (SEM)[70,71]. The precursor of the AFM was the Scanning Tunneling Microscopy (STM), but with this instrument it is only possible to explore charged surfaces[72].

For the first time Binning et al. studied the displacement of springs to determine forces at surfaces with an AFM, using cantilevers as springs for their technique[73]. This silicon spring acts as a probe while it scans over the surface. The cantilever interacts with an internal feedback and the signal is recalculated as a height profile of the surface[74].

In 1995 O'Connor et al. reported the analysis of hair surfaces under different conditions (e.g. pH change)[61]. Smith used an AFM also for high-resolution non-invasive structural studies of human hair[75].

The technique has also been demonstrated to be applicable in liquid environments, opening the way to *in situ* studies of the effects of hair-care products and treatments. Bhushan et al. studied the environmental effects on nanomechanical properties and cellular structure of human hair. They followed the film thickness, adhesive forces and Young's modulus of hair surface at various environments (humidity and temperature) using the force calibration plot technique[60]. The next Sections give a detailed illustration of how an AFM works:

- Design of the Instrument
- Modification of Cantilevers
- Principle of Force Curves
- Principle of Friction Loops

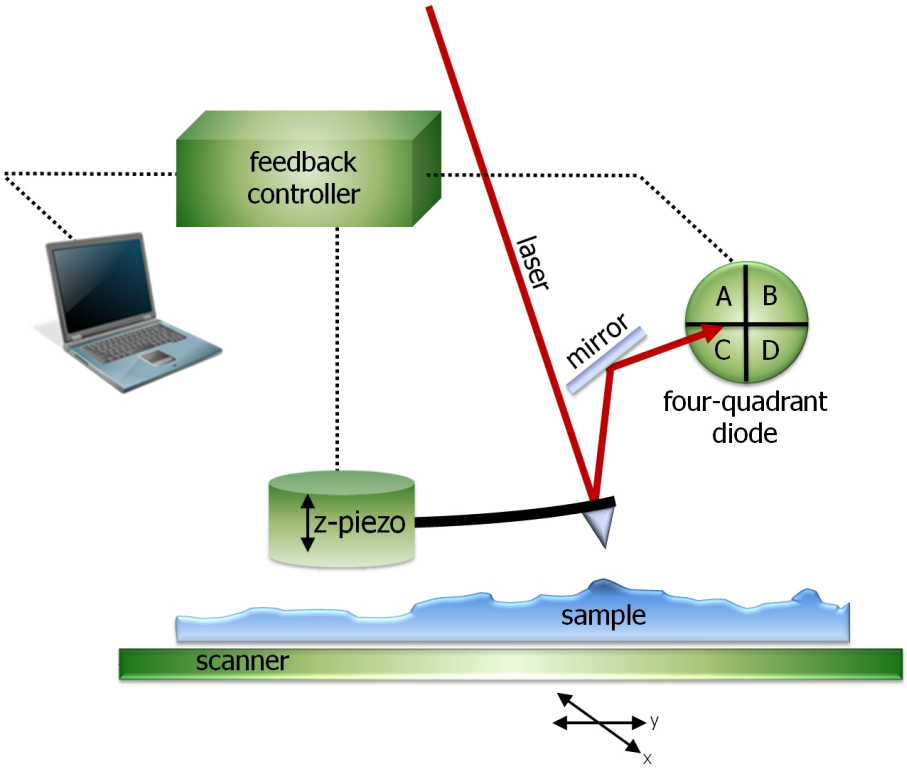

Figure 2.14: Optical Lever Technique (OLT) designed in an AFM set up. The laser of a solid state diode is reflected off the back of a cantilever. Vertical and lateral displacements can be detected by the four-quadrant photo diode. The controller is the linker between all of the important components.

Design of an AFM

There are different possibilities for the detection of cantilever deflection, one of the first of which was optical interferometry[76]. A simple alternative is the optical lever technique (see Figure 2.14)[67]. Under these conditions it is possible to detect simultaneously the two most important signals of such an instrument, the normal and the lateral deflection signals .

For imaging mode, the surface topography is measured by a lateral scan of the sample under the tip of the cantilever during either: the separation-dependent force, or the force-gradient between the tip and the surface. The interaction is either recorded directly on a four-quadrant photo diode, or used as control parameter for a feedback channel which

keeps the force or force derivative at a constant value. Due to the fact that imaging AFM was not used in this thesis it will be not discussed in detail (the avid reader is directed to: *Procedures in Scanning Probe Microscopies*[77]).
The other application is the detection of occurring forces. This is a potpourri consisting of different forces, like *Van der Waals* forces, capillary forces, chemical bonding, electrostatic forces, magnetic forces, *Casimir* forces, solvation forces and so on. Systematically here the cantilever moves as in imaging mode, but the main signal is collected from its vertical movement.
Figure 2.14 shows the schematic description of the optical lever principle which makes it possible to detect the deflection of the cantilever in nanometer range by guiding the laser beam to the four-quadrant photo diode. It consists of 4 different segments in one photo diode. If the cantilever is moving in an equilibrated state, the spot of the laser should be centered. Height profiles can be determined from the difference between the lower and upper segments of the detector. Lateral derivations between the left and right quadrants are proportional to the torsion of the cantilever and so to the occurring frictional forces between the tip and the sample after the cantilever is calibrated. The piezoelectric scanner moves the sample relative to the tip of the cantilever. The controller has the function to establish the z-piezo regulated cantilever and the scanning system.

Modification of Cantilevers

The geometry of cantilevers plays an important role during forces measurements via AFM. Problems are encountered when the measured force-distance profiles are compared with theoretical models due to the poorly defined geometry of the AFM tip, see Figure 2.15 (A)[79].
A solution to this problem was introduced in 1991 by Ducker et al.[80]. They replaced the tip by a colloidal particle with a well defined spherical shape. It was glued to the underside of the cantilever. The main contact area between this particle and another surface could be described in a more physical way. A SEM picture of a colloidal probe

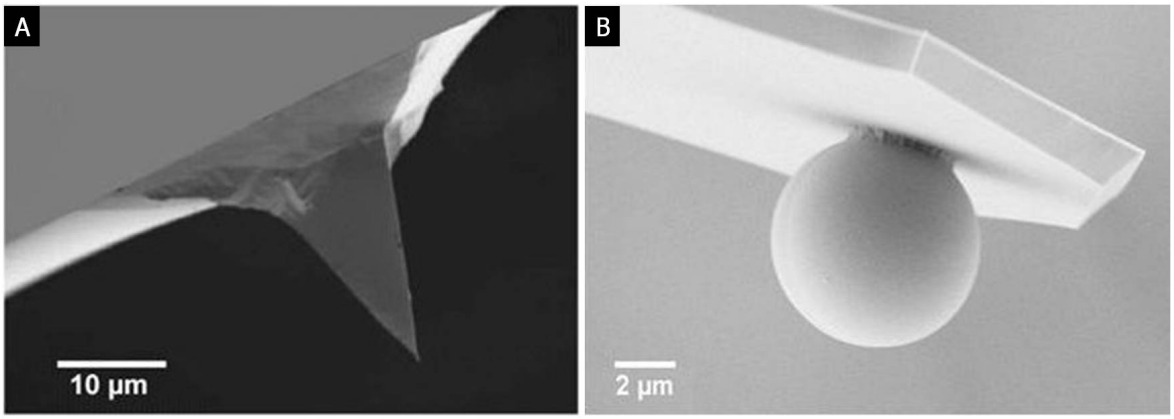

Figure 2.15: (A) SEM picture of a normal cantilever tip. It has not a exact defined geometry. (B) shows a particle, glued on a tipless cantilever with an optimal spherical geometry[78].

is depicted in Figure 2.15 (B). The well defined geometry allows calculations of the surface properties like the interfacial energy[79]. The *Langbein* approximation deals with the effective area of interaction when a sphere and a flat surface are close together:

$$A_{eff} = 2\pi RD, \text{ if } R \gg D \tag{2.8}$$

Hereby A_{eff} is the effective interaction area, D is the surface separation and R the radius of the surface. The colloidal particles attached to cantilevers usually have a radius of 1-50 μm which is three orders of magnitude higher than normal AFM tips. Therefore the resulting interaction forces increase.

Due to the limited range of the piezo movement and the dynamic range of the photo detector, shorter and therefore stiffer cantilevers have to be used to ensure the detachment of the particle after contact. The disadvantage is a loss of force resolution. In order to describe such interaction forces, the *Derjaguin* approximation is used, which relates the force law $F(D)$ between two spheres, where R_1 is one radius, $R_2 \to \infty$ and $R \gg D$:

$$F(D) \approx \int_D^\infty 2\pi(\frac{R_1R_2}{R_1+R_2})f(Z)dZ = 2\pi(\frac{R_1R_2}{R_1+R_2})W(D) \tag{2.9}$$

Here again D is the separation between the bodies and $W(D)$ is the interaction energy per unit area.
The attachment of the particle is realized by placing just a little amount ($10^{-18}\,\mathrm{m}^3$) of glue (usually epoxy resins) onto the end of the cantilever and bringing this spot in contact with the colloidal particle. The colloidal particles can be, in principle, made of any kind of material that can be glued to the cantilever.
In this work hair fragments (cylinders) are used instead of colloidal particles as probes for the cantilevers. The advanced *Derjaguin* approximation and the preparation of the new colloidal probe (*hair probe*) is described in more detail in Section 4.2.

Principle of Force Curves

A closer look at force-displacement curves gives first of all the voltage which is induced during equilibrium on the four-quadrant photo diode. If the cantilever is bent, different intensities occur between the two upper and two lower segments, therefore, according to Equation 2.10, ΔV is obtained from the induced voltage

$$\Delta V = (V_A + V_B) - (V_C + V_D) \tag{2.10}$$

ΔV is directly proportional to the deflection of the cantilever δ_c. The force between tip and sample is connected to the deflection by *Hooke's* law[81]:

$$F = -c_N \delta_c \tag{2.11}$$

Where c_N is the spring constant of the cantilever, the distance between the sample surface and the rest position of the cantilever is Z_p. The distance controlled during the measurement is not the actual distance D between sample surface and tip as it is shown in the graphic representation 2.16, these two forces differ due to the cantilever deflection

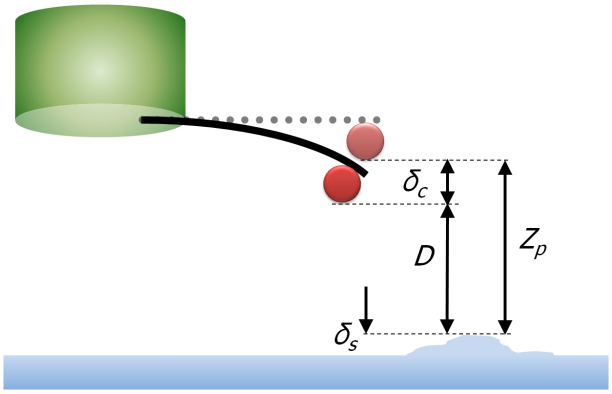

Figure 2.16: The tip-sample system, where Zp is the distance between the sample and the rest position of the cantilever, D is the actual tip-sample distance and δ_c being the deflection of the cantilever. These two distances are different based on the deflection of the cantilever δ_c and the sample deformation δ_s.

δ_c and the deformation of the sample δ_s. This leads to the relation:

$$D = -Z - (\delta_c + \delta_s) \tag{2.12}$$

When a measurement is performed, a plot of the detector signal ΔV, which is directly proportional to the force F, versus the corresponding piezo displacement in the z-direction Z_p is received. This is known as a force-displacement curve, the contributions to which are the force between the tip and the sample, and the elastic force of the cantilever (the latter is described by Equation 2.11). The tip-sample interaction can be approximated in the simplest case by an inter atomic *Lennard-Jones* potential, whose negative derivation yields the interaction force. The dependency of this force on the distance D between two particles is a combination of attractive *Van der Waals* interactions, which are proportional to $\frac{1}{D^7}$, and repulsive interactions due to the overlapping of the electron shells, which are proportional to $\frac{1}{D^{13}}$; yielding:

$$F(D) = -\frac{\alpha}{D^7} + \frac{\beta}{D^{13}} \tag{2.13}$$

α and β are material-dependent parameters.

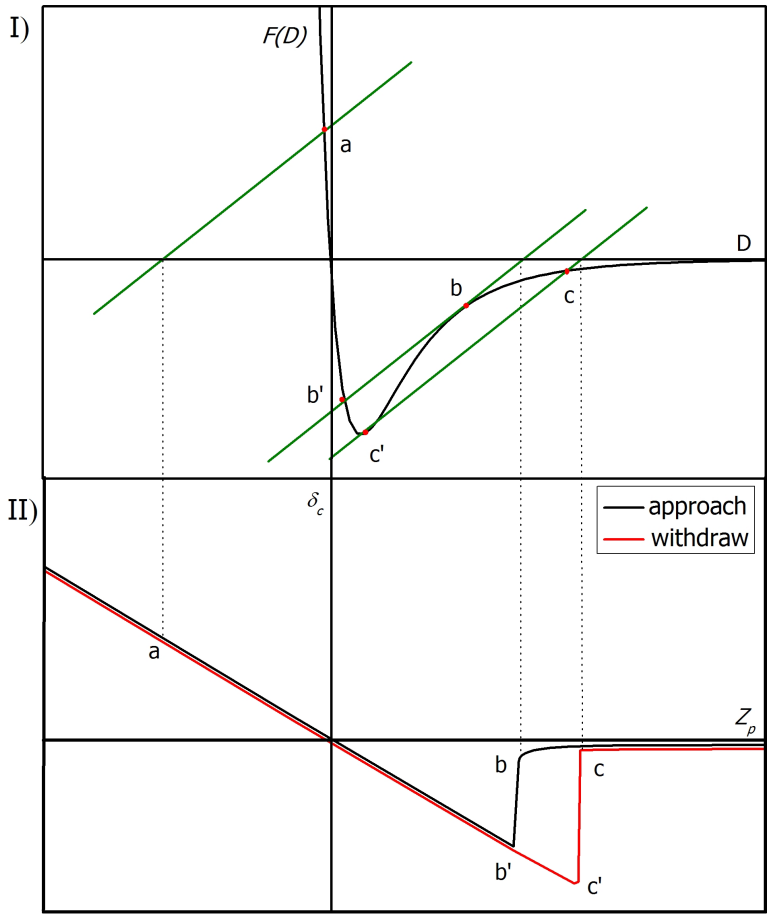

Figure 2.17: The inter atomic *Lennard-Jones* potential describes in the simplest case the interaction force $F(D)$ in I). The green lines visualize the elastic force of the cantilever at three different z-positions. II) depicts the graphical construction of a force-displacement curve from the plot of $F(D)$. The hysteresis between approach and withdrawal are due to two instable states which occur at two different piezo positions.

In Figure 2.17 the plot of $F(D)$ is depicted, the three green lines represent the elastic force of the cantilever at three different piezo positions, whereas the slope represents the spring constant c_N. At each distance the elastic force of the cantilever equals the tip-sample interaction force, thus the cantilever deflects until the system has reached an equilibrium. The deflection of the cantilever is defined by the intersection between the lines and the $F(D)$ curve. The rest position of the cantilever Z_p can be obtained

from the intersection between the lines and the horizontal axis, respectively. Figure 2.17 II) shows the resulting deflection versus Z_p for the approach of the tip and also for the withdrawal, which is a typical force-displacement curve (obtained by the construction of a graph from part I)). Initially, the tip is too far away from the sample so that no force is acting, and the deflection is consequently zero (this region is called baseline), upon approach of the tip to the sample, the system reaches a state of instability in b (this is the case, when the force gradient is higher than c_N).

$$F(D) = \frac{\delta F(D)}{\delta D} > c_N \tag{2.14}$$

Here the attractive interaction force between the tip and the sample is higher than the elastic force of the cantilever and the tip jumps from b to b' onto the surface of the sample (this is called *jump-to-contact*). Now by further approaching the cantilever changes nearly linearly, for the case that there is no sample deformation and taking into account that $D = 0$, Equation 2.12 leads to:

$$Z_p = -\delta_c \tag{2.15}$$

This region is called *constant compliance*. By retracting the tip again the cantilever detaches from the surface at a higher grade of force than at the approach, therefore a hysteresis is observed. The reason for this is the fact, that in this case the instable state does not occur at b' but at c'. Here again the force gradient is higher than c_N (first time for withdrawal). The elastic force is higher than the attractive adhesion force between tip and sample and the cantilever jumps away from the sample in a stable position at point c (this is called *jump-off-contact*). It is important to recognize, that the hysteresis is due to the combination of two forces acting on the tip and not to a real physical hysteresis, the interaction forces are constant during the measurement. Moreover c_N influences the shape of this hysteresis, for stiffer cantilevers it decreases, and if c_N is higher than the maximum value of the force gradient it disappears completely, and the

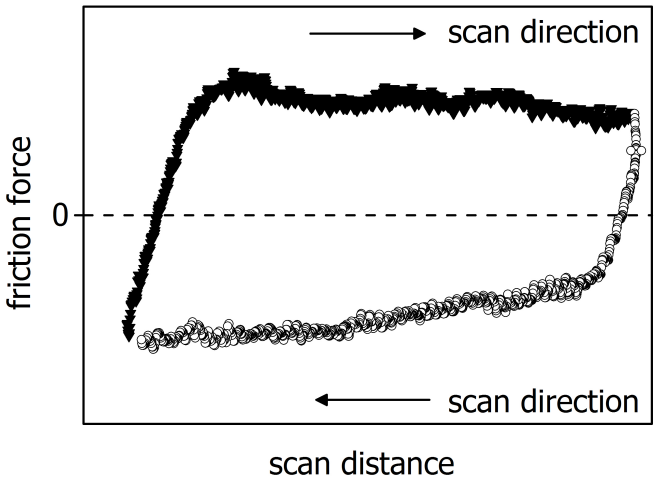

Figure 2.18: Lateral force (friction) vs. cantilever displacement. There is no torsion of the tip at the dashed line (friction force = 0).

entire curve is sampled. On the other hand, a higher value of c_N means reduced force resolution so a suitable compromise has always to be found.

Principle of Friction Loops

The relative sliding of tip and surface is usually also accompanied by friction. Shortly after Binnig et al. the first Friction Force Microscopy (FFM) was carried out by Mate et al. using a different method to detect lateral forces (optical beam deflection was published in 1990 first)[9,74,82].

As mentioned in the introduction to the Optical Lever Technique (OLT) in Section 2.4.3, friction forces between the tip and the sample are proportional to the lateral derivations of the laser between the left and right quadrants of the photo diode. This horizontal voltage signal V_L is related to the lateral force F_L according to the formula[83]:

$$F_L = \frac{3}{2} c_L \frac{h}{l} S_z V_L \tag{2.16}$$

Where S_z is the sensitivity of the photo detector. The sensitivity can be measured by a normal force versus distance curve on a hard substrate (for example on a glass slide), where the slope of the curve gives the required sensitivity. The lateral spring constant c_L is discussed in more detail in Chapter 4, as are h and l, as geometric values of the cantilever.

Figure 2.18 shows a friction loop plot. In this parallelogrammic loop the vertical signals are the stiction, whereas the plateau is reached and the stiction is fading in the sliding friction.

3 Materials

In the following chapter the polymers studied in this thesis are described in terms of their structure and physical behavior. There is also an introduction of a standardization process of laces (sewed bundle of hair), that were chemically treated to increase their homogeneity.

Table 3.1: Ingredients of a conditioning shampoo and their effects on hair[84].

benefit	content	approx. amount [%]
cleansing	main surfactants	8.0 ∼ 10.0
	co surfactants	3.0 ∼ 5.0
conditioning	cationic polymers	0.1 ∼ 1.0
	proteins, silicones	0 ∼ 4.0
appearance	thickening agents	0.1 ∼ 2.0
product statements	*active ingredients*	0.1 ∼ 3.0
sensoric acceptance	perfumes, dyes	q.s.
microbiological stability	preservatives	q.s.
	water	ad. 100

3.1 Polymers

Polymers have become important ingredients of cosmetics over the past few decades. A typical mixture of a purchasable conditioning shampoo is shown in Table 3.1, and as it is clearly evident, the concentration of cationic agents is not higher than 1.0%.
In this thesis most experiments were carried out with three different cationic polymers. All of them are used in industry as conditioning polymers in shampoo formulations. The

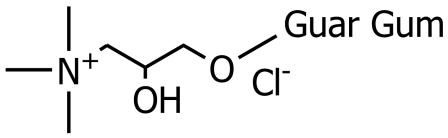

Figure 3.1: Molecular structure of Guar hydroxypropyltrimonium chloride (INCI), registered under the trade name Jaguar® C-13S. Guar gum is a branched polysaccharide consisting of mannose and galactose units.

chemical structure of Jaguar C-13S is drawn in Figure 3.1, the polymer is a cream-colored powder, that was delivered by C. H. Erbslöh, Germany. Figure 3.2 presents a UCARE^{TM} Polymer, so called JR-400, guar hydroxypropyltrimonium chloride in the International Nomenclature of Cosmetic Ingredients (INCI), delivered by Amerchol, Germany, in the form of a white to a off-white powder or granules. It has a cellulosic backbone and a regular, crystalline structure that is not readily water soluble. The addition of hydroxy ethyl groups to the cellulose backbone alters the crystalline structure and transforms the polymer into an easy-to-use, water-soluble chemical. PQ-10 is then produced by reacting trimethyl ammonium substituted epoxide with the hydroxyethylcellulose to form a polymeric, quaternary ammonium salt.

Luviquat® Sensation is a copolymer of vinyl pyrrolidone (VP) and vinyl imidazole (VI) and poly (diallyl dimethylammonium chloride) (DADMAC). It is purchasable as a clear

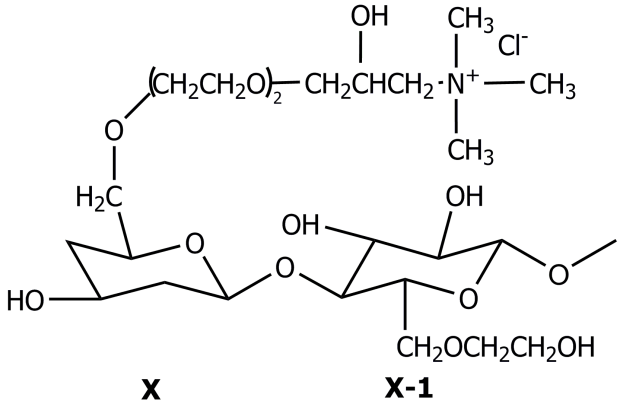

Figure 3.2: Polymer JR-400 is a N-trimethyl ammonium derivative of hydroxy ethyl cellulose (INCI) also called Polyquaternium-10. **X** is the ratio of the cationic monomers in mol% and has a value of 29.

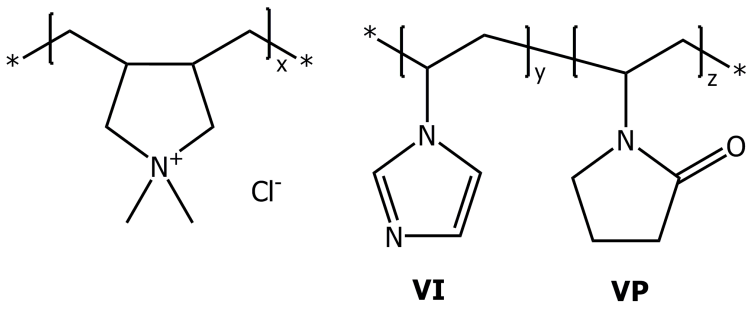

Figure 3.3: Luviquat® Sensation, Polyquaternium-87 (INCI) as a copolymer of vinyl pyrrolidone (VP) and vinyl imidazole (VI).

yellowish solution of 26% solids in water by BASF SE, Germany. The chemical structure is shown in Figure 3.3.

Table 3.2 shows the different charge densities and the molecular weights of these polymeric cations[84]. To mention in this context is also sodium laureth sulfate (SLES, TEXAPON NSO, FG:28-30%, with 2 M ethoxy, supplied by Cognis, Germany) which was utilized as a surfactant, the chemical structure of which is shown in Figure 3.4.

Table 3.2: Overview of polymers used in this work[84].

Comparison of molecular weight (M_w) and charge density (ρ) at pH = 7.0			
INCI	chemical compound	ρ [meq/g]	M_w [MDa]
Polyquaternium-10	Quaternized hydroxyethylcellulose	1.0	1.0
Guar hydroxypropyl triammonium chloride	Cationic guar gum	1.0	2.6
Polyquaternium-87	Poly(DADMAC)/ poly-(vinyl pyrrolidone-co-vinyl imidazole)	3.7	0.1

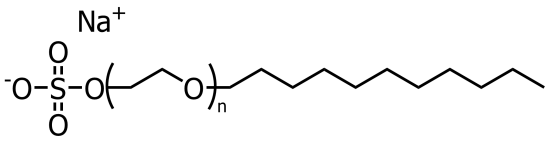

Figure 3.4: Molecular structure of sodium lauryl ether sulphate (SLES), a surfactant which is commonly used in hair care products.

3.2 Hair

To use hair from a standard source is more likely to yield reproducible results in science. There are worldwide standards for Asian, Indian, Afro-American or European hair, and different hairs have different needs. This is why the ingredients in conditioners varying. For example, there is more need of UV-protective ingredients in southern parts of the world.

In this study laces of European standard hair were used to focus on the European and North-American market of conditioner polymers. Figure 3.5 illustrates a 30 cm long bound hair lace supplied by Wernesgruen, Germany.

Figure 3.5: Purchasable European standard hair lace with approx. a length of 30 cm supplied by Wernesgruen, Germany.

Figure 3.6 shows three different locations on one hair. From left to right the cuticles from the root to the tip are illustrated. It is visible, that the cuticles are more damaged near

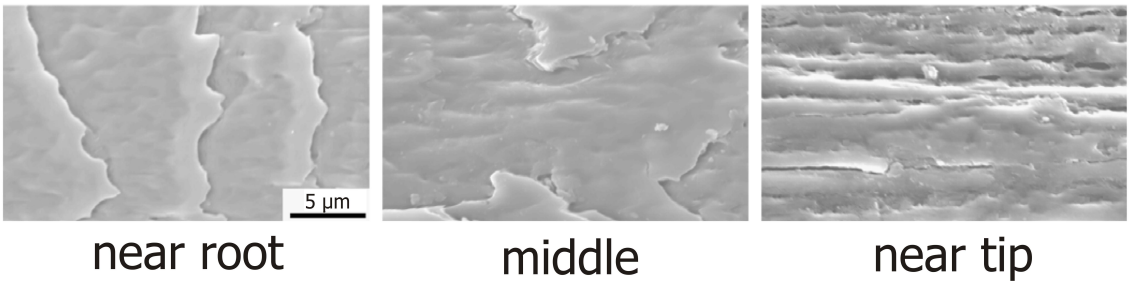

Figure 3.6: SEM pictures of European Caucasian standard hair on three different positions[13]. Near tip the cuticle structure is more damaged than near the root.

the tip. For all experiments just the middle part of the hair was used because in that region, both sides (namely the root and the tip) of each single hair are equally distanced and consequently this part is more representative for physical measurements[32].

To be sure of the consistency of different charges of laces, the laces were systematically treated before by BASF SE, Germany in the following way:

All supplied hairs were cleaned in a mixture of solvent, which consists of ethanol/isopropanol/acetone/water in the ratio of 1:1:1:1. Afterwards the hair was washed with sodium lauryl ether sulfate (SLES). The laces were completely dipped in a bleaching compound (see Table 3.3) to be sure that extensive wetting took place. Subsequently the hair were stripped off by gloved fingers to remove the redundant bleaching paste. The application time of the residual bleach depended on the quality of the hair.

Table 3.3: Ingredients of the bleaching paste all hairs were treated with.

bleaching compound	
component	amount [g]
ammonium carbonate	7.00
calcium carbonate	8.00
Aerosil 200	0.50
hydrogen peroxide (30%)	9.80
$\text{water}_{\text{dest.}}$	9.80

It was varied between 15 and 20 min, and conformed to the designated level of impairment. The bleached laces were subsequently flushed for 2 min under a water tap and washed with sodium lauryl ether sulfate (SLES) again. To avoid a creeping bleach the hair was brought into an aqueous, acidic solution (e.g. citric acid) and then rinsed again under water. After drying, the hair was stored in the dark.

4 Results and Discussion

This chapter contains a detailed description of the development of the different modifications of the experimental set ups. It is combined with existing measurement methods, which attempt to explain the different physical behavior of conditioning polymer treated hair in the micro- and in the nanoscale.

To detect friction forces in the micro regime, the Universal Surface Tester was modified in a way that allows a correlation to the so called Comb Force Method[50]. We could realize this in a calibration of a new-constructed scanning head and a self-constructed measuring cell. The reproducibility of the data collection is discussed. Correlation of the investigation of applied hair with different conditioner polymers leads to the conclusion, that a variety of different forces is acting.

To separate these forces from each other, the idea to identify single forces resulted in single hair measurements. One opportunity to realize such single hair measurements is given by an Atomic Force Microscope and based on the *Derjaguin* approximation. The set up for the instrument was modified which is presented and discussed in Section 4.2.1. After the first measurements between two single hairs were carried out, the reproducibility was checked and a statistical approach related to the adhesion force $F_{\text{adh.}}$ could be established. Focused on the occurring friction forces between two single hairs *in situ* experiments achieved effects which are also being discussed and presented in detail.

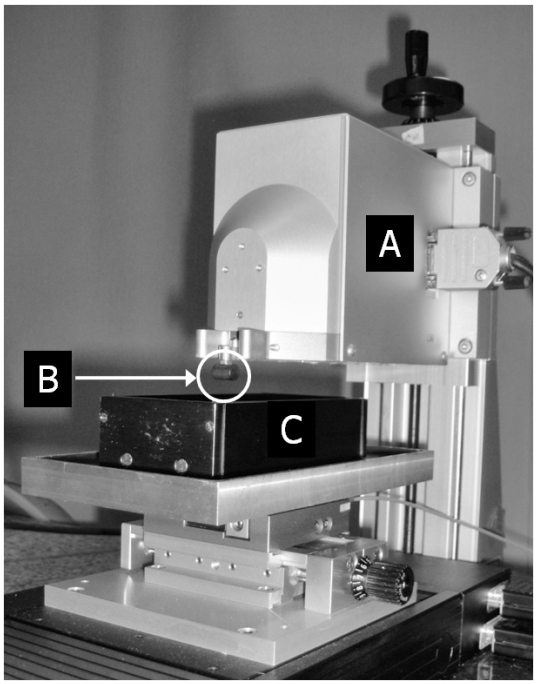

Figure 4.1: Picture of the Universal Surface Tester to measure friction of hair under optimized conditions. (A) is the stand in the z-direction. (B) is a modified scanning head (here: styrene-butadiene-rubber) to simulate a comb and (C) is the self-made measuring cell set up on a moving micro friction unit for the x- and y-direction.

4.1 UST Force Measurements

4.1.1 Development of UST Experiments

The Universal Surface Tester (UST) of Innowep, Germany allows quantitative friction measurements at the microscale. It should be mentioned that one ambition in this work was to correlate so called combing force measurements with more precisely defined physico-chemical parameters resulting from the experimental data obtained with the UST. All comb experiments were carried out by BASF SE, Germany, therefore the method is not discussed in further detail in this thesis.

The photography in Figure 4.1 shows the set up we developed tailored to the particular needs of the system. The instrument consists of a stand in z-direction (A). For

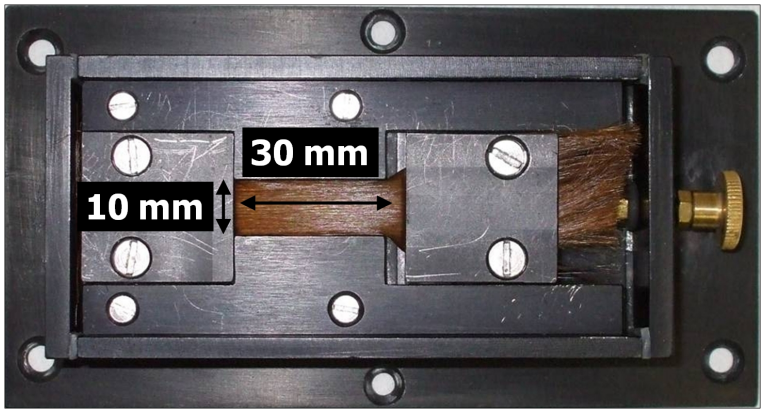

Figure 4.2: Top view of the self-constructed measuring cell. In the 30 mm long middle channel hairs are fixed.

detecting the friction the conventional scanning head (B) was replaced by a cylindric styrene-butadiene-rubber to simulate the interactions between hair and comb material. The measuring cell (C) was developed and optimized for the hair measurements as well. It is depicted in Figure 4.2 in a top view. This cell was finally adaptable for highly reproducible measurements. As is visible, the distance that was covered by the scanner is 30 mm. With this length and a breadth of 10 mm always the same amount of hair could be measured. As aforementioned in Section 3.2 the middle part of the hair laces were used[32].

The measuring cell was fixed to a table which was moved by an electrical motor in one dimension (x-dimension) and contained a piezo micro friction module. During this motion a certain load was applied by a tip that was attached to the upper part of the device (scanning head). The y- and z-direction could be varied manually before the measurement started. The load could be varied from 1.0 to 100.0 mN. After a certain measure distance was determined the table moved with a constant velocity and the friction forces were detected in intervals of at least 1 μm. Simultaneously, the tip scanned the profile of the sample, and up on completive of the experiment, a statistical evaluation was carried out with a software based on LabVIEW (visual programming language), which could give information about the mean friction force values.

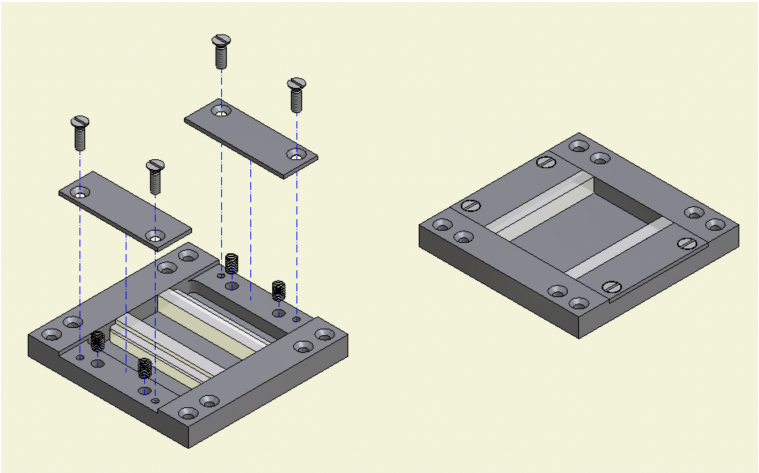

Figure 4.3: Construction of the first version of the measuring cell for fixing always the same amount of hair. After the hairs were brought into the cell the two poly-ethylene platelets were moved under strain to fix a hair strand from the inner to the outer part of the cell.

Development of Measuring Cell

For the investigation of measurements of hair strands with the UST, the following problems had to be solved with the measuring cell: a clamping tool had to be constructed for guaranteeing that the same amount of hair was mounted to the cell. In addition to that, it was important to avoid as much as possible the contact of the surface of hairs with other surfaces to retain the cuticles of mechanical damages, during fixation. Figure 4.3 depicts the construction of a measuring cell with two clamping fixtures consisting of poly-ethylene. With this cell the realization of the amount of hairs could be solved, but it was not possible to get a nearly homogeneous surface of the hairs. Therefore Figure 4.4 illustrates a measuring cell with swiveling ends. After the hairs were brought into the middle part of the cell, the strand was tried to fix with the two pivot bearing. The channel of hair had the same width of approx. 10 mm as the scanning head, and the reproducibility of scanning was optimized compared to the cell before. The pivot bearing process seemed not to work, the surface of the clamped hairs was still heterogeneous. This could be solved with the measuring cell illustrated in Figure 4.5. The strand of

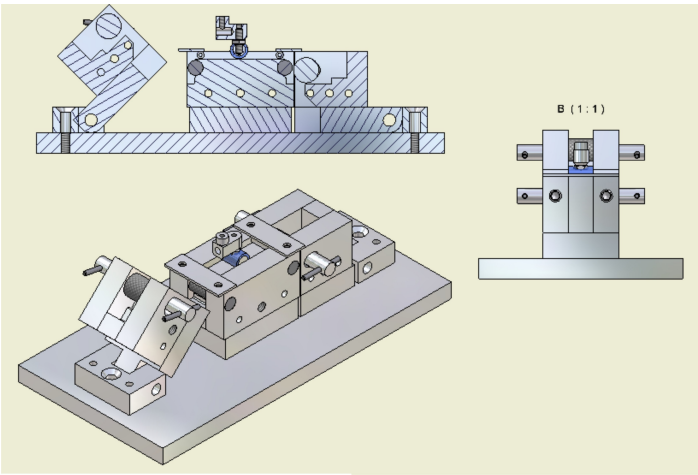

Figure 4.4: Construction for clamping a hair strand. Here the hairs could not be fixed homogeneously with the two pivot bearings because the hair glided off. Even by covering the pivot bearing with a rubber material no homogeneously surface of the strand could be reached.

hair was stretched by the big locking screw at the bottom end of the cell. Afterwards the cell was mounted to the friction table of the instrument. Another advantage of this cell compared to the other cells, was the possibility to carry out measurements under water.

Scanner

The scanner was manufactured based upon the particular needs of the system. With the intention of comparing the friction forces a cylindrically shaped scanner head was used, which fitted the channel of the measuring cell (width of approx. 10 mm). The contact between the hair strand and the measuring head was ideal. The head consists of a styrene-butadiene-rubber (SBR). This rubber is used for typical purchasable combs. A block of the raw material was delivered by New-York Hamburger Gummi-Waaren Compagnie AG, Germany. After the SBR block was molded to a cylindrical shape, experiments were carried out. It was possible to correlate the friction reduction results (received from UST) with the combing force reduction, as mentioned above.

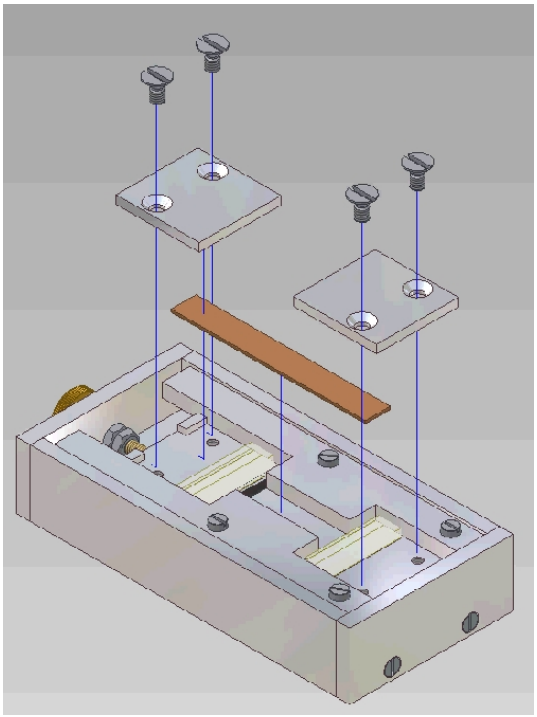

Figure 4.5: Construction of clamping procedure of a hair strand in the self-constructed measuring cell. After bringing the hair strand into the channel, it is possible to stretch it minimally by the locking screw to achieve a nearly homogeneously surface.

Humidity Control Chamber

During the UST measurements the humidity were kept constant to avoid effects on friction forces (thereby standardizing the procedure). Therefore, a chamber with a defined relative humidity (RH) of 60 $\pm$ 5% inside, was constructed. This value could be adjusted by an air flow which first passed through a saturated solution of sodium bromide salt (supplied by Merck, Germany) and heated up to 35°C. The exact humidity was controlled by a hygrometer and the temperature in the box was kept between 20 and 22°C. Figure 4.6 presents the set up. After passing the chamber the flow was divert.

Treatment of Hair Laces

The application of the shampoo formula to the hair laces was standardized. The procedure was used for the blank value formulation as well as for the conditioner products.

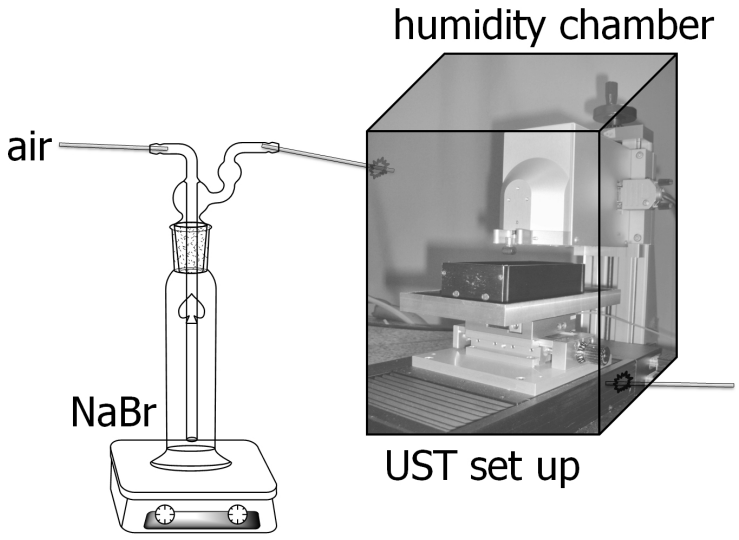

Figure 4.6: Complete set up of the UST, for keeping the humidity constant (approx. 60 ± 5% RH), a saturated NaBr solution is used. The flow of air passes the gas washing flask and enters the chamber.

First of all, 5 g of seven different shampoos were used. Table 4.1 depicts the main shampoo composition. Variations were only made in the concentrations of the active agents, i.e. the 3 different polymers (Jaguar C-13S, PQ-10 and PQ-87). Tego Betain L7 (INCI: co-coamidopropyl betaine, 29.5 wt%) was delivered from Goldschmidt, Germany and Euxyl K 100 (INCI: 5-chloro-2-methyl-2H-isothiazol-3-one/2-methyl-2H-isothiazol-3-one/benzyl alcohol) from Schülke & Mayr GmbH, Germany. The standard concentration of these compounds was 0.2 wt%. Furthermore in three formulations, 1.0 wt% silicone oil SM 2725 (supplied by GE Bayer, Silicones, Germany) was added. One shampoo had a concentration of 1.0 wt% PQ-87. Table 4.2 gives an overview of the basic formulae.

The hair sample was washed with water (T= 32 ± 2°C) under the water tap. Then the shampoo was applied and rinsed off afterwards. Every step took one minute. The hair sample was carefully dried with lab tissue and combed. Finally the lace was dried on lab tissue at room temperature over night and stored dry in the dark afterwards.

Table 4.1: Substance of content in wt% of a standard shampoo formulation.

component	[wt%]
water (dest.)	50.5
TEXAPON NSO	35.7
Tego Betain L	12.5
NaCl	1.0
Polymer	0.2
Euxyl K 100	0.1

Proceeding

Every sample was measured with the scanner under two different conditions (60 ± 5% RH and wet). Thus, in total, the samples were measured four times each. From the prepared hair laces a strand of hair, approx. with a length of 1 cm, was cut off and combed. Subsequently, the root end was placed on one side of the measuring cell. Afterwards the strand was combed again and put under strain in the channel to arrange the hair homogeneously. The tip end was then fixed with the second platelet and the rest of the strand was cut off. The measuring cell was fixed to the UST friction table

Table 4.2: The different concentrations $c_{Poly.}$ of polymer and silicone oil (SM 2725) used in the standard formula.

Mixture	PQ-10 [wt%]	C-13S [wt%]	PQ-87 [wt%]	SM 2725 [wt%]
1	0.2	-	-	-
2	0.2	-	-	1.0
3	-	0.2	-	-
4	-	0.2	-	1.0
5	-	-	0.2	-
6	-	-	0.2	1.0
7	-	-	1.0	-

Table 4.3: Parameters of the UST measurements.

settings of the software	
mode	value
measured section	10.00 [mm]
lead and trail	3.00 [mm]
load	50.00 [mN]
measured distance	1.90 [μm]
velocity	0.50 [$\frac{\text{mm}}{\text{s}}$]

and the SBR scanner was attached. The UST head was adjusted so that the scanner was in the correct measurement range when the load was applied.
The parameters used for the software are displayed in Table 4.3. A certain leader and trailer distance was chosen in order that only kinetic friction was taken into account. Subsequently, 20 single measurements were carried out in order to assure statistical significance. Afterwards the conditions were changed and the measurement cell was filled with 15 ml of water (dest.). The hair sample was completely under water. Finally the measurement cell was cleaned with ethanol, water and dried.

4.1.2 UST Statistics

To make sure that the UST device applies the correct load, the self-constructed scanners had to be calibrated, which was guided by the UST software. A balance was required. The scanner was fixed and the z-stand was varied manually until its software signal was determined to be acceptable by the software. The software increased the load gradually by approaching various scanner positions and the according weight was stated and calculated a calibration curve which was fitted by a polynomial of degree 6. Figure 4.7 shows the calibration for the SBR scanner.

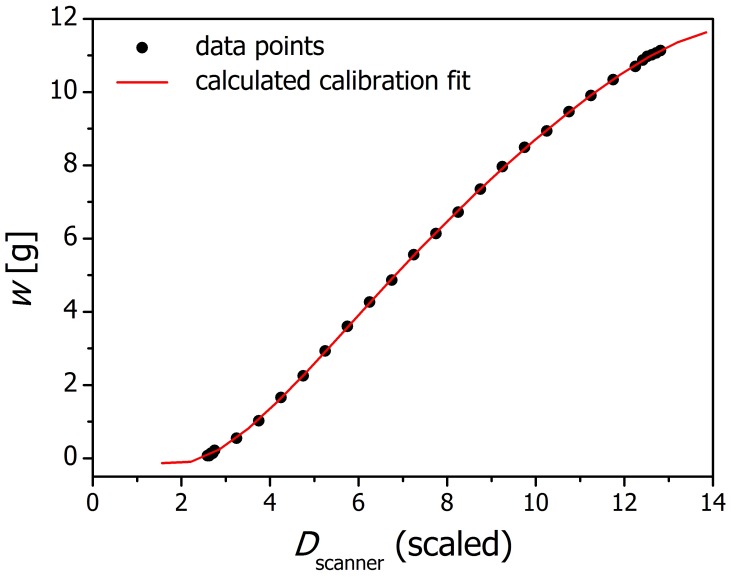

Figure 4.7: Calibration of the self-constructed SBR scanner of the UST as a model for a comb system between hair and material. The graph shows the weight w plotted against the scanner position D_{scanner}. This calibration curve was fitted by a polynomial of degree 6.

When a body is moved on a surface a force usually has to be applied to uphold this motion. The reason for this is sliding friction, which operates in the opposite direction. When the body moves with a constant velocity, the frictional force and the motional force are in equilibrium. The friction force is proportional to the load, which is perpendicular to the surface. This is described by the *Coulomb* friction:

$$F = \mu F_N \tag{4.1}$$

Dependency of Load and Velocity on Friction

Before the treated hair samples were measured, the dependency of friction on load and velocity was analyzed with an untreated hair sample.

All measurements were carried between 20 and 22°C. For analysis 20 single friction measurements were carried out and the mean average value was calculated. The UST

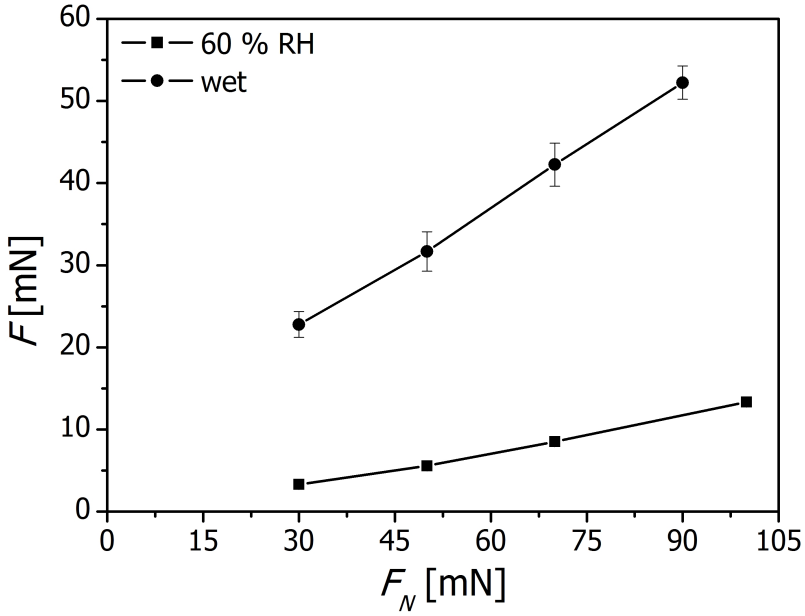

Figure 4.8: Friction F vs. load F_N at 60 ± 5% RH and under water. The load is proportional to the friction. Each measurement point results from the arithmetric mean of five different samples of one lace. The error in dry state is compared to the scale of the plot so small, that it is not visible in this graph.

parameters depicted in Table 4.3 were varied. According to Equation 4.1 the friction should be directly proportional to the load. This is in good agreement with Fig. 4.8, where the friction F versus the load F_N is plotted under wet and dry (60 ± 5% RH) conditions. The friction values under wet conditions are higher than under 60 ± 5% RH. The velocity behavior is depicted in Figure 4.9. The reproducibility of the measurements has an error in the range of the UST instrument itself. Five different samples and 20 measurements from the same lace were compared. The calculated deviation reached an error of 10%. In the following, all measurements were carried out with a velocity of 0.50 $\frac{\text{mm}}{\text{s}}$ under a load of 50.00 mN.

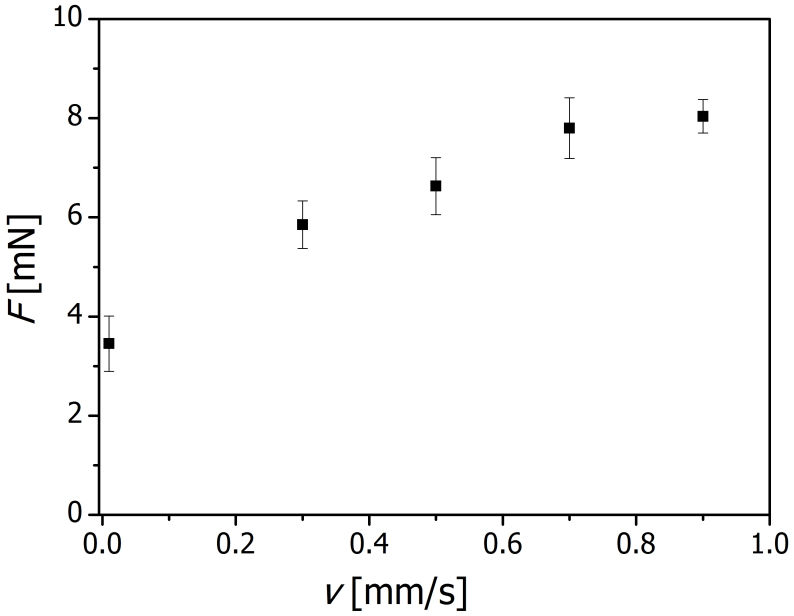

Figure 4.9: Friction F vs. velocity v at 60 ± 5% RH. The velocity is proportional to the friction.

Different Polymer Solutions

The wet combing force reduction F_R for the different conditioning polymers is shown in Fig. 4.10. The active levels of the cationic polymers are 0.2 wt%. The combination of 0.2 wt% cationic polymer and 1.0% silicone oil (SM 2725) was also tested. In addition to that Figure 4.10 illustrates the force reduction measured with the UST. The results indicate a higher combing force reduction when the amount of the cationic polymer was increased.

The addition of silicone oil has the strongest effect on combing when combined with Jaguar C-13S. However, Polyquaternium-87 shows the highest values for combing force reduction $F_R > 80\%$ at 1.0 wt% of the contents. This was not improved by the addition of silicone oil. The UST data showed pronounced friction decrease for samples with silicone oil. Furthermore the correlation aspect of both measurements is in the same error range with around 10%. Even with such an error it is clear that there is variation

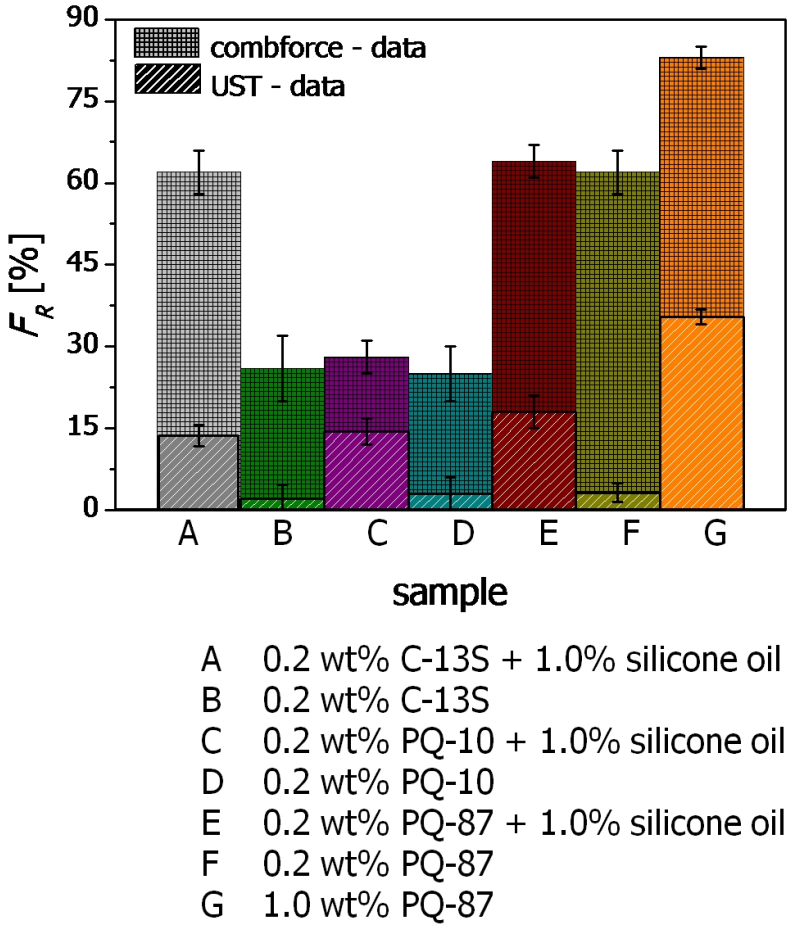

Figure 4.10: Correlation of wet comb force data and wet UST data. The graph shows the force reduction F_R in % versus the different samples.

in the hairs despite the fact that standardised hair is used.

Conclusion

It was also observed that the laces contained different numbers and orientations of hair relative to one another. In addition to the hair SBR interactions, hair-hair interactions occur. The main problem with these two methods is the *multi hair effect*[50].

Figure 4.11 depicts the various functions, along with the macro and micro/nanoscale mechanisms behind these interactions, that are responsible for the roughness of the sur-

face, friction, and adhesion between hair and skin, hair and hair and hair and material[85]. Friction between hair and skin should be reduced in wet and dry state to reach a smooth feel under both conditions, respectively. For a good feel in relation to bouncing and shaking of the hair during walking or running, friction between hair fibers and groups of hair fibers should be low.

The friction which can be felt during combing is a result of interactions between hair and the comb material, and this needs to be low to easily maintain, sculpt, and comb the hair.

To scale down entanglement, adhesive forces (the force required to separate the hair fibers) need to be low, as well. Sometimes, a certain level of adhesion may be acceptable and is often a function of the hair style. For individuals seeking hair alignment, where hair fibers lay flat and parallel to each other, a small amount of adhesive force between fibers may be desired. For more complex and curly styles, even higher adhesion between fibers may be optimal. To minimize this accumulation of forces we focused on the adhesive forces of single hair interactions in the next Section.

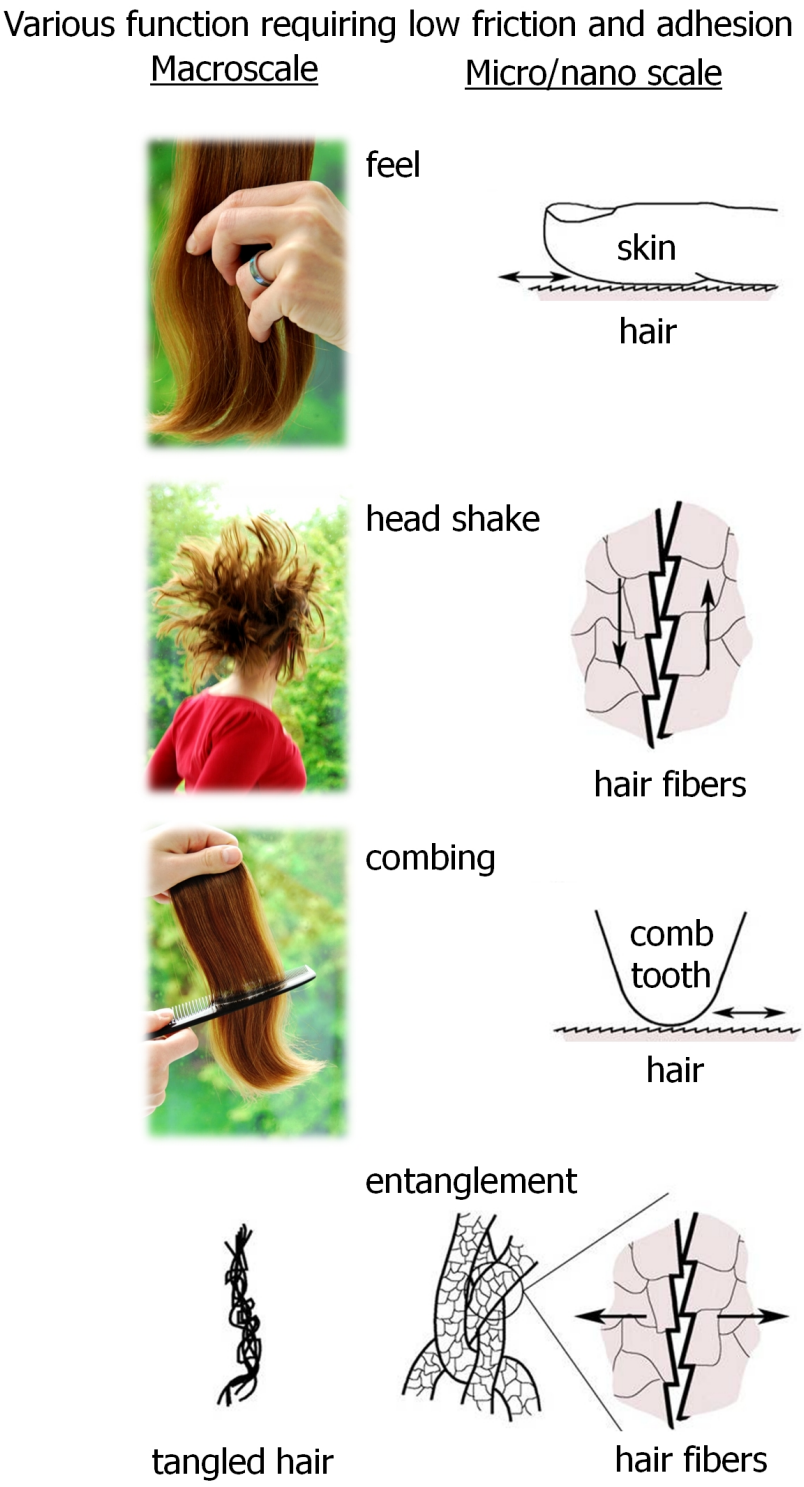

Figure 4.11: Schematics illustrating various functions with associated macroscale and micro/nanoscale mechanisms of hair and skin friction during feel or touch, shaking and bouncing of the hair, combing, and entanglement. Inspired by LaTorre et al.[85].

4.2 AFM Force Spectroscopy

4.2.1 Development of the AFM Experiment

Based on the previous findings, a further motivation of this thesis was to modify a cantilever for detecting interactions between single hairs with an AFM. Therefore a construction had to be investigated with respect to the following aspects:

1. Theoretical Base: *Derjaguin* Approximation
2. Modification of the Cantilever in Order to Meet Requirements of the Theory
3. Hair as Substrate in Order to Achieve the Theory

For normal cantilever calibration the thermal noise method was regarded[86]. In the following all three aspects and the calibration of the cantilever are illustrated.

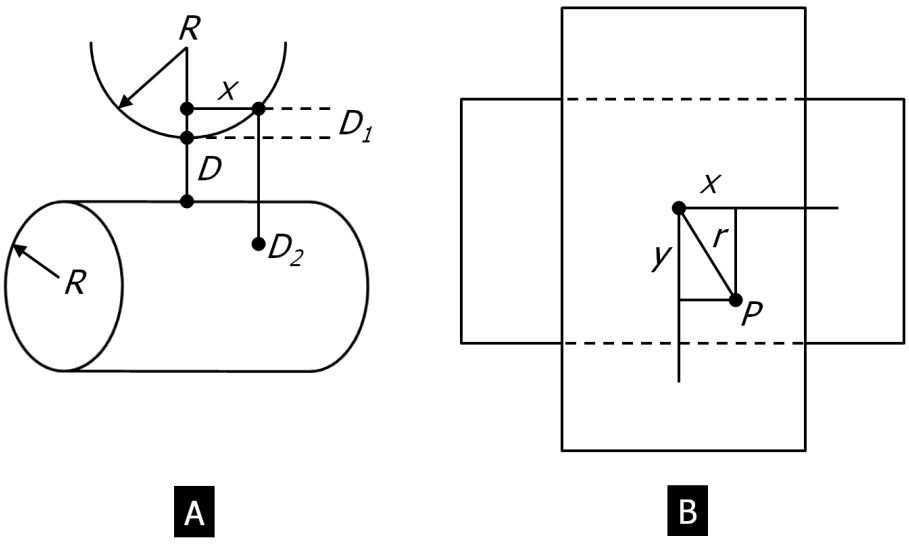

Figure 4.12: Geometry of two crossed cylinders. In (A) the *Chord* theorem in side view and in (B) the top view of the contact area is sketched.

Set Up and Geometry

During an experiment it is often easier to measure the forces between macroscopic bodies than the interaction energies between them. Therefore it is desirable to be able to relate

the force law $F(D)$ between two curved surfaces to the interaction free energy $W(D)$ between two planar surfaces.

In section 2.4.3, Equation 2.9 describes the *Derjaguin* approximation for two spheres. It relates the force law between two spheres, where R_1 is one radius and $R_2 \to \infty$. The approximation is displayed below:

$$F(D) \approx \int_D^\infty 2\pi(\frac{R_1 R_2}{R_1 + R_2}) f(Z) dZ = 2\pi(\frac{R_1 R_2}{R_1 + R_2}) W(D) \tag{4.2}$$

Here again D is the separation between the bodies and $W(D)$ is the interaction energy per unit area. It is applicable to any time of force law (attractive, repulsive or oscillatory) so long as the range of the interaction and the separation D is much less than the radii of the spheres ($D << R$).

If now two orthogonal cylinders with the same radius R, in this case the two hairs, are approximated by the distance D, Equation 4.2 is also valid[87]. Using purely geometrical arguments leads to the same contact region, to first order, as for a sphere of the same radius R at the same distance D from a sphere with $R_2 \to \infty$.

Referring to the geometric alignment of Figure 4.12 (A) a simple modification of the *Pythagorean* theorem is applied in the *Chord* theorem:

$$x^2 = 2RD_1 \;\&\; y^2 = 2RD_2 \tag{4.3}$$

With this and the geometry displayed in Figure 4.12 (B) it can be implied that:

$$2R(D_1 + D_2) = x^2 + y^2 = r^2 \tag{4.4}$$

If P is a circle than r is constant and thus $D_1 + D_2$. Because this Equation is indistinguishable from that for a sphere of the same radius near to a flat surface, it is proved that the two geometries are locally equivalent as far as interactions are concerned.

On the one hand this crossed cylinder geometry provides a good stability and on the

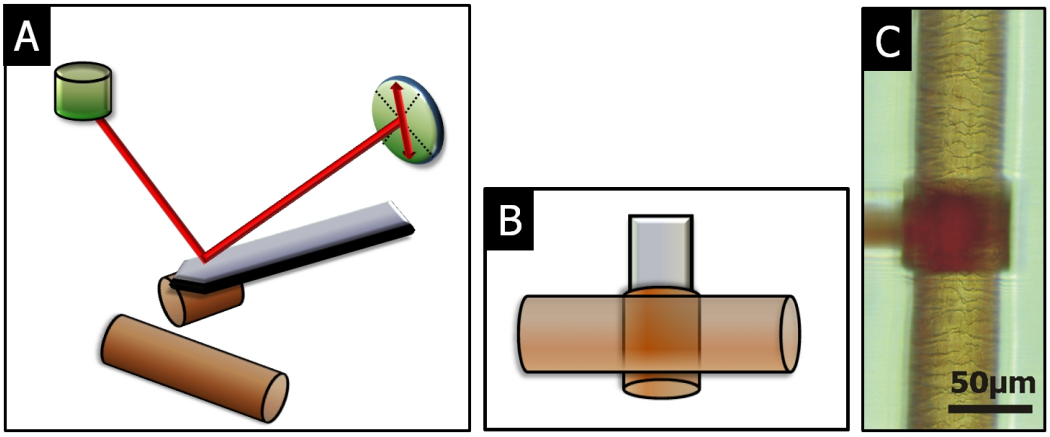

Figure 4.13: Optical image of the crossed cylinder *hair probe* set up. (A) is the schematic view of the complete AFM set up with the laser source reflected by a cantilever and detected by the segmented photo diode during the fixed defined *hair probe* on the cantilever interacts with the mounted substrate hair. (B) sketches the top view of the set up and (C) the optical image of the realized set up.

other hand there is a self-aligning of the contact region of the two single hairs.

Figure 4.13 schematically shows the upgraded realization of the *hair probe* set up of the discussed model in (A) and (B). The real geometry of two hairs is depicted in the optical image in (C). With this assumptions it is possible to relate the adhesion force $F_{\text{adh.}}$ to the energy per unit area $W(D)$ of two hairs. A detailed discussion and the exertion is presented in Paragraph **Adhesion Energy** in Section 4.2.2.

Hair Probe Cantilevers

Typically particles used in *colloidal probe* AFM are on the dimension of up to 50 microns diameter. A hair has to be cut into fragments whose length is smaller than the hair diameter in order to avoid problems due to inertia, hydrodynamic friction or weight of the attached object to the cantilever.

To investigate *hair probes* for AFM force measurements a cutting tool with special properties had to be found. Here several possibilities were considered:

- Mechanical Cutting by a Razor
- Technique of Microtomes
- Laser Cutting

Mechanical cutting by a razor results in the destruction of the hair as shown in Figure 4.14 (A). It is not suited for surface experiments on a small scale because the shape is not well defined enough for physical models.

Microtomes are often used for preparing samples in the micro- or even nanometer range. For this cutting process most of the samples have to be embedded. A typical material is resin. Robbins et al. studied a lot of cross sectioned hair via Scanning Electron Microscopy (SEM) and Transmission Electron Microscopy (TEM)[17]. The disadvantage of such techniques is the radical change of the surface of the sample and so the alteration of the physico-chemical properties, like force or friction. After cutting the embedding medium cannot be removed completely.

A third possibility was cutting hair by a micro laser (P.A.L.M. Microbeam System, 355 nm UV-light, gas laser, ZEISS, Germany). Laser cutting is mostly used for isolating single cells or cell areas via laser micro dissection[88]. Radiation in the UV-A range, between 320 nm and 400 nm lies well outside of the local absorption maxima of DNA and proteins, which are at 260 nm and 280 nm, respectively. With the highest width of cut of the laser (approx. 5-10 μm) using hair, the cutting procedure had to be optimized. The focus was manually readjusted during the procedure through the whole diameter of the hair sample. In the SEM picture 4.14 (B) the cut is nearly perfectly perpendicular to the fiber axis and the cuticle structure is not affected a few microns from the point of cutting.

As depicted in Figure 3.5, we used the middle part of a standard single bleached Caucasian hair from the laces in order to prepare a *hair probe*. Since contamination of the hair in this region is less than near the tip[32].

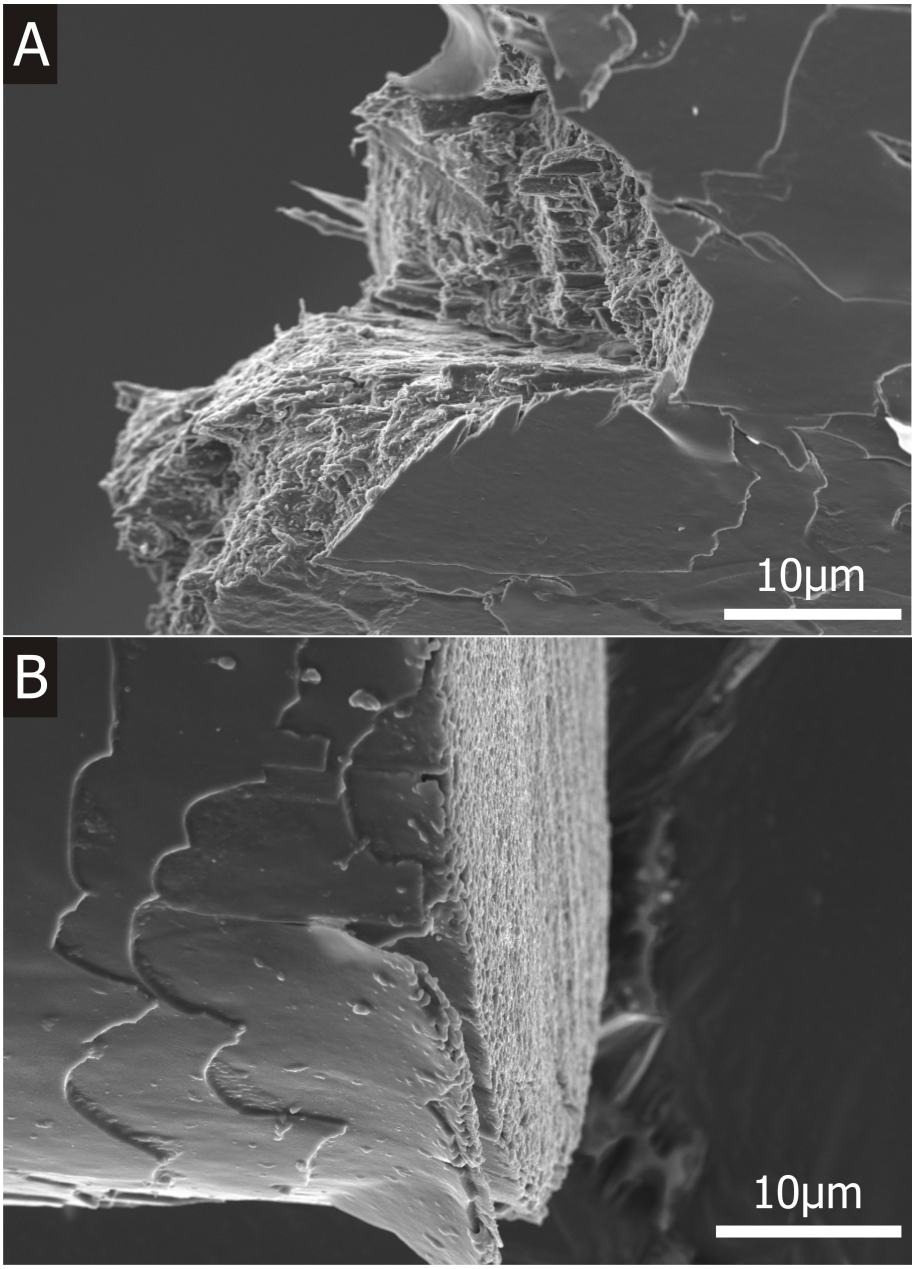

Figure 4.14: (A) SEM picture of a cut hair slice via a razor. (B) Precisely cut hair with a laser system after an optimization of the cutting procedure.

The fragments of hair with a amplitude of ∼50 μm and a diameter of 40-120 μm[19] were then glued to tipless cantilevers (NSC12/tipless/No AI, Micromash, USA). Figure 4.15 (A) illustrates a SEM picture of a glued hair fragment to such a cantilever and Figure

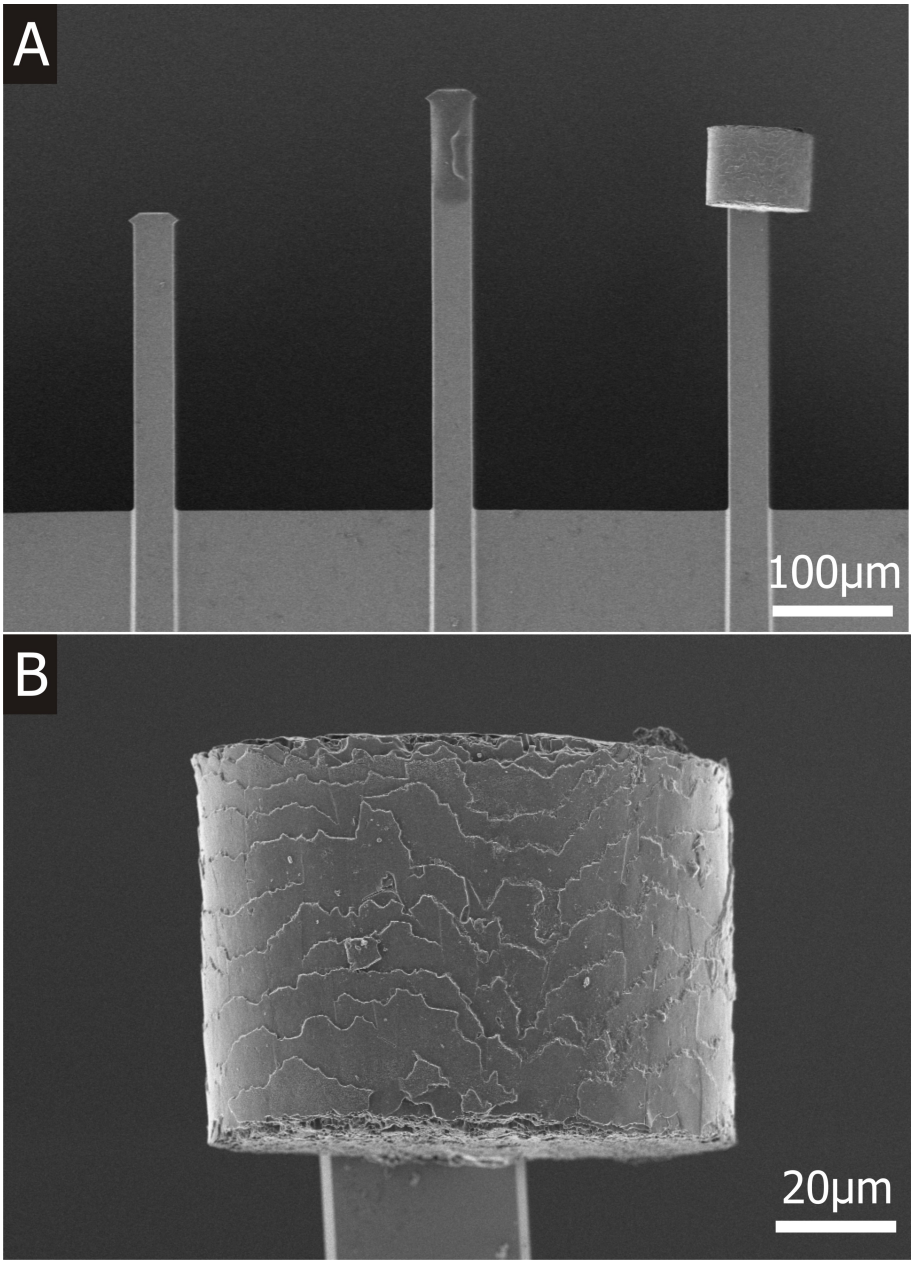

Figure 4.15: SEM picture of a hair fragment (∼50 μm) glued with 2-component adhesive on a tipless cantilever in (A). (B) presents a magnification of (A).

4.15 (B) represents the zoom into (A). We used a 2-component adhesive on an epoxy resin by UHU plus 300, UHU GmbH & Co, Germany. The complete process was controlled by a motorized micromanipulator, MP-285 from Sutter Instrument, USA. When using a *hair*

probe approach for hair studies, a major challenge is the sheer size of hairs which have diameters around 100 microns (Caucasian hair). The complete cutting procedure were carried out as a cooperation with the Max Planck Institute of Colloids and Interfaces in Golm, Germany, using their micro laser.

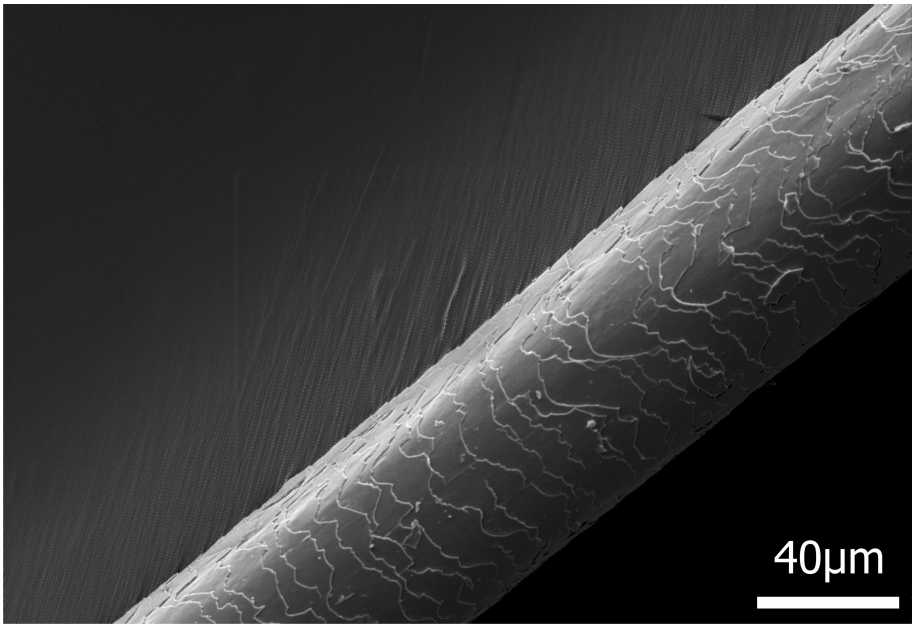

Figure 4.16: Hair as substrate glued on a ∼48 μm thick industrial double tape. Contamination of the polyester film of the tape on the upper side of the surface of hair is avoided.

Hair as a Substrate

For measuring real single hair interaction via AFM it is necessary to use a second hair as a substrate. An adaption to the optical set up of the MFP 3D AFM required a transparent material to fix this substrate hair. La Torre et al. mounted the specimens to the sample pucks using Liquid Paper® correction fluid[89]. For the adjustment of the cantilever hair to the substrate hair, we could not use Liquid Paper® correction fluid . The problem could be solved with an industrial double tape tesafixR® 4972 delivered by tesa AG, Germany. First, the tape was glued on glass slides (Microscope Slides, 76x26 mm, Menzel-GlaserR, Germany) and then the hair with a length of ∼10.00 mm

was attached to the tape. It was cut with normal scissors. With a tape thickness of $\sim$48 μm and a high shearing resistance the hair was steady enough to the surface and a contamination on the upper side could be avoided, due to its larger diameter. Figure 4.16 demonstrates that no depositioning of gluing material on the top of the hair surface took place.

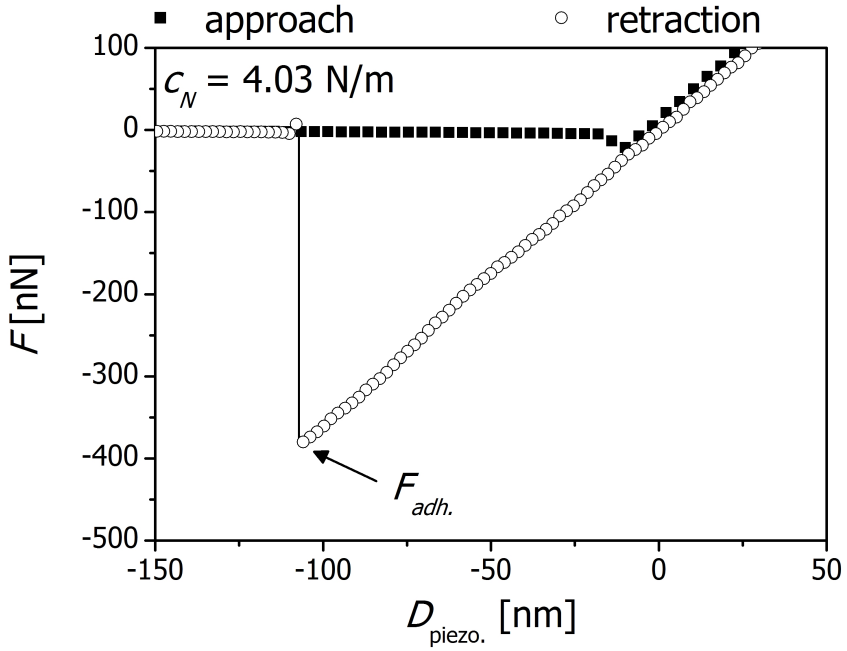

Figure 4.17: Characteristic force-distance curve of two untreated hairs brought into contact under air with 30 ± 5% RH. A cantilever with a spring constant of c_N= 4.03 N/m was used. The filled squares are the approach and the open circles are the retraction. The retraction is reaching a minimum in $F_{adh.}$.

4.2.2 Results on Adhesion Forces

Reproducibility

The measurements were carried out under two environmental conditions, firstly in air with around 30 ± 5% RH (dry state) and secondly under water (wet state). Both were done in a commercial (liquid) cell (Closed Fluid Cell, Asylum Research, Santa Barbara, USA). All data were collected with the MFP 3D AFM (Atomic Force, Germany).

Dry State

In the dry state, measured in air around 30 ± 5% RH, one calibrated *hair probe* and five different substrate hairs were used. This guaranteed that the data could be compared. To obtain usable data of force-distance measurements, the first experiments were carried out with a spring constant of c_N= 4.03 N/m of the cantilever. Figure 4.17 presents a

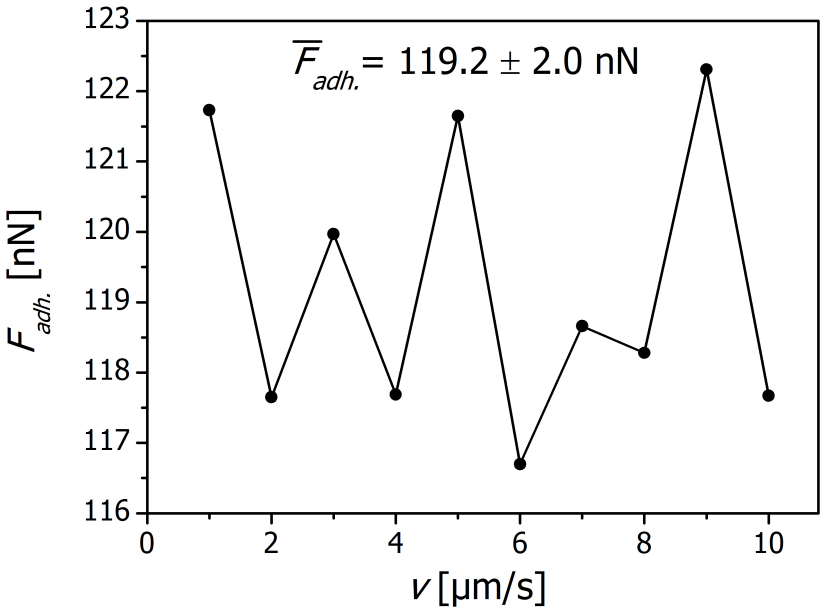

Figure 4.18: Graph of adhesion force $F_{\mathrm{adh.}}$ versus velocity v of an untreated hair.

typical force-distance curve between two single hairs. The approach are the filled squares and the retraction are the open circles. From left to right the filled squares demonstrate first the regime without a contact between the two hairs (baseline) until the slope is increasing (region of contact). From right to left the open circles are presenting that the two hairs are in contact with each other till the minimum is reached. This minimum is the adhesion force $F_{adh.}$. It is followed by the *jump-off-contact*, where the two hairs are not in contact any more. The graph shows an approx. ideal force-distance curve as it is described in Literature, where a normal cantilever tip or a *colloidal probe* is brought into contact to a hard substrate, for example to glass[90,91].

Influence of Velocity

To check if the velocity of approaching and retracting the hairs to each other has an influence on the shape of the force-distance curves, the dependency of adhesion forces from the approaching velocity was investigated. In Figure 4.18 the adhesion force is

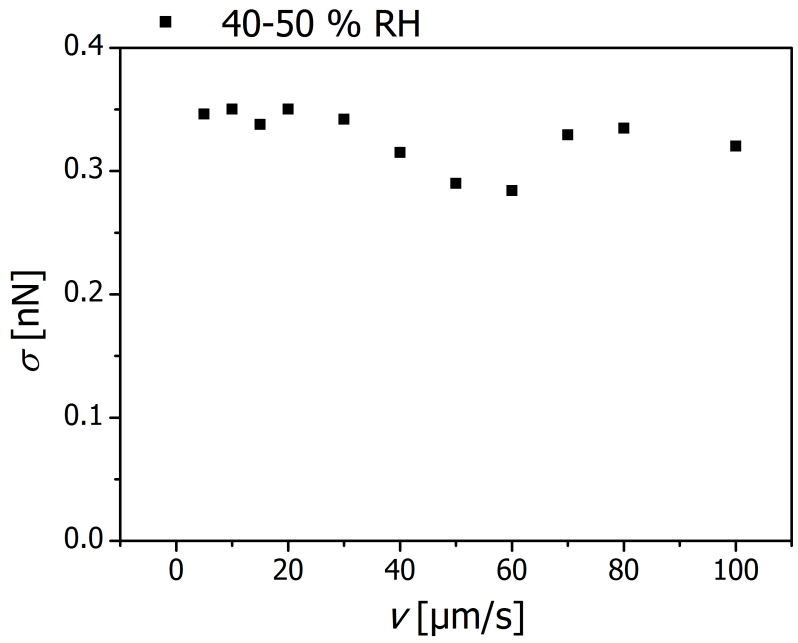

Figure 4.19: Deviation σ of baselines (approach and retraction) plotted against the velocity v of the piezo element by an environmental condition of a relative humidity of 40-50% RH. Within a negligible value the deviation is nearly constant and hydrodynamic aspects are insignificant.

plotted versus the velocity. The graph shows a range of the velocity from 1 to 10 μm/s within different steps between $\Delta v = 1.0$ μm/s. With an average value of $\overline{F}_{adh.} = 118.5$ $\pm$ 2.0 nN the influence of velocity is marginal. With the finding, that the two hairs are behaving like a normal tip which is in contact with a hard substrate, we could compare the results to Literature if the velocity is $v < 10.0$ μm/s. Hereby Lui et al. used a Si (100) as surface and a normal cantilever tip. They could show, that the occurring adhesion force $F_{\text{adh.}}$ is nearly constant if the velocity is under $v = 10.0$ μm/s. If the velocity is higher, an increase of $F_{\text{adh.}}$ was detectable[92].

To be sure that hydrodynamic aspects could be insignificant, the baselines (none contact region) of approach and retraction were reviewed under a relative humidity of 40-50% RH. A cantilever with a normal spring constant of c_N= 3.36 N/m was used. Figure 4.19 depicts the mean value of the deviation σ of the baslines versus the velocity v of the

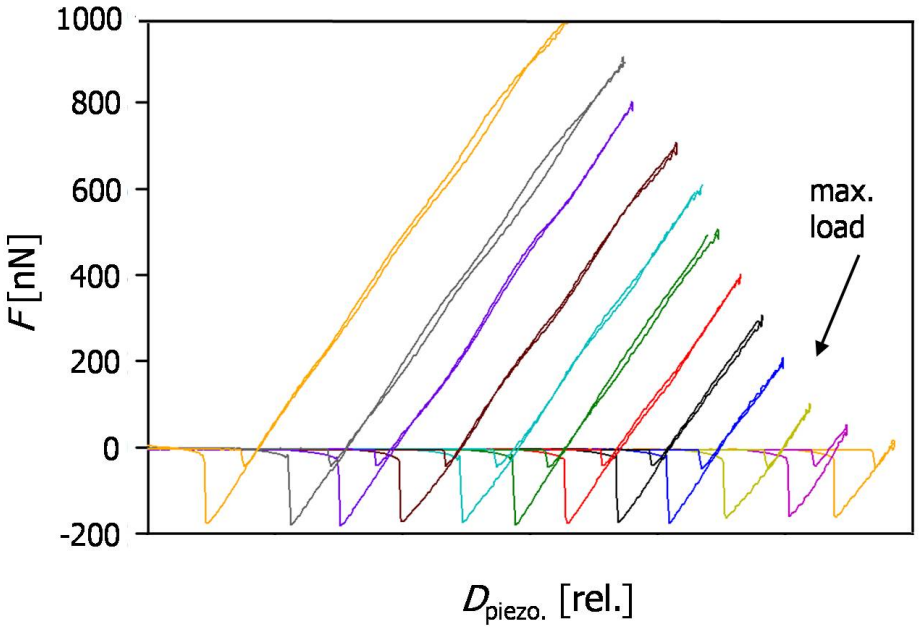

Figure 4.20: Force-distance curve (approach and retraction) of an untreated hair with different loads in a range of 10 - 1000 nN. Note, the x-axis is without any unit.

piezo element. The differences keep constant with negligible values. With that we can say that the hydrodynamic aspects play no important role in the dry state. Because of this findings all following experiments were carried out with velocity of 5.00 μm/s.

Influence of Load

To investigate the influence of an applied load on the cantilever to the adhesion force, in Figure 4.20 the maximum load force was stepwise changed from 10 nN to 1000 nN with a variation of $\Delta L = 100$ nN, except for the first and second step ($\Delta L = 50$ nN). The x-axis is without any unit because the different curves of load were set next to each other in this plot.

Testing its impact on the adhesion force resulted in no changes by varying the compression force. This leads to the conclusion that the adhesion force $F_{adh.}$ here is not influenced by the applied load and so we can say, that the single hair system is inelastic. Would it

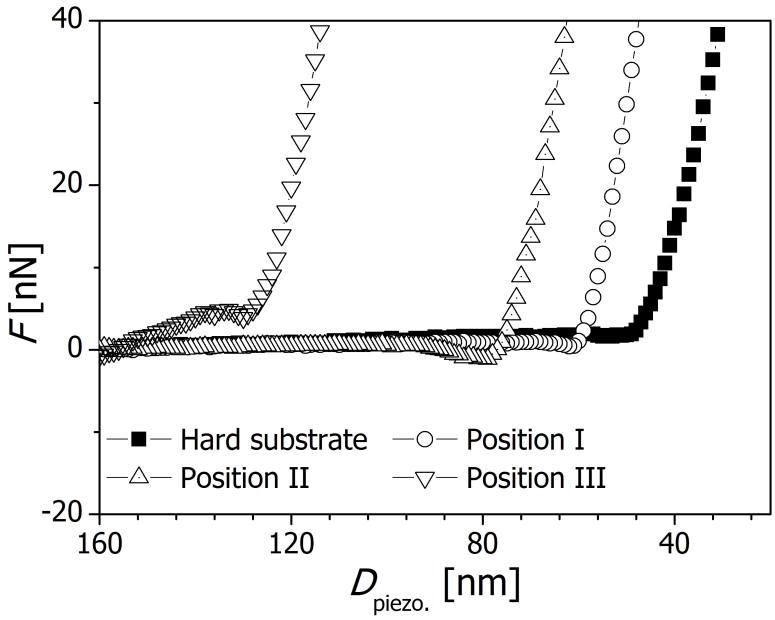

Figure 4.21: Force-distance curve (retraction) of two untreated hairs at three different positions on the substrate hair. Measurements were carried out under water.

be elastic, the contact area of the two crossed hairs would change non-proportional to the load, therefore the adhesion force $F_{adh.}$ would also differ.

Wet State

In order to clarify the nature of the attractive interactions, measurements were performed under water in the closed fluid cell. Figure 4.21 shows a typical force-distance curves under water for the single hair set up. Three different positions are plotted. Extension and retraction match within $\leq 2\%$ in the occurring force F, therefore only the retraction is highlighted. The adhesion is within values around 1.0 nN $\pm$ 0.5 nN an insignificant feature. This indicates that capillary forces dominate in the interaction between the hair fragments. This is in agreement with Literature, where adhesion forces are dissapearing under liquids[93].

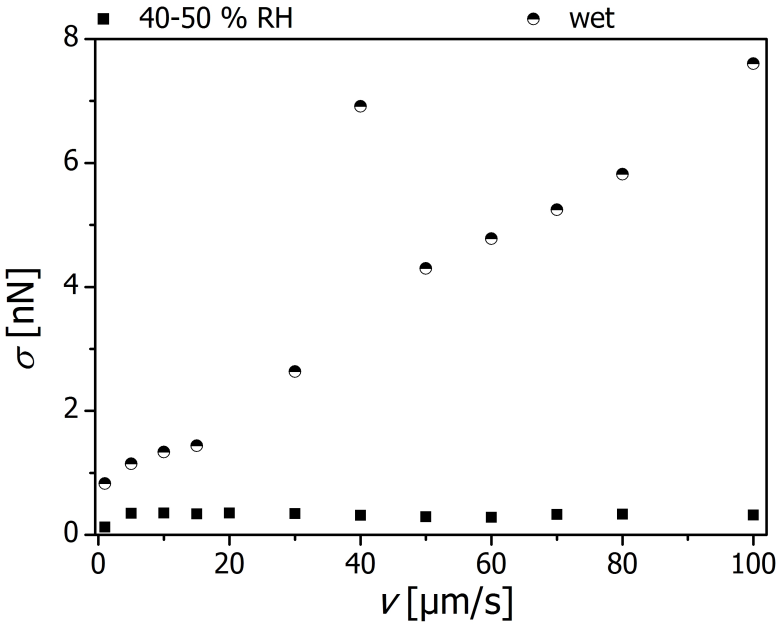

Figure 4.22: Deviation σ of baselines (approach and retraction) plotted against the velocity v of the piezo element. within a relatively humidity of 40-50% RH the deviation σ is constant with negligible values. In the opposite the deviation σ is increasing with the velocity v in wet state. This indicates a behavior of *Stokes* friction.

Influence of Velocity

To focus on the hydrodynamic behavior of the the single hair system also the non contact regime was checked carefully. The mean value of the deviation σ of the baselines versus the velocity v of the piezo element is depicted in Figure 4.22. To compare the data measured under dry conditions, they are also depicted in Figure 4.22. Under both environmental conditions, dry (40-50% RH) and wet (under water) a cantilever with a normal spring constant of c_N= 3.36 N/m was used. In wet state the standard deviation σ is increasing linear with the velocity v of the piezo. The system is behaving as the *Stokes* friction. Because of this strong influence of the hydrodynamics to our system, we focussed on the adhesion force in dry state[94].

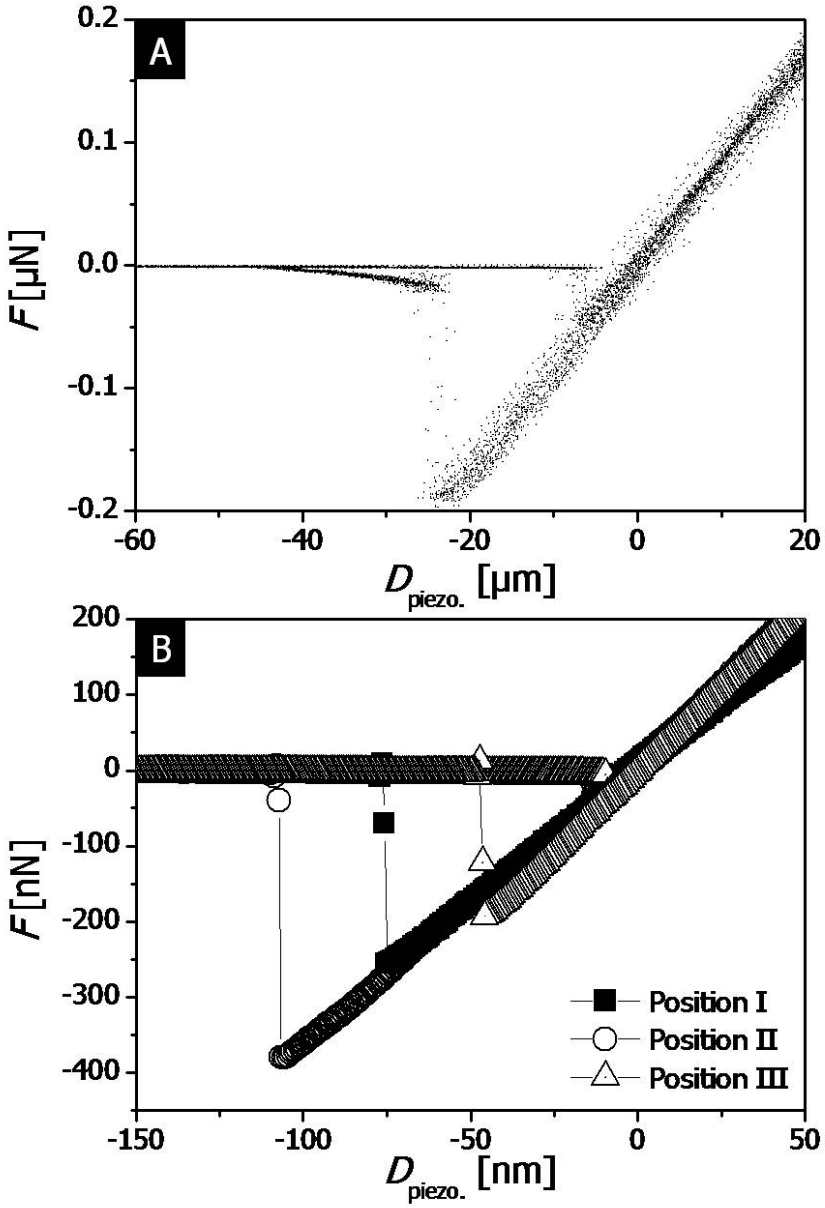

Figure 4.23: (A) 100 Force-distance curves of a single hair experiment to show the reproducibility on one spot of a hair in the dry state with a spring constant of 4.03 N/m. (B) Force-distance curve (approach and retraction) of an untreated hair on three different positions on the substrate hair, measured at room temperature and under a relatively humidity of 30 ± 5% RH.

Consistency of Adhesion Force

To extract adhesion forces from AFM data, it is sufficient to evaluate the withdrawal force-displacement curves since the *pull-off* force and therefore the adhesion force is the ΔF between absolute minimum and baseline.

Figure 4.23 (A) shows representative force-distance curves of a single hair measurement experiment in air with a relative humidity of 30 ± 5% RH. 100 curves are plotted to emphasize the reproducibility at one single position. The variation of adhesion force of one position was around 2.3 ± 0.4 nN and is good reproducible.

Also the variation for different positions on one substrate hair as well as between different hairs were investigated. Even if a high uniformity for individual measurements on one position is observed, however, there is a large scatter between the adhesion forces of different positions. That is clearly visible in Figure 4.23 (B). The adhesion force $F_{adh.}$ is three times different, and to this fact, statistic experiments were carried out for investigating the abrasion of the hair surface.

10000 force-distance measurements of a *hair probe* to a substrate hair were repeated to check the influence of mechanical abrasion of the surface. This is shown in the SEM pictures in Figure 4.24, where the damage of the cuticles is visible yet minor. With 10000 iterations the system was exposed wide over the maximum of measurements we investigated for the statistical approach.

Statistical Investigation of Adhesion Forces

To investigate the broad scatter of adhesion force $F_{adh.}$ of different positions over the samples, the adhesion forces of three different hair probes on fifteen different hairs were measured. Ten different positions on each and 150 different spots in total were carried out. First the mean adhesion force for different positions (dp) was calculated:

$$\langle F_{adh.} \rangle^{dp} = \frac{\sum F_{adh.}}{N} \tag{4.5}$$

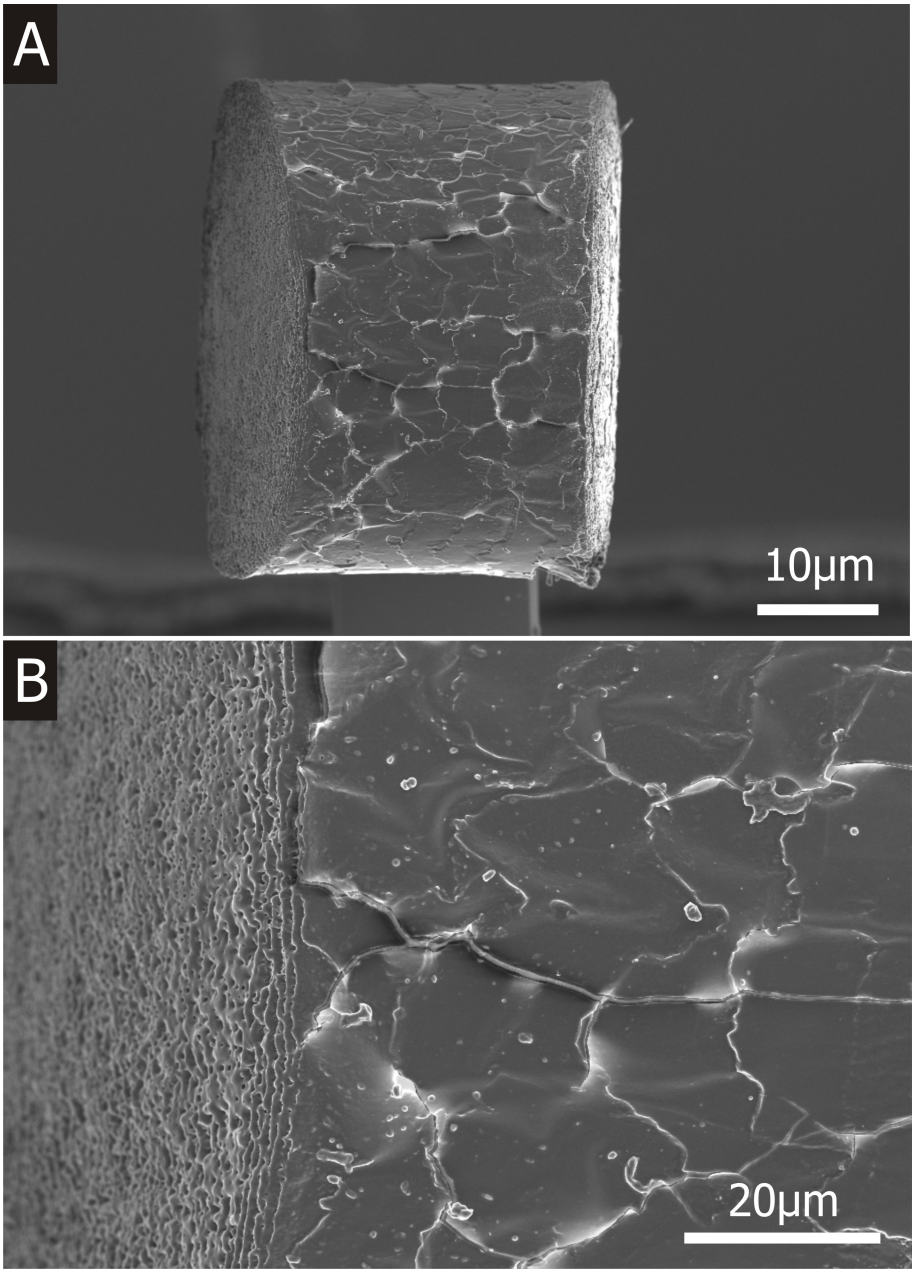

Figure 4.24: SEM images of the mechanical effect of abrasion on a cantilever hair after 10000 force distance curves.

The resultant standard deviation was determined with the following Equation:

$$\sigma^{dp}_{F_{adh.}} = \sqrt{\frac{\sum(F_{adh.} - \langle F_{adh.} \rangle)^2}{N-1}} \tag{4.6}$$

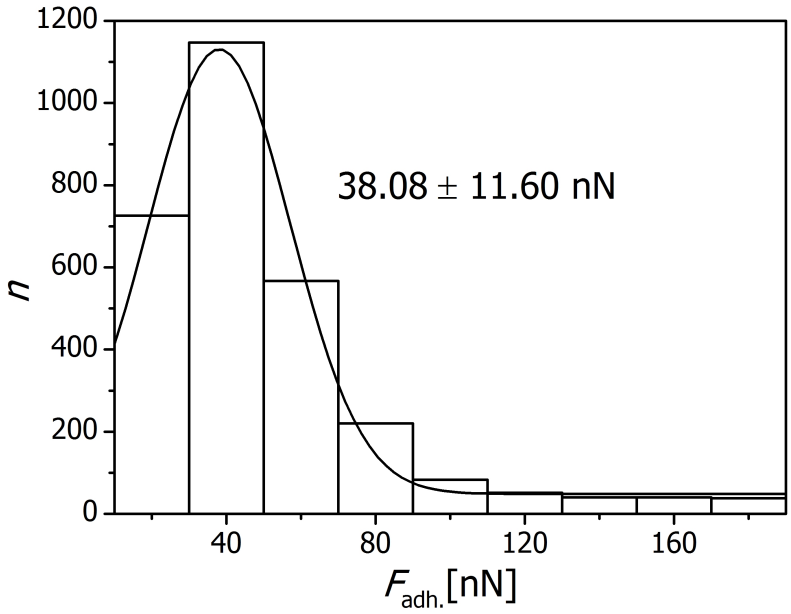

Figure 4.25: Gaussian fit of the adhesion force $F_{adh.}$ of three different *hair probes* on 150 different positions of 15 different untreated hairs. The adhesion force over all measurements was calculated to be $\langle F_{adh.} \rangle^{dp} = 38.08 \pm 11.60$ nN.

Under the same conceptional approach, all measurements were calculated for the same positions (sp), too.

To analyze this huge amount of data, a fitting procedure in **C** (general-purpose computer programming language) was developed. Wherein adhesion forces and additional data (e.g. baseline consistency) could be collected. The procedure is listed in Chapter 8, *Appendix*.

In the following the results of our statistical investigation are shown as $\langle F_{adh.} \rangle^{dp/sp} \pm \sigma^{dp/sp}_{F_{adh.}}$. The adhesion force and the standard deviation of an untreated hair on different positions is 43.5 ± 6.9 nN. On a single position it is 2.3 ± 0.4 nN as mentioned before. In all cases, adhesive interactions between the hair fragments in air were observed, but the surface appears to be highly heterogeneous. The human hair is quite rough which complicates analysis in the nano regime. The cuticle scales of a few microns along the

hair and a few hundred nanometers in thickness results a relatively large uncertainty of the size of the contact area between the *hair probe* and the sample hair at different positions[95].

For the whole statistical data, a Gaussian fit could be adducted. In Figure 4.25 the number of events n is plotted versus the adhesion force $F_{\mathrm{adh.}}$.

The full width at half maximum is consequently the adhesion force over all measurements and has a value of $\langle F_{adh.} \rangle^{dp} = 38.08 \pm 11.60$ nN (three different *hair probes* on 150 different positions of 15 substrate hairs). This is in the same range as the comparison of ten different positions on just one substrate hair. It is difficult to compare these results with Literature, since so far, no measurements between individual hairs have been carried out in this force range. The experiments that are the closest were carried out by Bhushan et al., but they used a normal tip of a cantilever for doing adhesion force statistics on hair surface[60]. The result at a humidity of around 40-50% RH led to a value of 44 nN and is in a good agreement with the statistics carried out here between single hairs.

Adhesion Energy

Based on the theory we introduced in Section 4.2 we will have a closer look now to existing models related to continuum physics to get a value for the adhesion energy per unit area.

If the sample is plastically deformed, the sample is exposed a deformation during the loading curve. When the tip is withdrawn, the sample does not get back its own shape as the load decreases, whereas the penetration depth remains the same. The most behavior of samples is mixed. Normally the force of the unloading curve is less than the force of the loading curve if the penetration depth is given.

From the assumption we made in Section 4.2.1 it is possible to calculate the energy per unit area between two hairs.

In the following we neglect plastic deformations and review theories related to elastic

continuum contact mechanics. Here the tip and sample are assumed to be continuous elastic media. The adhesive force $F_{\text{adh.}}$ is related to the energy W by the following two models:

- JKR Model (Johnson, Kendall and Roberts[96])
- DMT Model (Derjaguin, Muller and Toporov[97])

The JKR model applies normally to soft *probes* with large curvature radius (macroscopic bodies) and small stiffness. Such systems are called strongly adhesive. The model accounts for the influence of *Van der Waals* forces within the contact zone. The attraction arises which not only weakens the force of elastic repulsion but also results in a neck creation and in the negative force. The *pull-off* force, adhesion force $F_{\text{adh.}}$ is calculated by:

$$F_{\text{adh.}} = -\frac{3}{2}\pi W R \tag{4.7}$$

Here R is the radius of the contact between the two bodies.
The DMT model is adaptive to hard deformable bodies. With the assumption that there are no electrostatic components, the adhesion force $F_{\text{adh.}}$ is equivalent to the first power of the radius R and to the amount of work per unit area as required for effecting the equilibrium tearing-off:

$$F_{\text{adh.}} = -2\pi W R \tag{4.8}$$

To get the information, which of the two models is adaptable to the hair system, we calculated the so called *Tabor* factor. It is defined as *Tabor* parameter μ_T[98]:

$$\mu_T = \left(\frac{16RW^2}{9E_{\text{eff.}}^2 z_0^3}\right)^{1/3} \tag{4.9}$$

Herby R is again the effective radius and z_0 is the equilibrium separation of the atoms. To assume this Equation to our single hair system, some of the values had to be approximated. For z_0 a value of 5.0 $\times 10^{-10}$ m can be used in the Equations[99]. $E_{\text{eff.}}$ is the

effective modulus and is calculated by:

$$\frac{1}{E_{\text{eff.}}} = \frac{3}{4}\left(\frac{1-\nu_1^2}{E_1} + \frac{1-\nu_2^2}{E_2}\right) \tag{4.10}$$

E_1 and E_2 are the *Young's* modulus of the two bodies, which are in contact with each other. We used a value of 3000 MPa for the two crossed hair cylinders[14,24]. It was possible to use just one *Young's* modulus, because the material of the two bodies (in our case hair) is equal. In Equation 4.10, ν_1 and ν_2 are the *Poisson's* ratio. Again, here it was also possible to use just one value ($\nu = 0.48$)[17]. Equation 4.10 leads to an effective modulus of $E_{\text{eff.}} = 2598$ MPa.

For the radius R in Equation 4.9 the diameter (main two elliptic radii) was calculated by the following way over all measured hairs:

$$R = \sum \frac{R_{min} + R_{max}}{2} \tag{4.11}$$

To calculate the *Tabor* parameter the thermodynamic work of adhesion was appreciate first to $W = 10$ mJ/m^2 and the radius was calculated to $R = 7.2 \times 10^{-5} \pm 7.0 \times 10^{-6}$ m. With all taken values the *Tabor* parameter was calculated to $\mu_T = 2.46$.

If $\mu_T << 1$ then the limit of the DMT theory is valid. If $\mu_T >> 1$ then the JKR model should be taken. Even the calculated value for μ_T is not $\mu_T >> 1$ but $\mu_T > 1$, the JKR model yields to a value of the adhesive energy per unit area of $W = 0.1124$ mJ/m^2.

This value is very small. One reason for this can be that the real occurring contact area between the two hairs is very small as well, because of the heterogeneity of the surface. The cuticle scales of a few microns along the hair and a few hundred nanometers in thickness results a relatively large uncertainty of the size of the contact area between the *hair probe* and the sample hair at different positions[95]. The radius of the real hair is elliptical and not a perfect circle. We approximate a mean radii. In the JRK model the capillary forces, which play an important role in our system, are neglected. Also the roughness of surface is completely neglected.

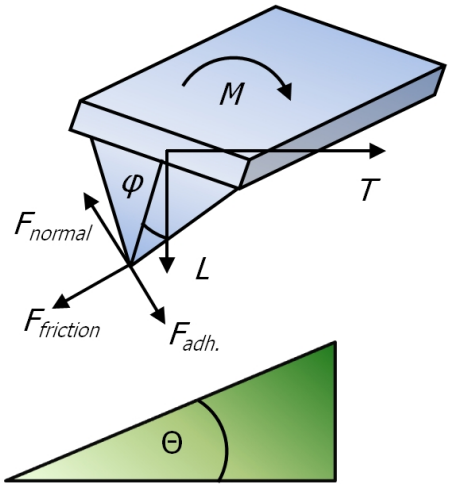

Figure 4.26: A surface with a known angle Θ, the occurring acting forces (the applied load L, the horizontal tractive force T, the adhesion force $F_{adh.}$, the reaction force from the surface acting on the tip with a component F_{normal} in the surface normal direction and a component $F_{friction}$ (friction force) parallel to the surface) and the torsion momentum M in equilibrium depend on the direction of motion-uphill and downhill. φ represents the torsion angle of the cantilever, which is proportional to the friction force.

4.2.3 Lateral Cantilever Calibration for Friction Detection

A further investigation of this thesis was the torsional spring constant of the *hair probe* cantilever to study friction forces with the AFM. Literature suggests different calibration methods for the lateral spring constant[100–107]. In comparison to the vertical spring constant calibration there is just few research on calibration techniques for the torsional spring constant, so far. In this thesis several possibilities for the lateral spring constant calibration were considered:

- Wedge Technique
- Colloidal Technique
- Enhanced Model

Tocha et al. developed a widely spread technique for calibration of purchasable cantilevers with a tip. With the Wedge Calibration Method (WCM), a cantilever is scanned across a calibration sample with two well-defined slopes.

Figure 4.26 shows the main principle of this method. While a cantilever is sliding across a sloped surface with a known angle Θ, the occurring acting forces (the applied load L, the horizontal tractive force T, the adhesion force $F_{adh.}$, the reaction force from the surface acting on the tip with a component F_{normal} in the surface normal direction, and a component $F_{friction}$ (friction force) parallel to the surface) and the torsion momentum M in equilibrium, depend on the direction of motion-uphill and downhill. φ represents the torsion angle of the cantilever, which is proportional to the friction force[108].

The friction signal is recorded as a function of the applied load. At a given load, friction and normal forces depend on the direction of motion. For the downhill motion, the torsion moment M about the tip-surface contact can be expressed.

In this thesis the lateral calibration of cantilevers was first carried out via the Wedge Calibration Method with the test structure TGG01 and cantilevers of the serie of NSC15/No AI delivered by Micromash, USA.

After this, a hair fragment was glued to the cantilever. This is explained in detail in section 4.2.1. The required orientation (for crossed cylinder geometry measurements) of the *hair probe* could not be achieved. Figure 4.27 presents an optical image of a hair fragment that turned 45°. A reason for this could be that the cantilever weas not tipless like used for the adhesion measurements, and therefore the tip influenced the drying process of the hair fragment. Even if the *hair probe* was much bigger than the tip.

Quintanilla et al. suggested a method for calibrating the torsional constant of a cantilever with *colloidal probe* attached[109]. It is based on the contact between a spherical particle and a flat substrate. Furthermore it deals with a combination of existing models. The theoretical values of ideal spherical bodies can be deduced from the dimensions of the cantilevers. In detail it is calculated via the spherical geometry, so it could not be adapted to the cylinder geometry.

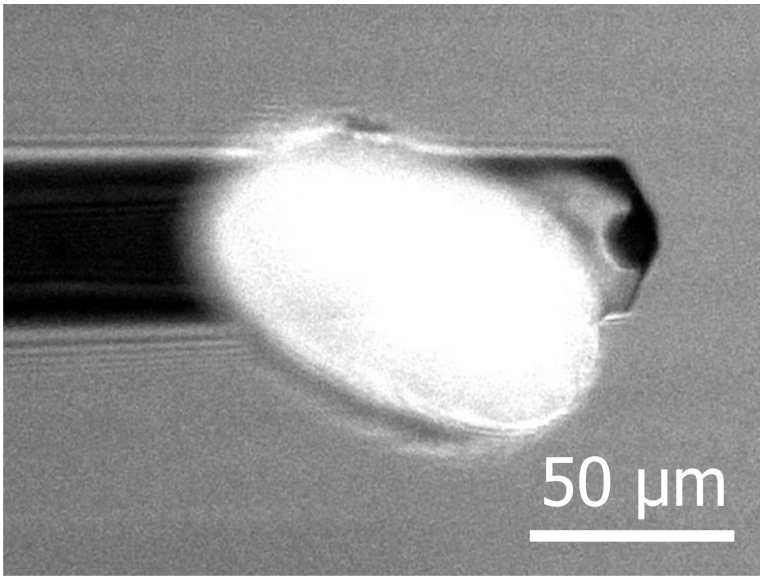

Figure 4.27: Calibrated cantilever via wedge method. The orientation of the hair changed within 45°. The occurred geometry of the *hair probe* could not require the crossed cylinder geometry.

The technique of Bhushan et al. formed the foundation of the cantilever calibration for the *hair probe*[110]. For that the width w and the length l was admeasured by the optical microscope of the AFM set up. The lateral spring constant c_L was calculated using the following Equation:

$$c_L = \frac{Gwt^3}{3h^2l} \tag{4.12}$$

Where G is the shear modulus of silicon with a value of G = $0.5{\times}10^{11}$ N/m^2. As height h we used the diameter of the hair (main two elliptic radii) plus the half height t of the cantilever ($t = 1.0 \pm 0.3$ μm).

This assumption represents just a rough estimation because the shear modulus of pure silicon was used. Figure 4.28 demonstrates this for the length l and width w of one cantilever. The height was calculated with a approximation of the radius R, because of the elliptical shape:

$$R = \frac{R_{min} + R_{max}}{2} \tag{4.13}$$

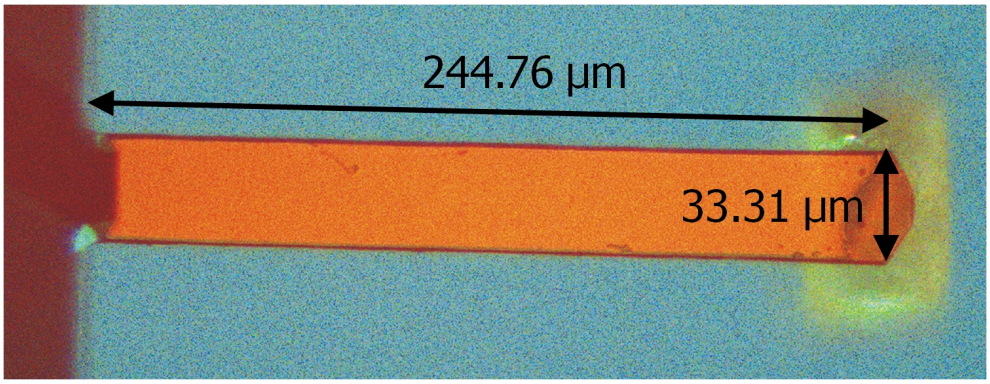

Figure 4.28: A picture of a cantilever for measuring its values in the width w and in the length l via optical imaging.

Nonetheless, it gave information about the range of the occurring friction forces of a *hair probe* set up. Subsequently, the occurring lateral force F_L was calculated using Equation 2.16, as discussed in Section 2.4.3:

$$F_L = \frac{3}{2} c_L \frac{h}{l} S_z V_L \tag{4.14}$$

Table 4.4: The different values used for calculating the lateral force F_L.

C	w[m]	h[m]	l[m]	c_N [N/m]	c_L [N/m]	S_N [m/V]
1	3.528×10^{-5}	7.000×10^{-5}	1.067×10^{-4}	8.997	0.40070	10.11
2	3.331×10^{-5}	8.019×10^{-5}	2.448×10^{-4}	2.822	0.09170	22.19
3	3.434×10^{-5}	7.678×10^{-5}	2.967×10^{-4}	2.618	0.06474	39.79
4	2.991×10^{-5}	7.635×10^{-5}	2.908×10^{-4}	2.908	0.10004	25.38
5	3.425×10^{-5}	6.801×10^{-5}	2.998×10^{-4}	3.292	0.13718	21.42
6	3.387×10^{-5}	7.781×10^{-5}	2.950×10^{-4}	2.529	0.08999	28.09

All values that were used for calculating the data in the following sections are listed in Table 4.4. Hair is a naturally system and every hair fragment is different, even it is

cutted from the same hair. With all the approaches, which were done so far the relation between the normal spring constant c_N and the lateral spring constant c_L is in good agreement with the Literature[111]. Herby the value of c_L is approx. 20 times smaller than c_N. The ratio between the spring constants calculated here are in the same order of magnitude.

4.2.4 Results on Friction Forces

The following Section presents the data we could achieve by using the Friction Force Microscopy (FFM). Therefore the main aspects are:

- Characteristic Friction Loops of Two Single Hairs
- *In situ* Investigation of Friction Forces with Different Polymers

Characteristic Friction Loops of Two Single Hairs

The principle of friction detection with an AFM is presented in detail in Section 2.4.3. Figure 4.29 (A) displays a typical friction loop of the *hair probe* set up. The measurement was carried out with a vertical movement of <1 μm of the cantilever hair.
As introduced in section 2.1.1, the cuticle of hair consists of flat cells which overlap each other (overlay$\sim$ 5μm). Their orientation is from the proximal end (root) to the distal end (tip) of the hair fiber. This navigation affects the frictional behavior of hair[18]. With the vertical movement of <1 μm the friction loop is just on one cuticle. No significant peaks are highlighted in Figure 4.29 (A). In the opposite, the scanning movement of >20 μm presents the edges of the cuticles. Wei et al. measured friction loops on human hair with a normal cantilever tip. They also could investigate a increasing friction signal provided from the cuticles of hair[11].
The measurements in Figure 4.29 were carried out at room temperature (RT) under dry conditions (30 $\pm$ 5% RH). The *hair probe* and the substrate hair were cut from one hair to guarantee the consistency of their radii. Following phenomenas were observed with a vertical movement of the piezo of <1 μm.

Influence of Environment

The measurements were carried out under two environmental conditions, in air with around 30 $\pm$ 5% RH (dry state) and under water (wet state). Figure 4.30 (A) demonstrates the friction force under 30 $\pm$ 5% RH and (B) under water. The possibility to

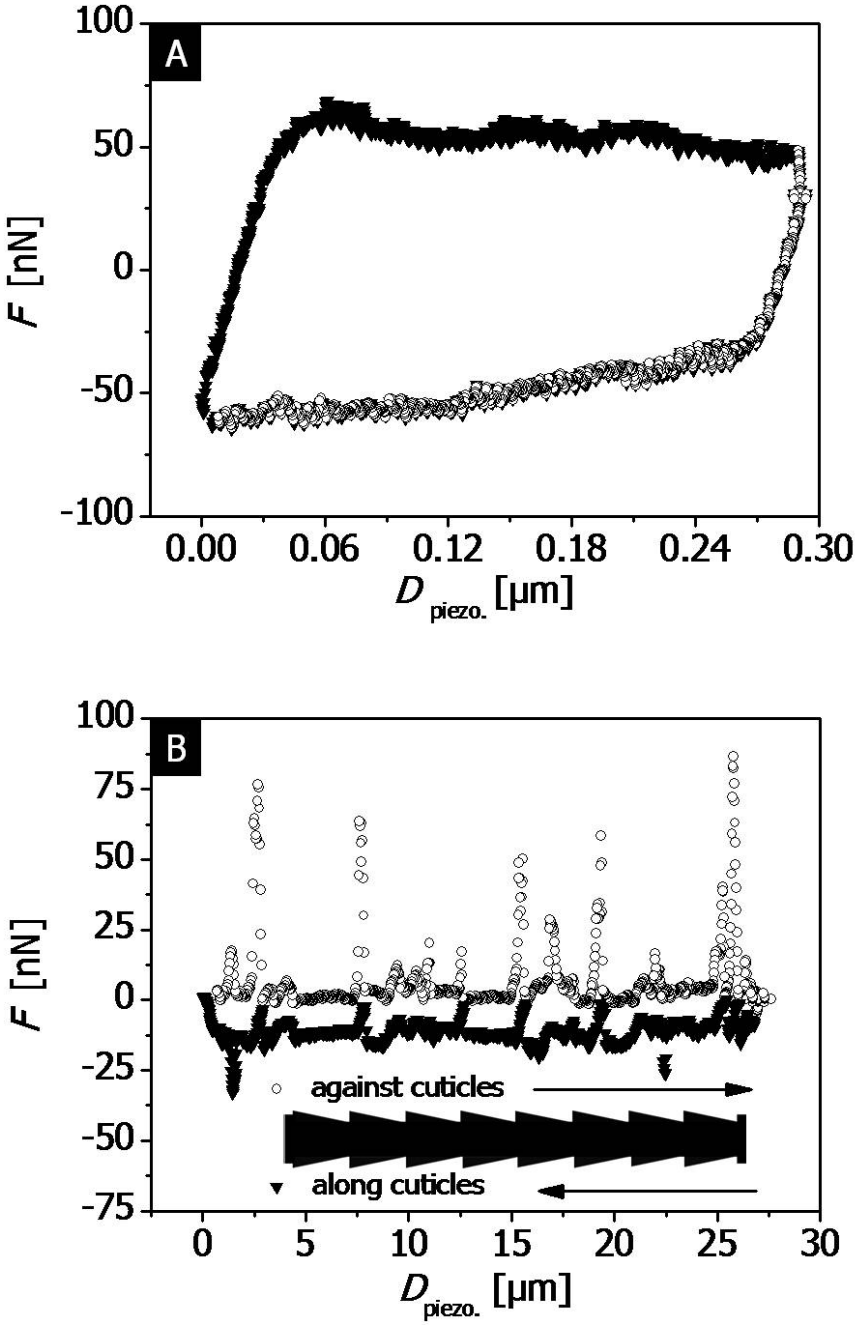

Figure 4.29: A typical friction loop measured with an AFM. The friction force F versus piezodisplacement D of a single hair measurement is depicted. The circles demonstrate one direction and the triangles the way back. In (A) a vertical range of <1 μm and in (B) a vertical range of >20 μm was scanned. The spikes in (B) depict the cuticles of hair, which aligning perpendicular to the axis of hair fiber and providing a local ratchet, that increases the friction signal. Measurement were carried out with C1, $c_L = 0.40070$ N/m.

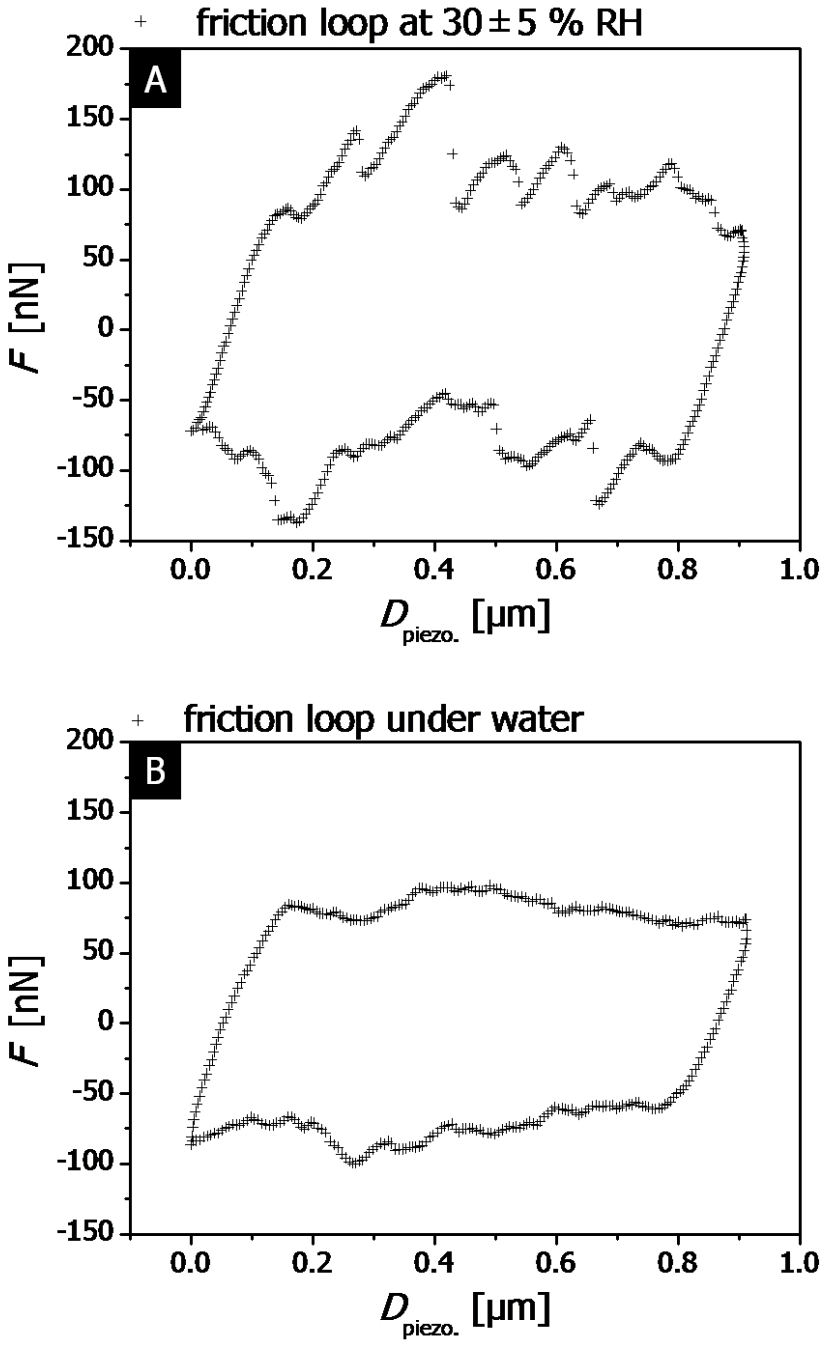

Figure 4.30: Friction loops under two different conditions with a vertical range of <1 μm. (A) shows the dry state with 30 $\pm$ 5% RH and (B) under water, where the intensity of the friction signal is higher in total. Measurements were carried out with C3, $c_L = 0.06474$ N/m.

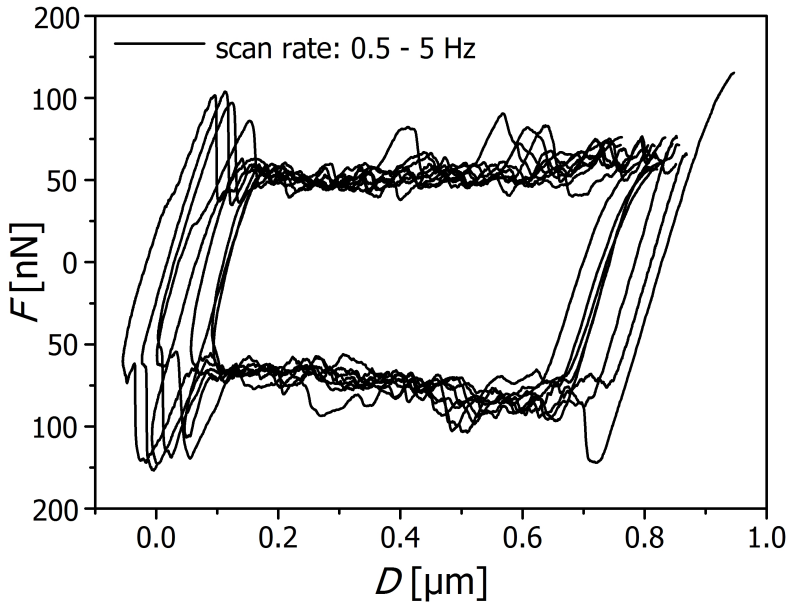

Figure 4.31: Friction loop with a variation of the scan rate. Measurements were carried out with C2, $c_L = 0.09170$ N/m.

compare these two graphs whith each other is given by the fact, that the same *hair probe* cantilever and substrate hair was used. It is clearly visible that the friction force under water decreases compared to the dry state.

In this thesis the focus was on the investigation of *in situ* measurements under different liquids. All following experiments were carried out under water, if another liquid is not mentioned especially.

Influence of the Scan Rate to Friction Loops

Several scan rates between 0.5 - 5 Hz were tested with the result of no/only minor influence to the the friction force F, see Figure 4.31. This is in contrast to the group around Gnecco. They studied the sliding friction between a normal cantilever tip and a NaCl (100) surface. They could describe the atomic friction mechanism within a logarithmically dependence[112]. The velocity behavior in our single hair experiments are also contrary to the measurements we achieved with the UST, where a linear dependence

could be achieved. A reason why the experiments presented in Figure 4.31 are showing an independent behavior could be that the hair system can not be clearly allocated to micro or nano scale[113]. Based on this finding all measurements were carried out with a scan rate of approx. 1 Hz.

Influence of Approach and Retraction to Friction Loops

In Figure 4.32 (A) the reproducibility of ten friction loops is clearly demonstrated, the data were collected under the condition that the *hair probe* cantilever was not losing the contact with the substrate hair.

The result on retraction of the cantilever and engaging it again to the substrate hair (three times) is depicted in Figure 4.32 (B). Even scanner position was not changed in x- and y-direction, it was not possible to scan exactly the same position after retracting the cantilever. Normally AFM friction measurements are carried out with systems in the nanometer range, sometimes in the sub micrometer regime. Here, with this huge rough cylindrical shape of the *hair probe*, the system is definitely not in the scale of nanometers, especially with a hair fragment of a length of 50 μm.

Nevertheless, we could study interesting investigations via *in situ* treatment of the single *hair probe* set up with different polymers.

As the main focus of this thesis was the investigation of *in situ* measurements, research was carried out on experiments under water .

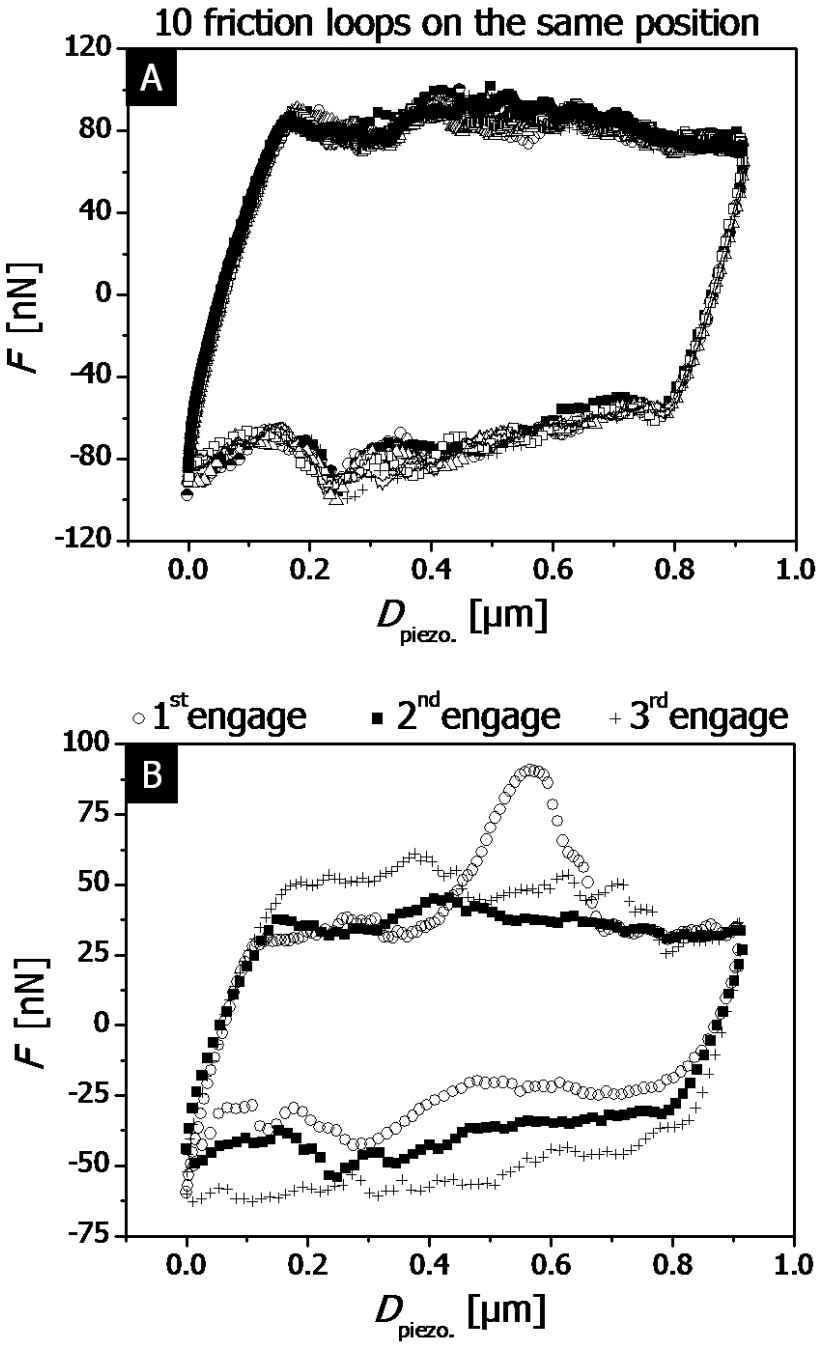

Figure 4.32: Friction loops with a vertical range of <1 μm. (A) Ten friction loops were carried out on the same position of substrate hair without losing contact of the *hair probe* to the substrate hair. (B) Three retraction followed by engages were carried out without varying the scanner position. Measurements were carried out with C3, $c_L = 0.06474$ N/m.

In situ Investigation of Friction Forces

Set Up Modification for Friction Forces

In Section 2.3 *State of the Art* the different methods to measure friction forces in the micro- and nanometer regime are introduced. In this thesis the friction forces were investigated with the AFM based on continuum contact mechanic theories, see Section 4.2.1 .

The crossed cylinder geometry of the *hair probe* and the substrate hair were prepared as in section 4.2.1. The main difference was an *in situ* treatment of the *hair probe* set up, where we could investigate the changes of friction forces by changing the environmental media.

The closed fluid cell was connected with a flow measuring method as depicted in Figure 4.33. An injection bottle was directly linked to the measuring cell and calibrated via the principle of hydrostatic pressure. The plot in Figure 4.33 presents the extrapolation of the flow rate R_{flow} versus the height difference Δh. All *in situ* experiments were carried out with a flow rate of $R_{flow} = 0.30$ ml/sec. During the measurements of the friction forces the flow had to be stopped because of the current of the liquid media.

Procedure of Friction Force Loops

The *in situ* measurements were carried out to mimic a cycle of *hair washing*. The procedure was standardized:

The calibrated and aligned set up was equilibrated with flowing $\text{water}_{\text{dest.}}$ for two minutes at a flow rate of $R_{flow} = 0.30$ ml/sec to be sure that the liquid cell with a volume of $V_{\text{cell}} = 5$ ml was completely flushed. After ten minutes, when the current of the liquid media was minimized, ten friction force measurements were carried out. The *hair probe* was retracted.

With a polymer concentration of $c_{\text{poly.}} = 200$ ppm $= 0.2$ wt% the system was applied for two minutes (again with a flow rate of $R_{flow} = 0.30$ ml/sec). The concentration of polymer was chosen because in marketed conditioners there is a concentration of $c_{\text{poly.}}$

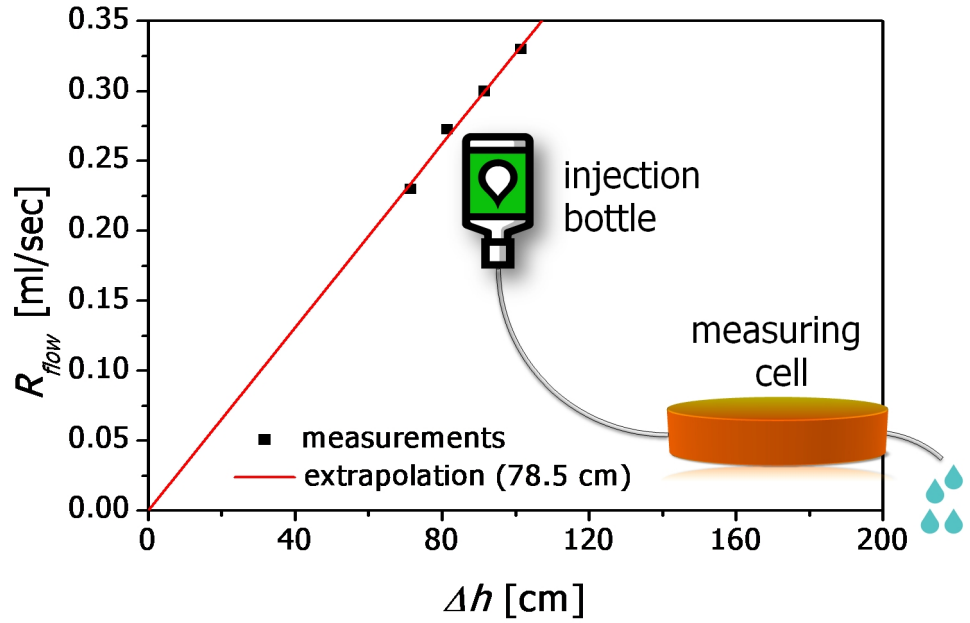

Figure 4.33: Extrapolation of the flow rate R_{flow} for the *in situ* measurements of single hair friction forces. A scheme of the flow set up is also illustrated.

$= 0.1 \sim 1.0\%$ (see also Table 3.1). Nylander et al. also used similar conditioner polymer concentrations for their *in situ* studies with an Ellipsometer[114].

After the equilibrium of the current was reached, 10 curves were measured. Finally after a rinse-off with destilled water, ten more friction loops were measured. As mentioned above, three different polymers were tested under this conditions.

Friction Loops without Cuticle Effects

Figure 4.34 demonstrates the friction loops of PQ-10 and its *washing cycle* with a horizontal movement of the cantilever hair of $D_{piezo.}$ <1 μm. For clarity just one of the ten measured friction loops is depicted.

The open circles were carried out after the system was flushed. The half-open circles reflecting a friction loop after the system was two hours under water. In the range of the inconsistency of retracting and approaching the *hair probe* from the surface of the substrate hair, the stability of the system could be verified. Hence it was derived from this that the swelling behavior of hair under water had no influence on the measurements

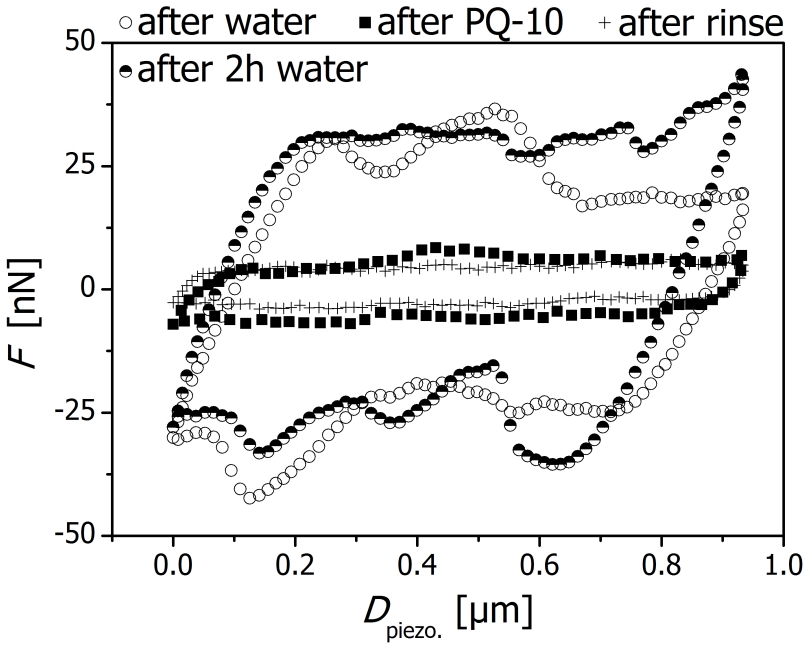

Figure 4.34: Friction loops of a washing cycle are depicted. The horizontal distance of the piezo was $D_{piezo.}$ <1 μm. The characteristic curves were measured after the *hair probe* set up was treated a) with $water_{dest.}$, b) with PQ-10 of a concentration of $c_{poly.}$ = 200 ppm and c) after rinse-off with $water_{dest.}$. In addition the stability of the system was checked after 2 h of a). Measurements were carried out with C4, c_L = 0.10004 N/m.

which were carried out here.

The filled squares show the friction behavior after the polymer PQ-10 was brought into the system. The plateau values decreased enormously after the polymer was added. The polymer layer deposited on the surface of hair and lowered the friction. The crosses demonstrating the effect on friction after a trial of rinse-off. As predicted from Literature, the polymer layer could not be removed completely from the hair surface as demonstrated by the fact that the friction force does not increase to the initial friction force any more. This is in good agreement with Literature, where Weigmann et al. studied the desorption of conditioner polymers[115].

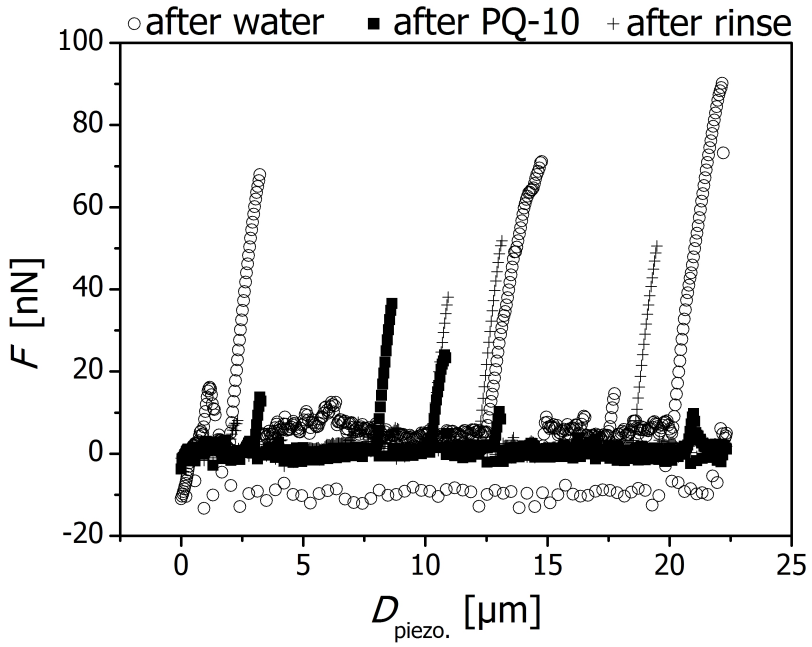

Figure 4.35: Friction loops of a washing cycle are depicted. The horizontal distance of the piezo was $D_{piezo.}$ >20 μm. The characteristic curve measured after the *hair probe* set up was treated a) with $\text{water}_{\text{dest.}}$, b) with PQ-10 of a concentration of $\text{c}_{\text{poly.}}$ = 200 ppm and c) after rinse-off with $\text{water}_{\text{dest.}}$. Collisions between cuticles increases the friction signal. Measurements were carried out with C4, c_L = 0.10004 N/m.

Friction Loops influenced by Cuticle Effects

Figure 4.35 demonstrates the friction loops of a *washing cycle* with a piezo movement of $D_{piezo.}$ >20 μm. The reduction of the friction forces after the polymer treatment of $\text{c}_{\text{poly.}}$ = 200 ppm is visible as for the distance $D_{piezo.}$ <1 μm.

The edge effects of the cuticles are showing higher values in friction compared to the vertical movement of $D_{piezo.}$ <1 μm. The region between the signals of cuticles (where $D_{piezo.}$ <1 μm) shows smaller values in total.

On closer inspection the characteristic signals of cuticles are affected after the treatment of polymer as well. The effect shows a decrease of the spikes after the polymer was applied. The followed increase after rinse-off can be interpreted as mentioned before.

The friction does not reach the initial maximum value of friction as before the polymer treatment. A complete deposition of polymer has also not taken place, as found in the Literature[115].

Comparison of the different Polymers

Measurements were also carried out with the polymers (C-13S and PQ-87) under the conditions of the washing cycle, mentioned above. Figure 4.36 depicts the friction loops of the polymer C-13S.

The behavior of the curves is very similar to the other polymer PQ-10. A direct relation between the friction values of the different polymers due to the different *hair probe* cantilever should be considered critical, see also Section 4.2.3.

To minimize these effects a normalization of the friction forces was carried out to compare the polymers to each other. The friction reduction F_R is defined as:

$$F_R = 100 - \frac{x_{\text{rinse}} \times 100}{x_{\text{water}}} \tag{4.15}$$

Hereby x_{rinse} refers to the friction force after the rinse-off, and x_{water} to the friction force of the untreated hair. The relative friction reduction of $F_R = 89.8 \pm 2.0\%$ at a scan rate of $D_{piezo.}$ <1 μm is similar between the C-13S treated *hair probe* set up and the PQ-10 treated one. For PQ-10 a friction reduction of $F_R = 84.9 \pm 2.1\%$ could be calculated. In principle this allows an estimation, that both polymers reduced the friction nearly equally. In contrast the polymer PQ-87 showed less friction reduction. It is different to the other polymers. Figure 4.37 shows the friction loops of PQ-87. The same trends like for the other polymers are noticeable in both vertical movements of the piezo, but a qualitative view of the data illustrates that the reduction of the friction is lower in the case of PQ-87. With a force reduction of $F_R = 35.3 \pm 2.1\%$ it decreased the friction least of the polymers, used in this thesis. A possible reason for this could be the high charge density ($\rho = 3.7$, see also Table 3.2) or the low molecular weight. In section 4.3 is a more detailed discussion about this phenomena.

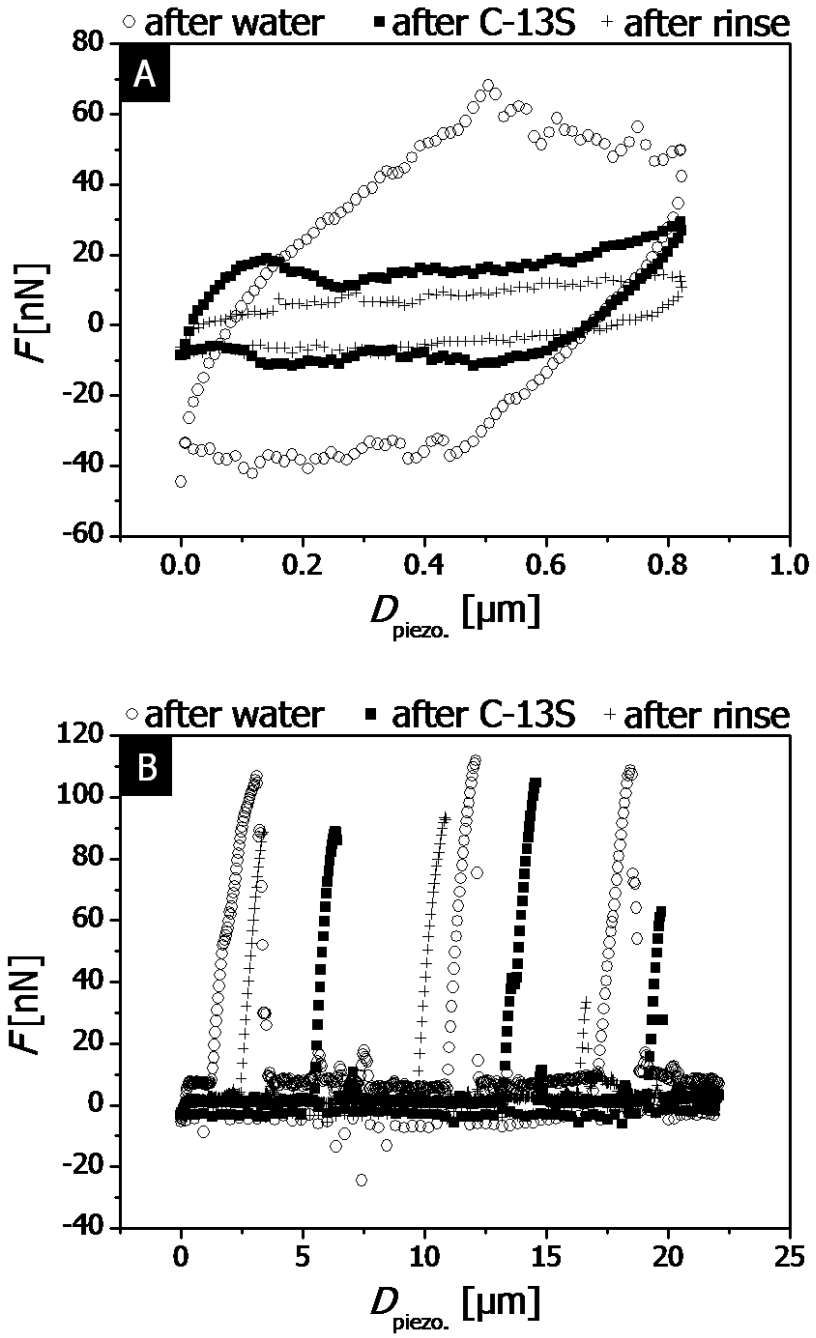

Figure 4.36: Friction loops of a washing cycle are depicted. The horizontal distance of the piezo was $D_{piezo.}$ <1 μm in (A) and $D_{piezo.}$ >20 μm in (B). The characteristic curve measured after the *hair probe* set up was treated a) with $water_{dest.}$, b) with C-13S of a concentration of $c_{poly.}$ = 200 ppm and c) after rinse-off with $water_{dest.}$. Measurements were carried out with C5, c_L = 0.13718 N/m.

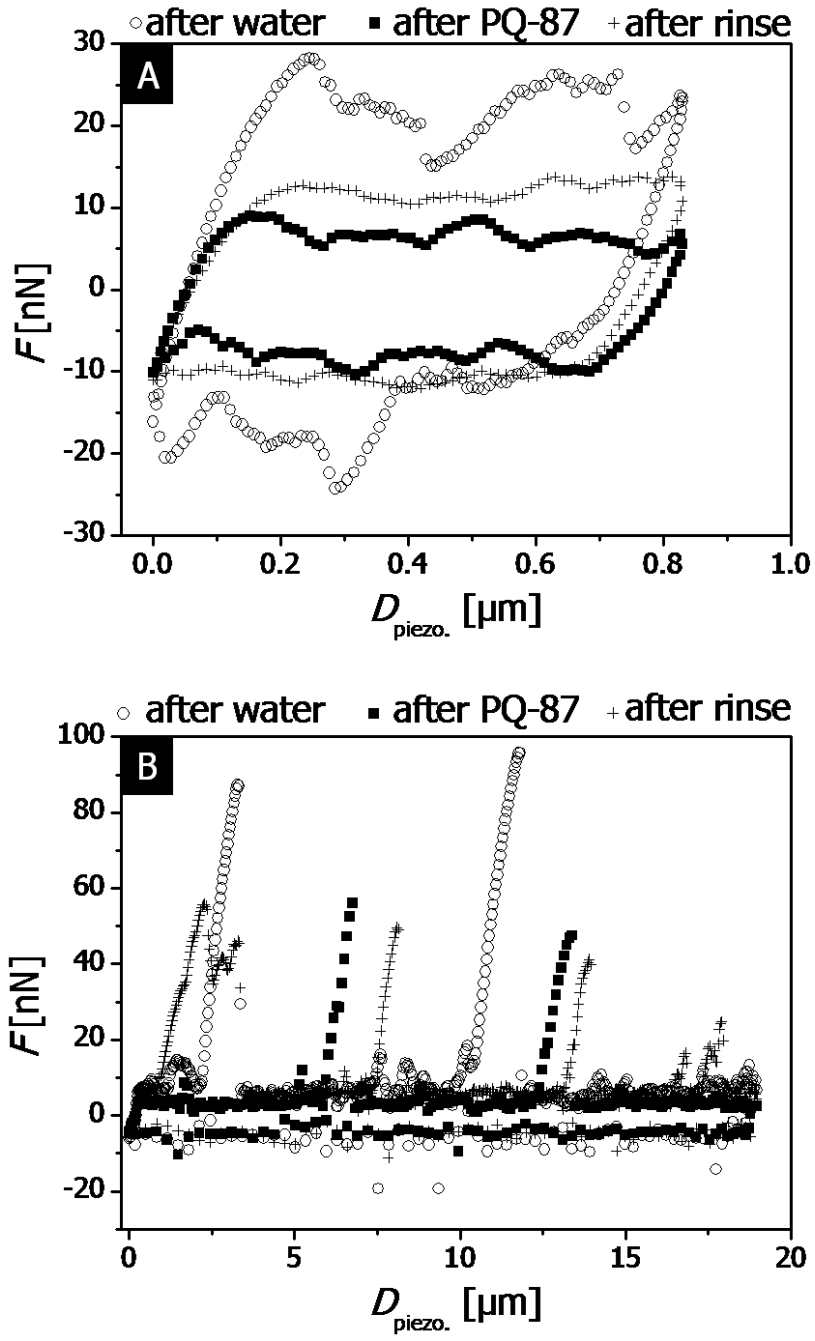

Figure 4.37: Friction loops of a washing cycle are depicted. The horizontal distance of the piezo was $D_{piezo.}$ <1 μm in (A) and $D_{piezo.}$ >20 μm in (B). The characteristic curve measured after the *hair probe* set up was treated a) with $water_{dest.}$, b) with PQ-87 of a concentration of $c_{poly.}$ = 200 ppm and c) after rinse-off with $water_{dest.}$.Measurements were carried out with C6, c_L = 0.08999 N/m.

Table 4.5: Friction reduction F_R of the different polymers. Different methods are presented: Universal Surface Tester (UST), Comb Force Method (CFM) and Atomic Force Microscopy (AFM). Further on the grades of the Haptic Panel Tests (HPT) are listed.

F_R			
Method	PQ-10 [%]	PQ-87 [%]	C-13S [%]
UST	4.0 ± 2.6	3.2 ± 1.7	2.0 ± 2.6
CFM	25.0 ± 5.0	62.0 ± 4.0	26.0 ± 6.0
AFM	84.9 ± 2.4	35.3 ± 2.1	89.8 ± 2.0
Grade			
HPT	2	1-	2

4.3 Nano Friction vs. Micro Friction

The modified set ups for different methods described in this thesis provided on the one hand friction measurements in the micrometer regime and on the other hand they lead to first results on friction measurements of single hair fibers in the nanometer regime.
A comparison of these new developed measurement to Haptic Panel Tests (HPT) and to the Comb Force Method (CFM) should help to understand the interaction behavior of cationic polymer with the surface of hair in more detail[50,51].
A summary of all the findings are given in Table 4.5 whereas three different polymers (PQ-10, PQ-87 and C-13S) are compared to each other. The friction force reduction F_R is the effect on the surface of hair after it was treated with the different polymers. It was calculated as described in the Sections before (see, Equation 2.7 and 4.15).
The values with UST show the lowest force reduction and indeed no real differences between the tested polymers. The reason for this could be the sample preparation. The laces were washed, treated and dried before measuring. Then to wet the samples for comparing it to the CFM and to the AFM, water was added to the system, a dilution

(15 ml) of the polymer concentration took place and decreased the effect on the friction reduction.

A good agreement can be achieved by the correlation of CFM and AFM. PQ-10 and C-13S show in friction force reduction F_R with both measurement methods the same tendency, even if the reduction is smaller in CFM. A reason for this could be that with the AFM a symmetric system of interactions was investigated:

hair $\leftrightarrow$ polymer $\leftrightarrow$ polymer $\leftrightarrow$ hair

In the opposite, the system of interactions of the CFM was asymmetric:

comb material $\leftrightarrow$ polymer $\leftrightarrow$ hair ($\leftrightarrow$ hair).

Furthermore the sample preparation was not exactly the same, because for the CFM measurements complete conditioner formulations were used. For the AFM measurement, the system was kept more simple to avoid side effects of the different ingredients of the conditioners. The focus lied on the active cationic polymers.

In the CFM the polymer PQ-87 represents with a value of $F_R = 62.0 \pm 4.0\%$ the highest friction reduction of the three polymers. This is in good agreement with the sensoric Haptic Panel Tests, that were also carried out with all three polymers. There PQ-10 and C-13S were graded with 2 (wet marginal well-kept, not waxy) and PQ-87 with 1- (wet well-kept, easy waxy)[50].

Comparing these results to the nanometer regime (AFM), PQ-87 displays the lowest force reduction of all three polymers. The value of the friction reduction was calculated to $F_R = 35.3 \pm 2.1\%$.

Nevertheless a direct comparison to the Haptic Panel Tests is also possible with that method. For PQ-87 the measured value is clearly different compared to the other polymers. Here just the friction between two single hairs were carried out. Based on the different friction reduction via AFM and CFM we suggest that the HPT is mainly influenced by the friction between skin and hair for that kind of polymer.

Normally the use of high molecular weight cationic polymers (C-13S, PQ-10), in relaxing or straightening systems also improves hair manageability and provides other benefits

desired by consumers. For example the hair is more easily combed and styled, and has reduced breakage and friction and increased hair fiber smoothness. With its molecular weight of $M_w = 0.1$ MDa, PQ-87 is relatively low compared to other conditioner polymers.

Instead of molecular weight, the effect of charge density could play a more important influence of the friction properties. With a charge density of $\rho = 3.7$ meq/g, it is higher than the other polymers (PQ-10, C-13S: $\rho = 1.0$ meq/g).

Based on these two values, it is easier for the small molecular weighted and a highly charged cationic polymer chain to interact with the negatively charged net of the hair surface. This results in attraction of the polymer to the edges of the cuticle and this leads to a smoothening effect because of the decrease in friction.

5 Perspectives

The presented experiments could give quantitative results from force measurement of hair fibers via the Universal Surface Tester (UST), as well, with the Atomic Force Microscope (AFM). From this AFM data, we could calculate the adhesional statistics and therefore the adhesion energy between the contact area of two single hairs. Also first *in situ* friction force measurement between single hairs could be investigated. This provides motivation to carry on upgrading the here modified measurement systems.
Focusing on the AFM experiments, a simplification of the preparation of samples, of the measurements and of the data analysis could help to establish this technique to existing standard analytics like imaging AFM. To find a way to optimize the developed calibration method for the lateral spring constant of the fiber fragment (hair) to receive more accurate values is also an important point in this context. Whereas the contact area between the two fibers is getting more precise.

Upgradability of the presented System: Hair

By investigating the measuring cell/head of the UST in some way the possibility to measure *in situ* is also given. Then a direct comparison between multi-hair friction (UST) and single hair friction (AFM) is realizable in a more precisely way.
In consideration of the developed *in situ hair probe* set up for the AFM, statistics in both vertical ranges ($D_{piezo.}$ <1 μm and $D_{piezo.}$ >20 μm) could be very helpful to rely on the existing results. In consideration of the occurring surface roughness, a closer look to different theories should be made to improve the adhesion energy (e. g. the *Robinovich* theory)[116,117].
Hairs of different ethnic sources could also be measured and compared to each other. As well different damaged hair (bleached or permanent waved hairs) to get a better

understanding about the friction reduction because of the treatment of different active agents to them. Therefore it could be figured out, which ingredients are the most essential for those type of hairs.
Moreover, the temperature could be varied and tested in the experiments with the AFM. The variation of chemicals that could be tested in consideration to the friction is very large. It is possible now to test polymer/surfactant complexes and their influence on the friction. Then it is possible to relate these findings indirectly to existing results from Literature, even they were measured with different techniques[35,118,119].
Therefore it would be interesting to varying the pH and control the isoelectric behavior of hair. Also addition of normal conditioner formula like silicone oil could be tested.
Surely, there could be investigations to correlate the occurring nano friction with the macroscale. It could also be useful to find another way how the different treatments and the resulting friction values affect the senses of humans, like the haptic properties. This could open the way to optimize hair care products better under the main focus of human well-being.

Beyond Hairs

It would be very interesting to test other fibers. Natural ones like hemp or cotton, even the synthetic ones like polyester, which play important roles in the textile industry.
With the here used measurement systems, especially the crossed cylindric geometry of the single fibers, it would be possible to find a direct relation to the handling of this sources.
To investigate the effect of washing cycles on the nanoscale of friction could lead to new findings relating to the choices of surfactants in detergents, for example.
By adding friction reducer, for example, the abrasion of textiles could be improved. There is definitely room for a lot of different variations, not only for the textile industry, but also for all kind of materials, which consist of microfibers.

6 Summary

In conclusion, we have developed techniques for the investigation of physical forces on microfiber surfaces. The experiments were carried out on hair fiber surfaces and their treatment with different conditioning formulas. We studied the physical behavior on the macro/micro- and on nanoscale.
Shampoo treatment and hair conditioning have a direct impact on the well-being of humans by improvements to the combability and haptic perception of hair. Therefore, systematic investigations should lead to a dramatic quality improvement of hair care products. The active substances in conditioning shampoos are cationic polymers. In this thesis, three commercially available polymers (Polyquaternium-10, Polyquaternium-87 and Jaguar C-13S) were tested with a focus on their interaction behavior with the negatively charged hair surface net.

A modified set up of the Universal Surface Tester informed us about the friction forces occurring in the micrometer range. Hereby the instrument was optimized for the hair fiber system. We developed a novel measuring cell that adapted the instrument for measurement of hairs and we calibrated a self-constructed novel measuring head. This new head consists of styrene-butadiene-rubber, because this is the material used to produce normal combs. This allowed us to compare the achieved friction force reduction after the hairs were treated with the different polymers, with existing data, investigated from the so called and Comb Force Method[50]. All three polymers cause a friction reduction on the hair surfaces and Polyquaternium-87 shows the highest reduction. However, when using these methods multiple forces occur, including the interaction between the hairs, the entanglements of hairs, the interaction of conditioning polymers with the hair and the comb material, and the comb material and the hair, and therefore we tried to find a

way to separate these forces from each other.

To this end, we investigated a set up to measure single hair interactions with an Atomic Force Microscope. Based on different models of continuum contact mechanics we modified the instrument in such a way that we could study the interactions of two hairs in a crossed cylinder geometry, which were brought in contact to each other. We glued a hair fragment with a length of $\sim$50 μm (which was cut with a micro laser) to a tipless cantilever spring, so that it was possible to detect with this modified measuring head the forces between the *hair probe* and another hair. First we investigated the adhesion forces occurring between the *hair probe* set up. After a statistical approach for the adhesive force of 38.08 $\pm$ 11.60 nN, we could calculate the adhesive energy per unit area of two hairs to 0.1124 mJ/m^2, based on the theory of JKR (Johnson, Kendall and Roberts[96]). A reason for this relatively small value is that the cuticle scales which are a few microns along the hair and a few hundred nanometers in thickness result in a relatively large uncertainty of the size of the contact area between the hairs[95].

In addition to that, we used the modified set up to investigate friction forces between two hairs. The main difference to the measurements of the adhesion forces was an *in situ* treatment of the *hair probe* set up, where we could investigate the changes of friction forces by adding the different conditioner polymers. This was achieved by mimicking a cycle of hair washing. Hereby a similar behavior appears, like the friction force reduction achieved with the Comb Force Method. The polymer Polyquaternium-87 demonstrated different behavior compared to the others, for example, with the single hair measurement the level of friction reduction was the lowest.
A comparison between Haptic Panel Tests and the results achieved from the different techniques of this work allowed the quantification of these tests of sense in a physico-chemical way.

7 Zusammenfassung

Die Zielsetzung dieser Arbeit ist die Weiterentwicklung verschiedener physikalischer Messmethodiken zur Untersuchung von Mikrofaseroberflächen. Das zugrunde liegende System hierbei hat das Augenmerk auf die Veränderungen der Oberflächen von Haaren durch applizieren mit unterschiedlichen Shampooformulierungen. Fokussiert werden die physikalischen Veränderungen, einerseits in der Makro - und Mikroskala und andererseits in der Nanoskala.
Haarpflegemittel wie Shampoos oder Conditioner spielen eine wichtige Rolle für unser Wohlbefinden und bieten einen weltweit attraktiven Markt für die Industrie. Von Seiten der Forschung wurde die Wirkungsweise und Adsorption von aktiven Wirkstoffen in Haarpflegemitteln deshalb intensiv untersucht. Im Gegensatz dazu stecken quantitative Messungen der Veränderungen in den Reibungs- und Wechselwirkungseigenschaften, die durch die Behandlung erreicht werden noch in den Anfängen.
Unser Ziel ist hier, Methoden zu entwickeln, die es erlauben solche Eigenschaften zu untersuchen und damit die Basis für eine gezielte Optimierung von Haarpflegeprodukten zu bieten. Die wichtigsten aktiven Substanzen in Haarpflegemitteln sind kationische Polymere. In dieser Arbeit wurden drei der auf dem Markt käuflich erwerbbaren Polymere (Polyquaternium-10, Polyquaternium-87 und Jaguar C-13S) in Hinblick auf ihr Wechselwirkungsverhalten mit dem negativ geladenem Netzwerk der Haaroberfläche untersucht.

Ein modifizierter Aufbau des so genannten Universal Oberflächen Testers lieferte Ergebnisse zu den Reibungseigenschaften von Haaren im Mikrometerbereich. Mit der Entwicklung einer neuen Messzelle und der Kalibrierung eines selbst konstruierten Messkopfes wurde das Instrument an das Haarfasersystem angepasst und optimiert. Das Material des Messkopfes (Styrol-Butadien-Kautschuk) wurde dem Material von herkömmlichen

Kämmen angeglichen, um einen direkten Vergleich mit Ergebnissen, die aus der so genannte Kämmkraftmethode hervorgingen, zu ermöglichen. Der Schwerpunkt lag auf der Veränderung der auftretenden Reibungskräfte nachdem die Wirkstoffe auf das Haar aufgebracht wurden. Alle drei Polymere verursachten eine Reduktion der Reibungskräfte, die höchste konnte dabei dem Polymer Polyquaternium-87 zugeschrieben werden. Bei beiden Methoden werden jedoch viele verschiedene Wechselwirkungen detektiert, nämlich die Reibung zwischen den einzelnen Haaren, deren Verwicklungen untereinander, die Reibungen zwischen den kationischen Polymereren mit den Haaren und mit dem Kammmaterial und die Wechselwirkungen der Haare mit dem Styrol-Butadien-Kautschuk. Mit dieser Erkenntnis galt es einen Weg zu finden, der diese auftretenden *Multikräfte* voneinander separiert.

Hierfür wurde der Aufbau eines Rasterkraftmikroskop so modifiziert um die Wechselwirkungen zwischen zwei einzelnen Haaren zu detektieren. In einem Rasterkraftmikroskop dienen mikrofabrizierte Blattfedern (Cantilever) als ultra-sensitive Kraftdetektoren, wodurch Kräfte im Bereich von 10^{-11} bis 10^{-5} N gemessen werden können. Um dieses Werkzeug zur Untersuchung von Wechselwirkungen zwischen einzelnen Haaren zu nutzen, wurden mit einem Laser-Skalpell Haarfragmente passender Größe ($\sim$50 μm) zurecht geschnitten und an den Cantilever fixiert. Dadurch konnten die direkten Wechselwirkungs- und Reibungskräfte zwischen einem Haarfragment und einem weiteren, auf der Oberfläche immobilisierten Haar, gemessen werden. Zunächst lag der Fokus darin, die auftretende Adhäsionskraft zu charakterisieren und mit einem statistischen Ansatz zu quantifizieren. Mit einem Wert der Adhäsionskraft von 38.08 $\pm$ 11.60 nN war es möglich anhand eines Kontinuumskontaktmechanikmodells nach Johnson, Kendall und Roberts die daraus resultierende Adhäsionsenergie pro Kontaktflächeneinheit zu 0.1124 mJ/m^2 zu ermitteln. Dieser relative kleine Wert kann unter anderem darin begründet liegen, dass die eigentliche Kontaktfläche zwischen dem Haarfragment und dem Substrathaar in Wirklichkeit relativ ungewiss ist, da die Schuppen auf der Haaroberfläche einige Mikro-

meter lang sind und eine Höhe von mehreren hunderten Nanometern besitzen[95]. Solche Größenordnungen sind für rasterkraftmikroskopische Untersuchungen von Wechselwirkungskräften riesig.

Des Weiteren wurde unter der eben erwähnten Aufbausmodifikation des Rasterkraftmikroskops ein Schwerpunkt auf die Ermittlung der auftretenden Reibungskräfte zwischen zwei einzelnen Haaren gelegt. Ein entscheidender Unterschied zu den vorangegangenen Messungen liegt darin begründet, dass die beiden Haare *in situ* mit den verschiedenen Polymeren behandelt wurden. Hierbei wurde einem Waschzyklus nachempfunden. Somit war es möglich nach der Behandlung mit den verschiedenen Polymeren die Änderung der Reibungskraft festzustellen. Die auftretende Reduktion der Reibung konnte in einem guten Einklang mit den Kämmkraftdaten gebracht werden. Genau wie bei diesen, erzielte das Polymer Polyquaternium-87 ein anderes Verhalten, verglichen zu den anderen beiden Polymeren. Bei den Einzelhaarmessungen wurde mit dem Polymer Polyquaternium-87 die geringste Reibungsreduktion gemessen.
Ein Vergleich zwischen sogenannten Haptikprüftests und den Ergebnissen, die von den verschiedenen Messmethodiken dieser Arbeit erzielt wurden, eröffnet neue Wege solche Sinnestests physikochemisch zu quantifizieren.

Bibliography

[1] Mayer, W. V. *Anatomical Record* **1950**, *108*, 602–603.

[2] Myers, R. J. *Journal of the Association of Official Agricultural Chemists* **1958**, *41*, 368–376.

[3] Pauling, L.; Corey, R. B. *Proceedings of the National Academy of Sciences of the United States of America* **1951**, *37*, 261–271.

[4] Orfanos, C.; Ruska, H. *Archiv für Klinische und Experimentelle Dermatologie* **1968**, *231*, 97–110.

[5] Reese, G. *Fette Seifen Anstrichmittel* **1966**, *68*, 763–765.

[6] Bories, M. F.; Martini, M. C.; Bobin, M. F.; Cotte, J. *International Journal of Cosmetic Science* **1984**, *6*, 213–229.

[7] Ehrenstein, D.; Iwase, K. H. *Biophysical Journal* **1996**, *71*, 1087–1094.

[8] Marti, C. J. M. J., O. *Nanotechnology* **1990**, *1*, 141.

[9] Meyer, G.; Amer, N. M. *Applied Physics Letters* **1990**, *57*, 2089–2091.

[10] Ruetsch, S. B.; Kamath, Y. K.; Kintrup, L.; Schwark, H. J. *Journal of Cosmetic Science* **2003**, *54*, 579–588.

[11] Wei, G. H.; Bhushan, B. *Ultramicroscopy* **2006**, *106*, 742–754.

[12] Cao, G. X.; Chen, X.; Xu, Z. H.; Li, X. D. *Composites Part B-Engineering* **2010**, *41*, 33–41.

[13] Wei, G. H.; Bhushan, B.; Torgerson, P. M. *Ultramicroscopy* **2005**, *105*, 248–266.

[14] Orfanos, C. E. *Haar und Haarkrankheiten.*; Fischer, Stuttgart und New York, 1979.

[15] Menkart, J.; Wolfram, L. J.; Mao, I. *International Journal of Cosmetic Science* **1984**, *35*, 21–43.

[16] Dekoi, S.; J., J. *Journal of Dermatology* **1988**, *15*, 393–6.

[17] Robbins, C. R. *Chemical and physical behavior of human hair*, 4th ed.; Springer-Verlag: New York, 2002.

[18] Feughelman, M.; Haly, A. R. *Biochimica Et Biophysica Acta* **1959**, *32*, 596–597.

[19] Bogaty, H. *Journal of the Society of Cosmetic Chemists* **1969**, *20*, 159–175.

[20] Wolfram, L. F.; Lindeman.Mk, *Journal of the Society of Cosmetic Chemists* **1971**, *22*, 839–930.

[21] Negri, A. P.; Cornell, H. J.; Rivett, D. E. *Textile Research Journal* **1993**, *63*, 109–115.

[22] Swift, J. A.; Holmes, A. W. *Textile Research Journal* **1965**, *35*, 1014–1019.

[23] Hersh, S. Ph.D. thesis, Princeton University, 1954.

[24] Robbins, C. R.; Crawford, R. J. *Journal of the Society of Cosmetic Chemists* **1991**, *42*, 59–67.

[25] Robbins, C. R.; Reich, C.; Patel, A. *Journal of the Society of Cosmetic Chemists* **1994**, *45*, 85–94.

[26] Scott, G. V. R. C. R.; Barnhurst, J. . D. *Journal of the Society of Cosmetic Chemists* **1969**, *20*, 135–152.

[27] Steinhardt, J.; Zaiser, E. M. *Journal of Biological Chemists* **1950**, *183*, 789–802.

[28] Pauling, L. *Cornell University Press* **1948**, 3.

[29] Maron, S. H. P. C. F. *Principles of Physical Chemistry*; Macmillan, 1958.

[30] Fuller, C. S. *Journal of Chemical Education* **1943**, *20*, 466–491.

[31] Wilkerson, V. A. *Journal of Biological Chemists* **1935**, *112*, 329–335.

[32] Bhushan, B. *Progress in Materials Science* **2008**, *53*, 585–710.

[33] Schwuger, M. *Journal of Colloid and Interface Science* **1973**, *43*, 491–498.

[34] Jonsson, B.; Lindman, B.; Kronberg, B.; Holmberg, K. *Surfactants and Polymers in Auqueous Solution*, 2nd ed.; John Wiley & Sons, LTD, 2003; ISBN-10: 0471974226.

[35] Terada, E.; Samoshina, Y.; Nylander, T.; Lindman, B. *Langmuir* **2004**, *20*, 6692–6701.

[36] Goddard, E. D.; Hannan, R. B. *Journal of Colloid and Interface Science* **1976**, *55*, 73–79.

[37] Manuszak Guerrini, M.; Daly, W. H. **1999**, 214–233.

[38] Lodge, R. A.; Bhushan, B. *Journal of Vacuum Science & Technology A* **2006**, *24*, 1258–1269.

[39] Wolfram, L. J.; Lennhoff, M. *Journal of the Textile Institute Transactions* **1966**, *57*, 590–591.

[40] Rebenfeld, W. H.-D., L.; Dansizer, C. *Journal of the Society of Cosmetic Chemists* **1966**, *17*, 525–538.

[41] Robbins, C. R.; Scott, G. V. *Journal of the Society of Cosmetic Chemists* **1970**, *21*, 639–641.

[42] Garson, J. C.; Vidalis, M.; Rousspoulos, P.; Leveque, J. L. *International Journal of Cosmetic Science* **1980**, *2*, 231–241.

[43] Randebrook, L., R.; Eckert *Fette Seifen Anstrichmittel* **1965**, *67*, 775–779.

[44] Robbins, C. R.; Kelly, C. H. *Textile Research Journal* **1970**, *40*, 891–896.

[45] Wolfram, L. J.; Albrecht, L. *Journal of the Society of Cosmetic Chemists* **1985**, *36*, 87–99.

[46] Robbins, C. R.; Scott, G. V. *Journal of the Society of Cosmetic Chemists* **1978**, *29*, 469–485.

[47] Robbins, C. R.; Scott, G. V. *Journal of the Society of Cosmetic Chemists* **1980**, *31*, 179–189.

[48] Schwartz, A. M. K. D. C. *Journal of the Society of Cosmetic Chemist* **1963**, *14*, 455–463.

[49] Gamez-Garcia, M. *Journal of the Society of Cosmetic Chemists* **1993**, *44*, 69–87.

[50] Wood, C.; Bartels, W. F.; Max, E.; Fery, A. *IFSCC Congress* **2008**, *25*, 1–5.

[51] Wood, C.; Bartels, W. F.; Max, E.; Fery, A. *56. SEPAWA Congress and European Detergence Conference* **2009**, *25*, 1–4.

[52] Bhushan, B.; Wei, G. H.; Haddad, P. *Wear* **2005**, *259*, 1012–1021.

[53] Swift, J. A. *International Journal of Cosmetic Science* **1991**, *13*, 143–159.

[54] Jachowicz, J.; McMullen, R. *Journal of Cosmetic Science* **2002**, *53*, 345–361.

[55] Barnes, H. A.; P., R. G. *International Journal of Cosmetic Science* **2000**, *22*, 259–264.

[56] Lodge, R. A.; Bhushan, B. *Journal of Applied Polymer Science* **2006**, *102*, 5255–5265.

[57] Chen, N.; Bhushan, B. *Journal of Microscopy-Oxford* **2006**, *221*, 203–215.

[58] Chen, N.; Bhushan, B. *Journal of Microscopy-Oxford* **2005**, *220*, 96–112.

[59] Swift, J. A.; Smith, J. R. *Scanning* **2000**, *22*, 310–318.

[60] Bhushan, B.; Chen, N. H. *Ultramicroscopy* **2006**, *106*, 755–764.

[61] O'Connor, S. D.; Komisarek, K. L.; Baldeschwieler, J. D. *Journal of Investigative Dermatology* **1995**, *105*, 96–99.

[62] Swift, J. *International Journal of Cosmetic Science* **2001**, *21*, 227–239.

[63] McMullen, R. L.; Kelty, S. P. *Scanning* **2001**, *23*, 337–345.

[64] LaTorre, C.; Bhushan, B. *Ultramicroscopy* **2006**, *106*, 720–734.

[65] Sadaie, M.; Nishikawa, N.; Ohnishi, S.; Tamada, K.; Yase, K.; Hara, M. *Colloids and Surfaces B-Biointerfaces* **2006**, *51*, 120–129.

[66] Breakspear, S.; Smith, J. R.; Luengo, G. *Journal of Structural Biology* **2005**, *149*, 235–242.

[67] Alexander, S.; Hellemans, L.; Marti, O.; Schneir, J.; Elings, V.; Hansma, P. K.; Longmire, M.; Gurley, J. *Journal of Applied Physics* **1989**, *65*, 164–167.

[68] Wortmann, A., 2003.

[69] Knoll, M. *Zeitschrift für technische Physik* **1935**, *16*, 467–475.

[70] Clarke, D. R. *Journal of Materials Science* **1973**, *8*, 279–285.

[71] Danilatos, G. D. *Advances in Electronics and Electron Physics* **1988**, *71*, 109–250.

[72] Binnig, G.; Rohrer, H. *Ibm Journal of Research and Development* **1986**, *30*, 355–369.

[73] Binnig, G.; Quate, C. F.; Gerber, C. *Physical Review Letters* **1986**, *56*, 930–933.

[74] Binnig, G.; Gerber, C.; Stoll, E.; Albrecht, T. R.; Quate, C. F. *Europhysics Letters* **1987**, *3*, 1281–1286.

[75] Smith, J. R. *Journal of the Society of Cosmetic Chemists* **1997**, *48*, 199–208.

[76] Erlandsson, R.; Mcclelland, G. M.; Mate, C. M.; Chiang, S. *Journal of Vacuum Science & Technology a-Vacuum Surfaces and Films* **1988**, *6*, 266–270.

[77] Colton, R. J. *Procedures in scanning probe microscopies*; John Wiley & Sons, LTD, 1998; ISBN-10: 047195912X.

[78] Bosio, V. Ph.D. thesis, Max Planck Institute of Colloids and Interfaces in Golm, Germany, 2003.

[79] Kappl, M.; Butt, H. J. *Particle & Particle Systems Characterization* **2002**, *19*, 129–143.

[80] Ducker, W. A.; Senden, T. J.; Pashley, R. M. *Nature* **1991**, *353*, 239–241.

[81] Cappella, B.; Dietler, G. *Surface Science Reports* **1999**, *34*, 1–104.

[82] Mate, C. M.; Mcclelland, G. M.; Erlandsson, R.; Chiang, S. *Physical Review Letters* **1987**, *59*, 1942–1945.

[83] Bhushan, B. *Nanotribology and Nanomechanics*; Springer, 2008; ISBN-10: 9783540776079.

[84] Wood, C.; Basilan, J.; Rausch, M.; Knab, A.; Seidel, S. *Cosmetic Science Technology* **2009**, *6*, 1–11.

[85] LaTorre, C.; Bhushan, B. *Ultramicroscopy* **2005**, *105*, 155–175.

[86] Hutter, B. J., J. L. *Review of Scientific Instruments* **1993**, *64*, 1868–1873.

[87] Israelachvili, J. N. *Intermolecular and surface forces*, 2nd ed.; Academic Press: London, 2006.

[88] Vogel, A.; Venugopalan, V. *Chemical Reviews* **2003**, *103*, 577–644.

[89] LaTorre, C.; Bhushan, B. *Journal of Vacuum Science & Technology A* **2005**, *23*, 1034–1045.

[90] Capella, B.; Baschieri, P.; Frediani, C.; Miccoli, P.; Ascoli, C. *Ieee Engineering in Medicine and Biology Magazine* **1997**, *16*, 58–65.

[91] Maxwell, J. M.; Huson, M. G. *Micron* **2005**, *36*, 127–136.

[92] Liu, H. W.; Bhushan, B. *Ultramicroscopy* **2003**, *97*, 321–340.

[93] Butt, H. J.; Cappella, B.; Kappl, M. *Surface Science Reports* **2005**, *59*, 1–152.

[94] Vinogradova, O. I.; Butt, H. J.; Yakubov, G. E.; Feuillebois, F. *Review of Scientific Instruments* **2001**, *72*, 2330–2339.

[95] Max, E.; Häfner, W.; Bartels, F. W.; Sugiharto, A.; Wood, C.; Fery, A. *Ultramicroscopy* **2010**, *110*, 320 – 324.

[96] Johnson, K. L.; Kendall, K.; Roberts, A. D. *Proceedings of the Royal Society of London Series a-Mathematical and Physical Sciences* **1971**, *324*, 301–313.

[97] Derjaguin, B. V.; Muller, V. M.; Toporov, Y. P. *Progress in Surface Science* **1994**, *45*, 131–143.

[98] Tabor, D. *Journal of Colloid and Interface Science* **1977**, *58*, 2–13.

[99] Erath, J.; Schmidt, S.; Fery, A. *Soft Matter* **2010**, *6*, 1432–1437.

[100] Green, C. P.; Sader, J. E. *Journal of Applied Physics* **2002**, *92*, 6262–6274.

[101] Feiler, A.; Attard, P.; Larson, I. *Review of Scientific Instruments* **2000**, *71*, 2746–2750.

[102] Bogdanovic, G.; Meurk, A.; Rutland, M. W. *Colloids and Surfaces B-Biointerfaces* **2000**, *19*, 397–405.

[103] Morel, N.; Ramonda, M.; Tordjeman, P. *Applied Physics Letters* **2005**, *86*, 163103:1–3.

[104] Cumpson, P. J.; Hedley, J.; Zhdan, P. *Nanotechnology* **2003**, *14*, 918–924.

[105] Li, Q.; Kim, K. S.; Rydberg, A. *Review of Scientific Instruments* **2006**, *77*, 065105:1–13.

[106] Jeon, S. J.; Yi, G. R.; Koo, C. M.; Yang, S. M. *Macromolecules* **2007**, *40*, 8430–8439.

[107] Liu, W. H.; Bonin, K.; Guthold, M. *Review of Scientific Instruments* **2007**, *78*, 063707:1–7.

[108] Tocha, E.; Schonherr, H.; Vancso, G. J. *Langmuir* **2006**, *22*, 2340–2350.

[109] Quintanilla, M. A. S.; Goddard, D. T. *Review of Scientific Instruments* **2008**, *79*, 1–11.

[110] Bhushan, B. *Nanotribology and Nanomechanics An Introduction*, 2nd ed.; Springer, Berlin, 2008; ISBN-10: 3540242678.

[111] Green, C. P.; Lioe, H.; Cleveland, J. P.; Proksch, R.; Mulvaney, P.; Sader, J. E. *Review of Scientific Instruments* **2004**, *75*, 1988–1996.

[112] Gnecco, E.; Bennewitz, R.; Gyalog, T.; Loppacher, C.; Bammerlin, M.; Meyer, E.; Güntherodt, H.-J. *Phys. Rev. Lett.* **2000**, *84*, 1172–1175.

[113] Bhushan, B.; Liu, H. W.; Hsu, S. M. *Journal of Tribology-Transactions of the Asme* **2004**, *126*, 583–590.

[114] Nylander, T.; Samoshina, Y.; Lindman, B. *Advances in Colloid and Interface Science* **2006**, *123-126*, 105–123.

[115] Weigmann, H. D.; Kamath, Y. K.; Ruetsch, S. B.; Busch, P.; Tesmann, H. *Journal of the Society of Cosmetic Chemists* **1990**, *41*, 379–390.

[116] Rabinovich, Y. I.; Adler, J. J.; Ata, A.; Singh, R. K.; Moudgil, B. M. *Journal of Colloid and Interface Science* **2000**, *232*, 10–16.

[117] Rabinovich, Y. I.; Adler, J. J.; Ata, A.; Singh, R. K.; Moudgil, B. M. *Journal of Colloid and Interface Science* **2000**, *232*, 17–24.

[118] Scott, G. V. R. C. R. *Journal of the Society of Cosmetic Chemists* **1980**, *31*, 179.

[119] Terada, E.; Samoshina, Y.; Nylander, T.; Lindman, B. *Langmuir* **2004**, *20*, 1753–1762.

8 Appendix

- The macro to export the force-distance curve was written for IGOR Pro 6.1, WaveMetrics:

```
#pragma rtGlobals=1              // Use modern global access method.
macro export_em
Silent 1
NewPath /C DataPath, "D:\Users\Max\diss\Memory" + root:ForceCurves:
    TestingFolder:MasterFPList[0] + ":"
setdatafolder root:ForceCurves:
Duplicate  /O root:ForceCurves:TestingFolder:MasterFPList
    MasterFPList
Make/O/T/N=0 xy_namen
variable invisible_dirs =-1
do
        invisible_dirs += 1
while (DataFolderExists("InvisibleSubFolder" + num2str(
    invisible_dirs)))
invisible_dirs -=1
//print invisible_dirs
variable max_files = numpnts(root:ForceCurves:MasterFPList) -1
//print max_files
//print(root:ForceCurves:MasterFPList[3] + "LVDT")
//string file_name=root:ForceCurves:MasterFPList[29] + "LVDT"
//print exists(file_name)
variable files=0
variable dirs
variable found
variable help=-1
do
        files += 1
        found = 0
        setdatafolder ("root:ForceCurves:")
        if (exists(root:ForceCurves:MasterFPList[files] + "Force")
           && exists(root:ForceCurves:MasterFPList[files] + "LVDT"))
                found =1
                Save/O/M="\n"/U={0,0,0,0}/G/P=DataPath $((root:
                    ForceCurves:MasterFPList[files] + "LVDT")), $((
```

```
                root:ForceCurves:MasterFPList[files] + "Force"))
                as (root:ForceCurves:MasterFPList[files] +".xy")
        else
                dirs=-1
                do
                        dirs += 1
//                      setdatafolder ("root:ForceCurves:" + root:
    ForceCurves:MasterFPList[0] + ":" + "InvisibleSubFolder" +
    num2str(dirs))
                        if (exists(root:ForceCurves:MasterFPList[
                            files] + "Force") && exists(root:
                            ForceCurves:MasterFPList[files] + "LVDT")
                            )
                                found = 1
                                Save/O/M="\n"/U={0,0,0,0}/G/P=
                                    DataPath $((root:ForceCurves:
                                    MasterFPList[files] + "LVDT")), $
                                    ((root:ForceCurves:MasterFPList[
                                    files] + "Force")) as (root:
                                    ForceCurves:MasterFPList[files]
                                    +".xy")
                        endif
                while (dirs < invisible_dirs)
        endif
        if (found == 0)
                print (root:ForceCurves:MasterFPList[files] +  "
                    Sorry, not available")
        else
                help +=1
//              print (num2str(help) + "  " + num2str(files))
                setdatafolder ("root:ForceCurves:")
                InsertPoints help,1,  xy_namen
                xy_namen[help]= root:ForceCurves:MasterFPList[files]
                     +".xy"
        endif
while (files<max_files)
Save/O/M="\n"/U={0,0,0,0}/G/P=DataPath xy_namen as "xy_namen"
KillWaves/Z xy_namen
print files
endmacro
```

- The procedure for analyzing the force-distance curves, written in **C**:

```
/*****************************************************************
**
**              This is file eval_force_distance.h
**              Copyright (C) 2008
**              developed by Wolfgang Haefner and Eva Max
**              Stand: 29.05.08
**
*****************************************************************/
#include <stdio.h>
#include <stdlib.h>
#include <fcntl.h>
#include <unistd.h>
#include <string.h>
#include <math.h>
#include <errno.h>
#ifdef powermac
#define high_endian
#endif
#ifdef x86
#define low_endian
#endif
#define ROB O_RDONLY
#define RWB O_RDWR|O_TRUNC|O_CREAT,0644

/*------------------------- allgemeine deklarationen
   -------------------------*/

#ifndef ROUND
#define ROUND(a)        ((a)>=0  ? (LONG)((DOUBLE)((a)+0.5)) \
                                 : (LONG)((DOUBLE)((a)-0.5)))
#endif
#ifndef ABS
#define ABS(a)          ((a)>=0 ? (a) : -(a))
#endif
#ifndef MOD
#define MOD(a,b)        ((a)%(b))
#endif
#ifndef SIGNUM
#define SIGNUM(a)       ((a)<0 ? (-1) : ((a)>0 ? (1) : (0)))
#endif
#ifndef MAX
#define MAX(a,b)        ((a)<(b) ? (b) : (a))
```

```
#endif
#ifndef MIN
#define MIN(a,b)        ((a)>(b) ? (b) : (a))
#endif
#ifndef SQUARE
#define SQUARE(a)        ((a)*(a))
#endif
#ifndef MAXCHAR
#define MAXCHAR          256
#endif
#ifndef TINY
#define TINY             1.0e-86
#endif
/*-------------------------------------------------------------*/
/*
/*                  Variablen fuer User- Funktionen
/*
int              err;
char             funktion[MAXCHAR], ausgabename[MAXCHAR];
/*

   */
/*-------------------------------------------------------------*/

/*              Variablen fuer elementare - Funktionen

char             *name_des_files;

double           *hilf;
double           *x_hin, *y_hin, *x_weg, *y_weg;
double           x_noncontact, x_contact, y_noncontact, y_contact,
   contact;
double           xsp[2], chi[2], a[2][2], da[2][2], x_schnitt,
   y_schnitt;
double           x_schnittpunkt, y_schnittpunkt, adhaesionsenergie;
FILE             *fd;
int              npts, npts_hin, npts_weg;
int              index_unten, index_oben;
int              index_hin_unten, index_hin_oben, index_weg_unten,
   index_weg_oben;

/*------------------------------ funktionen
   ----------------------------------------*/
```

```
int     namen_feld_anlegen ();
int     felder_freigeben_eval_force_distance ();
int     analyse_filename (char *filename, int *point_position);
int     lies_file (char *filename);
int     schreib_file (char *filename, int anzahl, double *xx, double
    *yy);
int     contact_suchen (char *filename, int anzahl, int *
   index_nach_unten, int * index_nach_oben, double *xx, double *yy);
int     anpassung (char *filename, int anzahl, int i_unten, int
   i_oben,\
                       double *xx, double *yy, double h_tolleranz);
int     adhaesions_energie (double *xx, double *yy, int grenz_index,
    double *m, double x_sp);
int     schreib_ergebnis_file (char *name);
void    did_not_work (char *filename);
#endif
```

Acknowledgments

My thesis would not have been possible without the help and support of so many people. Among those, I am deeply grateful to my advisor **Prof. Dr. Andreas Fery**. The years under his supervision were very essential for my development as a scientist and a researcher.

I also want to thank my former supervisor **Prof. Dr. Georg Krausch**, who opened the door to the opportunity to do a PhD in collaboration with an industry partner.

I want to thank **BASF SE** for financial support during these years.

Working together with the industry means having access to good collaborators in order to discuss and to solve problems. Therefore I want to thank the project managers from BASF SE: **Dr. Michael Kutschera**, **Dr. Frank W. Bartels** and **Dr. Albert B. Sugiharto**. Special thanks are due to **Dr. Claudia Wood** for her insightful suggestions and support. Numerous other colleagues at BASF SE also contributed to this project. They are **Dr. Bernhard v. Vacano**, **Monika Rausch**, **Sabine Seidel**, **Guido Lupa** and **Peter Boeshans**.

During my three months in Sweden I want to thank **Prof. Dr. Tommy Nylander** and **Dr. Pauline Vandoolaeghe** for introducing me to *the Swedish way of life*, even though Rudolph (the Ellipsometer) was not on my side.

Dr. Markus Rüggeberg from the Max Planck Institute of Colloids and Interfaces in Golm introduced me to the working principle of the micro laser, which was used for preparing my samples.

I am especially thankful to **Dr. Wolfgang Häfner**, who helped me with the statistical analysis of my data.

Thanks also to the complete crew of the machine shop under the direction of **Heinz Krejtschi** for processing my orders rapidly.

I should also mention Mr. Klaus Ehlers from New-York Hamburger Gummi-Waaren Compagnie AG in Hamburg and Mrs. Cornelia Graudenz from tesa AG in Hamburg for supplying me with samples of commercial products.
Thanks to **Dr. John Hardy** for proofreading this thesis. Also all of my colleagues from Physical Chemistry II at the University of Bayreuth for providing a fun environment in which to work.

I want to thank my office mate **Melanie Pretzl** for being such a great person to work next to. I really enjoyed all of the thought-provoking conversations and also the time we spent together. My other office mate **Johann Erath** has always been helpful in discussions regrading physics. *Frau* **Sybille Zimmermann** made life much easier with her administrative support and much sweeter by always being ready with a piece of chocolate or candy.

For being always there I want to thank my bff☺ **Margarete Wurst** and **Ulrike Lichtenau**.
I also want to thank my friends from study, especially **Dr. Felix Schacher**, **Michael Möller** and **Dr. Dominik Erhard** for having always an open ear and many great times outside of work. Last but not least, I want to thank my climbers out there for understanding me, even if I was preoccupied with work.

Am Ende möchte ich von ganzem Herzen meinen Eltern danken, dass sie mir während meines gesamten Studiums und während meiner gesamten Promotion immer ein stützender Pfeiler waren. Vielen Dank auch, dass Ihr mir so viel Verständnis entgegengebracht habt.

Erklärung

Die vorliegende Arbeit wurde von mir selbstständig verfasst, und ich habe dabei keine anderen als die angegebenen Hilfsmittel und Quellen benutzt.

Ferner habe ich nicht versucht, anderweitig mit oder ohne Erfolg eine Dissertation einzureichen oder mich der Doktorprüfung zu unterziehen.

Bayreuth,

Eva Max